

Fall 2014

Algorithm Development and Analysis for Advanced Engine Technologies including Piezoelectric Fuel Injection and Variable Valve Actuation

Bradley W. Pietrzak
Purdue University

Follow this and additional works at: https://docs.lib.purdue.edu/open_access_theses



Part of the [Automotive Engineering Commons](#), and the [Mechanical Engineering Commons](#)

Recommended Citation

Pietrzak, Bradley W., "Algorithm Development and Analysis for Advanced Engine Technologies including Piezoelectric Fuel Injection and Variable Valve Actuation" (2014). *Open Access Theses*. 367.
https://docs.lib.purdue.edu/open_access_theses/367

This document has been made available through Purdue e-Pubs, a service of the Purdue University Libraries. Please contact epubs@purdue.edu for additional information.

**PURDUE UNIVERSITY
GRADUATE SCHOOL
Thesis/Dissertation Acceptance**

This is to certify that the thesis/dissertation prepared

By Bradley W. Pietrzak

Entitled

Algorithm Development and Analysis for Advanced Engine Technologies including Piezoelectric Fuel Injection and Variable Valve Actuation

For the degree of Master of Science in Mechanical Engineering

Is approved by the final examining committee:

Gregory M. Shaver

Peter H. Meckl

Oleg Wasynczuk

To the best of my knowledge and as understood by the student in the Thesis/Dissertation Agreement, Publication Delay, and Certification/Disclaimer (Graduate School Form 32), this thesis/dissertation adheres to the provisions of Purdue University's "Policy on Integrity in Research" and the use of copyrighted material.

Gregory M. Shaver

Approved by Major Professor(s): _____

Approved by: Ganesh Subbarayan

10/14/2014

Head of the Department Graduate Program

Date

ALGORITHM DEVELOPMENT AND ANALYSIS FOR ADVANCED ENGINE
TECHNOLOGIES INCLUDING PIEZOELECTRIC FUEL INJECTION AND
VARIABLE VALVE ACTUATION

A Thesis

Submitted to the Faculty

of

Purdue University

by

Bradley W. Pietrzak

In Partial Fulfillment of the

Requirements for the Degree

of

Master of Science in Mechanical Engineering

December 2014

Purdue University

West Lafayette, Indiana

ACKNOWLEDGMENTS

I would like to thank my advisor, Professor Gregory M. Shaver, for enabling my graduate research and providing me with advice along the way. I would also like to thank my other committee members, Professor Peter Meckl and Professor Oleg Wasynczuk for their feedback and support.

Without the assistance of a knowledgeable and experienced technical shop staff, I could not have completed my research. Accordingly, a special thanks goes out to Bob Brown, Ron Evans, Frank Lee, and David Meyer.

Thank you to my colleagues Dat Le, David Fain, Mayura Halbe, Aswin Karthik, Leighton Roberts, Chuan Ding, Soumya Nayyar, and Lucius Wang. Their assistance with the conducting of experiments and the troubleshooting of hardware and software issues has repeatedly prevented the pace of my research grinding to a halt.

I would also like to thank Cummins Inc. and Eaton Corporation for sponsoring my research. Specifically, a very special thanks goes to Mike Ruth, Ed Koeberlein, Douglas Memering, Shankar Venkataraman, Jalal Syed, and Rod Hemmerlein of Cummins, and Jim McCarthy and Doug Nielsen of Eaton.

Last but certainly not least, I would like to thank my parents and sister for their support and encouragement as I worked to complete this thesis.

TABLE OF CONTENTS

	Page
LIST OF TABLES	v
LIST OF FIGURES	vi
SYMBOLS	ix
ABBREVIATIONS	xii
ABSTRACT	xiii
1. INTRODUCTION	1
1.1 Motivation	1
1.2 Literature Review	4
1.2.1 Fuel Injection Rate Shaping	4
1.2.2 Cylinder Deactivation	5
1.3 Experimental Hardware	7
1.3.1 Piezoelectric Fuel Injector Experimental Setup	7
1.3.2 CDA and Oil Accumulation Experimental Setup	9
1.4 Contributions	14
1.4.1 LabVIEW FPGA Code Optimization	14
1.4.2 Model-Based Estimation of Piezoelectric Fuel Injector Parameters	15
1.4.3 Oil Accumulation Measurement and Analysis	15
1.4.4 First-Fire Readiness Analysis	15
1.4.5 Fired Recharge Algorithm Development and Validation for a Diesel Engine Utilizing CDA	15
2. MODEL-BASED ESTIMATION OF PIEZOELECTRIC FUEL INJECTOR PARAMETERS	17
2.1 Injector System and Parameters of Interest	17
2.1.1 Injector System	17
2.1.2 Available Measurements	19
2.2 Parameter Estimation	20
2.2.1 Injector Simulation Model	20
2.2.2 State Estimator	21
2.2.3 Flow Rate Measurement Technique	21
2.2.4 Needle Seat Area Identification	23
2.3 Simulation Results	25
2.3.1 Parameter Estimation Simulation	25

	Page
2.3.2 State Estimator Simulation	27
2.4 Discussion and Conclusion	32
2.5 Summary	33
3. OIL ACCUMULATION MEASUREMENT AND ANALYSIS	35
3.1 Heat-Release-Based Analysis of Oil Accumulation	35
3.2 Test Plan for the Experimental Analysis of Oil Accumulation	41
3.3 Results and Discussion	43
3.4 Summary	72
4. FIRST-FIRE READINESS ANALYSIS	73
4.1 Analytical Procedure	73
4.2 Experimental Results	74
4.3 Summary	80
5. FIRED RECHARGE ALGORITHM DEVELOPMENT AND VALIDATION FOR A DIESEL ENGINE UTILIZING CDA	83
5.1 The Fired Recharge Algorithm	83
5.2 The Implementation and Validation of the Fired Recharge Algorithm	85
5.3 The Effect of Recharge Events on Oil Accumulation and First-Fire Readiness	92
5.4 Summary	92
6. SUMMARY AND FUTURE WORK	94
6.1 Parameter Estimation for a Piezoelectric Fuel Injector	94
6.2 Oil Accumulation, First-Fire Readiness, and Cylinder Recharging Anal- ysis for a Diesel Engine Utilizing CDA	95
LIST OF REFERENCES	97

LIST OF TABLES

Table	Page
1.1 Nominal engine parameters.	10
2.1 Injected Fuel Quantity Error	30
3.1 Waschni heat transfer model tuning constant for each cylinder.	40
3.2 Magnitudes of error bars for each cylinders cumulative heat release and accumulated oil mass in data set 1.	45
3.3 Magnitudes of error bars for each cylinders cumulative heat release and accumulated oil mass in data set 2.	46
3.4 Accumulated oil masses for data set 1.	71
3.5 Accumulated oil masses for data set 2.	71
5.1 ECM variables used in fired recharge algorithm.	86

LIST OF FIGURES

Figure	Page
1.1 US EPA regulations for on-highway heavy-duty diesel engines [1]. . . .	1
1.2 Example of boot-shaped fuel injection profile.	2
1.3 Schematic of Off-Engine Injector Experimental Setup	8
1.4 Photograph of Off-Engine Injector Experimental Setup	9
1.5 Photograph of Off-Engine Injector Control and Measurement Hardware	11
1.6 Schematic of engine testbed.	12
1.7 Experimental testbed with VVA.	13
1.8 Schematic of fully flexible electro-hydraulic VVA actuator.	14
2.1 Piezoelectric Fuel Injector Schematic Diagram	18
2.2 Expanded view of injector needle seat	19
2.3 Parameter Estimation Strategy	21
2.4 Flow Rate Measurement Technique	22
2.5 Piezostack Voltage for Typical Boot-Shaped Injection	24
2.6 Flow Rate for Typical Boot-Shaped Injection	25
2.7 Parameter Estimator Simulation Results for $\alpha = 0.75$	26
2.8 Parameter Estimator Simulation Results for $\alpha = 1.25$	27
2.9 State Estimator Simulation Results for $\alpha = 1.25$, 40% Toe Height . . .	28
2.10 State Estimator Simulation Results for $\alpha = 1.25$, 50% Toe Height . . .	29
2.11 State Estimator Simulation Results for $\alpha = 0.75$, 50% Toe Height . . .	31
2.12 State Estimator Simulation Results for $\alpha = 0.75$, 20% Toe Height . . .	32
3.1 Cumulative heat release in cylinder 1 for 0.5, 5, 10, and 20 minute CDA times. Active cylinder cumulative heat release shown for comparison. .	37
3.2 Gross, net, and wall heat transfer rates for a fired recharge in cylinder 6	40
3.3 Test plan used to study oil accumulation	42

Figure	Page
3.4 Cumulative heat release per cycle in cylinder 1 after 20 minutes of CDA.	44
3.5 Cumulative heat release per cycle in cylinder 1 after 20 minutes of CDA with sum shaded.	47
3.6 Cumulative heat release per cycle in cylinder 1 after 10 minutes of CDA with sum shaded.	48
3.7 Cumulative heat release per cycle in cylinder 1 after 5 minutes of CDA with sum shaded.	49
3.8 Cumulative heat release per cycle in cylinder 1 after 0.5 minutes of CDA with sum shaded.	50
3.9 Heat release rate as a function of crank angle in cylinder 1 after 20 minutes of CDA.	51
3.10 Heat release rate as a function of crank angle in cylinder 1 after 0.5 minutes of CDA.	52
3.11 Calculated oil masses in cylinder 1 for data sets 1 and 2.	53
3.12 Cumulative heat release per cycle in cylinder 1 after 10 minutes of CDA in data set 2.	54
3.13 Calculated oil masses in cylinder 2 for data sets 1 and 2.	55
3.14 Cumulative heat release per cycle in cylinder 2 after 10 minutes of CDA in data set 1.	56
3.15 Calculated oil masses in cylinder 3 for data sets 1 and 2.	57
3.16 Cumulative heat release per cycle in cylinder 3 after 5 minutes of CDA in data set 2.	58
3.17 Cumulative heat release as a function of crank angle in cylinder 3 after 5 minutes of CDA in data set 2.	59
3.18 Heat release rate as a function of crank angle in cylinder 3 after 5 minutes of CDA in data set 2.	60
3.19 Cumulative heat release per cycle in cylinder 3 after 20 minutes of CDA in data set 1.	61
3.20 Heat release rate as a function of crank angle in cylinder 3 after 20 minutes of CDA in data set 1.	62
3.21 Calculated oil masses in cylinder 4 for data sets 1 and 2.	63
3.22 Calculated oil masses in cylinder 5 for data sets 1 and 2.	64

Figure	Page
3.23 Cumulative heat release per cycle in cylinder 5 after 20 minutes of CDA in data set 1.	65
3.24 Cumulative heat release as a function of crank angle in cylinder 5 after 20 minutes of CDA in data set 1.	66
3.25 Heat release rate as a function of crank angle in cylinder 5 after 20 minutes of CDA in data set 1.	67
3.26 Calculated oil masses in cylinder 6 for data sets 1 and 2.	68
3.27 Calculated oil masses in all cylinders for data set 1.	69
3.28 Calculated oil masses in all cylinders for data set 2.	70
4.1 Heat release rate as a function of crank angle in cylinder 5 after 20 minutes of CDA.	75
4.2 GIMEP after 20 minutes of CDA for data sets 1 and 2.	76
4.3 Heat release rate as a function of crank angle in cylinder 1 after 10 minutes of CDA.	77
4.4 GIMEP after 10 minutes of CDA for data sets 1 and 2.	77
4.5 Heat release rate as a function of crank angle in cylinder 3 after 5 minutes of CDA.	78
4.6 GIMEP after 5 minutes of CDA for data sets 1 and 2.	79
4.7 GIMEP after 0.5 minutes of CDA for data sets 1 and 2.	80
4.8 Heat release rate as a function of crank angle in cylinder 5 after 0.55 minutes of CDA.	81
4.9 Cumulative heat release per cycle in cylinder 5 after 0.5 minutes of CDA in data set 2.	82
5.1 Order of events during a non-fired recharge event	84
5.2 Order of Events During a Fired Recharge Event	85
5.3 Fired recharge in cylinder 4 at 800 rpm	87
5.4 Fired recharge in cylinder 5 at 800 rpm	88
5.5 Fired recharge in cylinder 6 at 800 rpm	89
5.6 Fired recharges in cylinders 4, 5, and 6 at 800 rpm, all on the same time axis	91

SYMBOLS

α	Parameter Error Multiplier for Piezoelectric Fuel Injector Model
β	Waschni Heat Transfer Tuning Coefficient
$A(\theta)$	Inside Surface Area of Cylinder as a Function of Crank Angle
$A_{1,true}$	True Value of $A_1(x_2)$ Parameter
$A_{1,estimator}$	Value of $A_1(x_2)$ Parameter used in State Estimator
$A_1(x_2)$	Area of Needle Seat as a Function of Needle Lift
$\hat{A}_1(x_2)$	Estimate of $A_1(x_2)$ Parameter
A_2	Area of Spray Holes
$Area_{total}$	Total Area Under Boot-Shaped Injection Profile
$Area_{shank}$	Area Under Shank of Boot-Shaped Injection Profile
B	Cylinder Bore Diameter
c_1	In-Cylinder Gas Velocity Model Coefficient
c_2	In-Cylinder Gas Velocity Model Coefficient
C	Celsius
CO	Carbon Monoxide
CO_2	Carbon Dioxide
$dQ_{gross}/d\theta$	Gross Heat Release Rate
$dQ_{net}/d\theta$	Net Heat Release Rate
$dQ_{wall}/d\theta$	Heat Transfer Rate
$d\theta$	Delta Crank Angle Degree
dV	Delta Volume
$ft - lbs$	Foot-Pounds
g	Gram
$g/hp - hr$	Gram/Horsepower-Hour
γ	Specific Heats Ratio

$h(\theta)$	Instantaneous Heat Transfer Coefficient Through Cylinder Walls
hp	Horsepower
J	Joule
K	Kelvin
kg	Kilogram
$kPag$	Kilopascals (gage)
L	Liter
L_{stroke}	Piston Stroke Length
LHV_{fuel}	Lower Heating Value of Diesel Fuel
LHV_{oil}	Lower Heating Value of Engine Lubricating Oil
m_{fuel}	Mass of Fuel Burned In-Cylinder
m_{oil}	Mass of Engine Lubricating Oil Burned In-Cylinder
Nm	Newton-Meters
ρ	Density of Fuel Inside Piezoelectric Injector
P	Pressure
P_{bv}	Body Volume Pressure
P_{line}	Line Pressure
P_{mot}	Motored In-Cylinder Pressure
P_r	In-Cylinder Pressure at Reference Condition
P_{sac}	Sac Volume Pressure
Q_{gross}	Gross Heat Release
$Q_{gross,deactive}$	Gross Heat Release During Oil and Fuel Combustion
$Q_{gross,active}$	Gross Heat Release During Fuel Combustion
r	Connecting Rod Length
R_{need}	Flow Resistance of Needle Seat
R_{sh}	Flow Resistance of Spray Holes
\bar{s}_p	Mean Piston Speed
t_{injend}	End Time of Boot-Shaped Injection Event
t_{shank}	Shank Time of Boot-Shaped Injection Event

t_{start}	Start Time of Boot-Shaped Injection Event
t_{toe}	Toe Time of Boot-Shaped Injection Event
t_{toeend}	Time at which Toe of Boot-Shaped Injection Ends
T	Bulk Temperature of Cylinder Contents
T_r	In-Cylinder Temperature at Reference Condition
T_{wall}	Temperature of Cylinder Walls
θ	Crank Angle Degree
V_r	Cylinder Volume at Reference Condition
V_s	Piezostack Voltage
$w(\theta)$	In-Cylinder Gas Velocity
w_{stc}	Output Fuel Flow Rate of Piezoelectric Injector Model
w_{toe}	Fuel Flow Rate During Toe Portion of Boot-Shaped Injection
$W_{c,i}$	Gross Indicated Work per Cycle Delivered to Piston i
W_c	Total Gross Indicated Work per Cycle
x_2	Needle Lift

ABBREVIATIONS

AFR	Air-to-Fuel Ratio
BMEP	Brake Mean Effective Pressure
CDA	Cylinder Deactivation
DOC	Diesel Oxidation Catalyst
DPF	Diesel Particulate Filter
ECM	Engine Control Module
EPA	Environmental Protection Agency
GSI	Generic Serial Interface
GIMEP	Gross Indicated Mean Effective Pressure
MRAC	Model Reference Adaptive Control
NO _x	Oxides of Nitrogen
NVH	Noise, Vibration, and Harshness
PM	Particulate Matter
PPM	Parts per Million
RLS	Recursive Least Squares
rpm	Revolutions Per Minute
SCR	Selective Catalytic Reduction
TH	Toe Height
VVA	Variable Valve Actuation

ABSTRACT

Pietrzak, Bradley W. M.S.M.E., Purdue University, December 2014. Algorithm Development and Analysis for Advanced Engine Technologies including Piezoelectric Fuel Injection and Variable Valve Actuation. Major Professor: Gregory M. Shaver, School of Mechanical Engineering.

As vehicle emissions standards and fuel economy constraints become increasingly strict, the automotive industry must employ the use of advanced engine technologies to overcome these challenges. Fuel injection rate shaping and cylinder deactivation (CDA) are two such technologies, and both of them require the design and implementation of algorithms using various hardware and software tools.

Fuel injection rate shaping is one path towards cleaner and more efficient diesel engines. Piezoelectrically-actuated fuel injectors are well-suited for rate shaping operation, but are difficult to control. Control-related challenges arise primarily due to the lack of measurements available in a fuel injection system on-engine, the inherent complexity in the dynamics of a piezoelectric fuel injector, and variability from injector-to-injector and over the life of a given injector. Although these challenges are significant, model-based fuel flow rate estimation and control is of the utmost importance due to the fact that the brake torque in a diesel engine is primarily influenced by the total amount of injected fuel per engine cycle. This thesis studies the effect of injector model parameter uncertainties on the model-based estimate of the injector's output fuel flow rate. Specifically, the relationship between the injector's needle seat area and needle lift is investigated. While off-engine experiments can be conducted to determine this parameter, this study presents an on-engine parameter estimation strategy that can accommodate for some of the aforementioned injector variability. In the presence of an initial parameter error of 25%, the parameter estimator improved

the model-based prediction of total injected fuel by approximately 10% in Matlab simulations.

CDA is another technology that enables improved fuel economy and reduced tailpipe emissions in diesel engines. As the name suggests, CDA involves deactivating some combination of an engine's cylinders in order to temporarily reduce the total displacement of the engine. Reduced engine displacement can improve fuel economy and reduce harmful engine emissions (by means of reduced air-to-fuel ratio and reduced pumping work), especially at low engine speed and load conditions. However, there are a few challenges that CDA presents. First, engine lubricating oil can accumulate in deactivated cylinders as time progresses. Second, cylinders may not perform normally immediately upon reactivation (a concept referred to as "first-fire readiness") due to this oil accumulation as well as low in-cylinder temperatures that are the result of a prolonged deactivation. Third, changing the combination of firing cylinders can yield undesirable torsional vibrations during CDA operation. This thesis analyzes the first and second of these issues using in-cylinder pressure measurements to study combustion in cylinders that have been reactivated after prolonged periods of deactivation. Experiments show that as more time is spent in CDA mode, more oil accumulates in deactivated cylinders. This oil accumulation can be as much as 500 mg for cylinders that have been deactivated for 20 minutes. CDA durations of 5 and 10 minutes yield accumulated oil masses of up to 376 mg and 255 mg, respectively, while a CDA duration of 0.5 minutes yields an oil accumulation of less than 1 mg. Since the combustion of this accumulated oil causes abnormally large cumulative heat releases in the engine cycles following the transition from CDA to six cylinder mode, the brake torque does not smoothly transition between these two engine modes. For CDA times of 5, 10, and 20 minutes, these torque fluctuations make such long periods of CDA-only operation unacceptable from a first-fire readiness perspective.

Finally, this thesis presents a basic cylinder recharging strategy that can be used in future work to mitigate the effect of oil accumulation and improve first-fire readiness. While improvements in piston ring design can prevent oil accumulation, this cylinder

recharging strategy uses software to reactivate all deactivated cylinders for a single engine cycle at regular intervals in an effort to raise in-cylinder pressures enough to prevent oil from seeping into deactivated cylinders. The ability to perform these “recharge events” has been added to the engine test cell used in this study and has been validated experimentally. Although CDA-only operation is unacceptable for periods of time greater than or equal to 5 minutes, CDA operation with regularly-spaced recharge events could enable prolonged CDA operation by mitigating the effects of oil accumulation and first-fire readiness.

CHAPTER 1: INTRODUCTION

1.1 Motivation

In diesel engines, harmful emissions primarily appear in the form of oxides of Nitrogen (NO_x) as well as particulate matter (PM), and their reduction often inherently involves some increased use of fuel. Figure 1.1 shows the evolution of EPA-mandated emissions standards for on-highway heavy-duty diesel engines from 1994 through 2010 in the US. This approximately ten-fold decrease in emissions limits has motivated the development of a variety of novel diesel engine technologies, including advanced fuel injection techniques and cylinder deactivation.

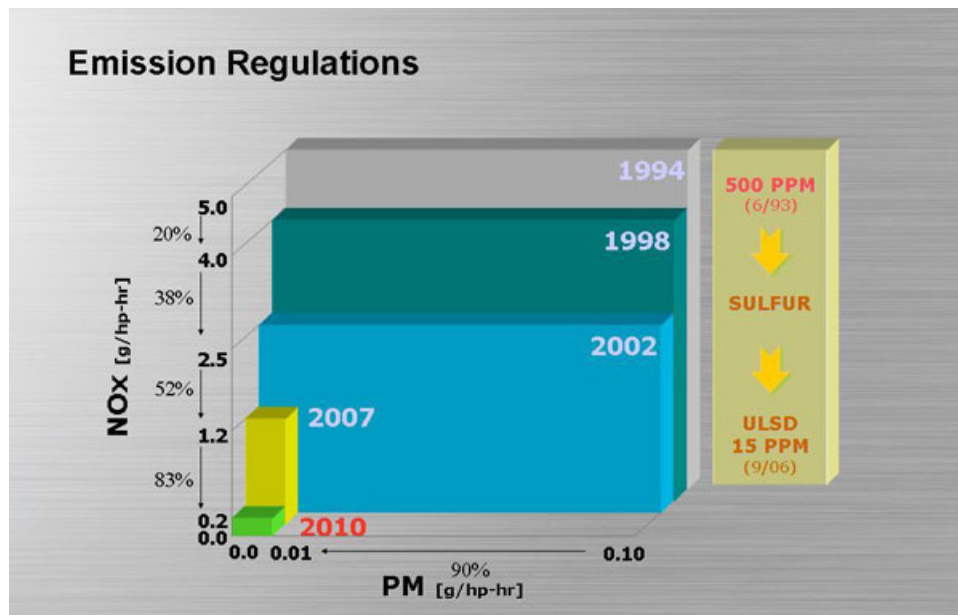


Figure 1.1. US EPA regulations for on-highway heavy-duty diesel engines [1].

Fuel injectors capable of high pressure, multi-pulse operation with precise control of both fueling quantity and spacing is a key enabler for the development of engines that offer reduced emissions, as well as quieter and more efficient operation [2–4].

Further improvement in fuel injection technology can be made via the use of a more complex type of injection event known as “rate shaping” [5].

Piezoelectric actuators have very fast response times enabling the creation of a variety of injection events [6], including rate shaping [7]. For the purposes of reduced emissions and improved fuel economy, a special type of rate shape known as the “boot profile” is of interest [8–10]. Fig. 1.2 shows an example of a boot-shaped injection profile, and while it will be discussed in detail later in this thesis, it should be mentioned here that its generation poses a unique set of problems compared to conventional pulse-shaped fuel injections. Because the injector is hovering somewhere

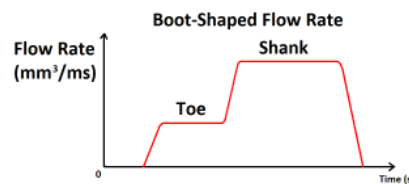


Figure 1.2. Example of boot-shaped fuel injection profile.

between fully on and fully off during the “toe” portion of a boot shaped injection event, injector models which account for complex phenomena including piezostack hysteresis and needle compliance must be used. Additionally, parameter variations with time and from injector-to-injector become more significant. The development of the parameter estimation algorithm presented in this thesis improves the closed-loop control of fuel injection rate in piezoelectric injectors.

CDA is another technology that aims to improve fuel economy while also reducing NOx and PM emissions by improving the efficacy of exhaust gas after-treatment systems. The primary mechanism by which CDA improves fuel economy is a reduction in engine pumping losses via a reduction in the number of cylinders that are drawing charge gas from the intake manifold. Fuel economy benefits are particularly noteworthy at low load conditions, and often result in improvements on the order

of 10-26% [11–16]. Of at least equal importance is the ability of CDA to increase exhaust gas temperatures. The “light-off” temperatures of many modern exhaust after-treatment systems is approximately 250 °C, and this represents the lowest exhaust gas temperature at which the after-treatment systems - including a diesel oxidation catalyst (DOC), diesel particulate filter (DPF), and selective catalytic reduction (SCR) - can function effectively. At low load and idle engine conditions, exhaust gas temperatures are well below 250 °C. By lowering the engine’s air-to-fuel ratio (AFR), CDA significantly raises exhaust gas temperatures, thereby reducing emissions at low speed and load conditions.

The implementation of CDA poses a few unique problems, including the accumulation of engine lubricating oil in-cylinder during prolonged CDA operation, difficulty in the reactivation of deactivated cylinders due to their cooling-down during CDA mode (referred to as “first-fire readiness”), and noise, vibration, and harshness (NVH) issues that may arise due to undesirable torsional vibrations that arise in CDA mode. The first two of those three issues can be addressed in a few ways. Since oil seeps into deactivated cylinders via imperfections in the piston ring seal, improved piston ring design could reduce oil accumulation. Additionally, reformulating the engine oil itself could reduce its tendency to accumulate via changes in fluid properties such as viscosity. However, this thesis focuses on the development of an algorithm that reactivates each deactivated cylinder for a single engine cycle periodically during CDA operation in an effort to mitigate oil accumulation and first-fire readiness in future work.

Previously, several of the author’s colleagues successfully implemented an algorithm that opens and closes the intake and exhaust valves one time in deactivated cylinders at user-specified intervals. These single-cycle valve events are referred to as “recharge events,” and they serve to occasionally increase the pressure in each deactivated cylinder in order to prevent oil from seeping into the combustion chambers via the imperfect seal created by the piston rings. While this technique is effective to some degree, it is beneficial to also inject fuel during the recharge event so that

a normal combustion event can occur. Such a recharge event is known as a “fired recharge” because the deactivated cylinders experience a combustion event during the single recharge engine cycle.

Compared to non-fired recharges, fired recharges have the additional ability to raise cylinder temperatures during a recharge event. Furthermore, the increase in in-cylinder pressure created by a fired recharge is greater than that of a non-fired recharge, at least initially. Accordingly, this thesis investigates the potential need for fired recharges by studying the effect of long periods of CDA-only (i.e. without fired or non-fired recharges) operation on oil accumulation and first-fire readiness. Using the fired recharge algorithm presented in this thesis to reduce oil accumulation and improve first-fire readiness is the subject of future work.

1.2 Literature Review

1.2.1 Fuel Injection Rate Shaping

While multi-pulse fuel injectors are somewhat common in modern engines, injectors capable of rate shaping operation are comparatively rare. Rate shaping has been accomplished via rail pressure modulation in [17], and needle displacement modulation in [18]. While the injector used in this thesis also achieves rate shaping by the modulation of its needle, it does so using a piezoelectric actuator. The injector in [18], on the other hand, does this using a hydro-mechanical feedback circuit.

Parameter estimation for fuel injection systems has been accomplished in the literature. In [19], the parameters of an injector model for a Bosch V fuel injection system were determined using vibration measurements recorded during fuel injection events. While no online parameter estimator was proposed, the method used in this paper could be incorporated into an online technique because of the non-intrusive nature of vibration measurements. [20] presents an offline parameter estimation technique for a port fuel injection system.

Online parameter estimators are rarely found in the literature for any type of fuel injector, especially piezoelectric injectors. However, piezoelectric actuators have been adaptively controlled outside of fuel injector applications. In [21], a least-mean-square algorithm was used to adaptively control a piezoelectrically-actuated micro-positioning system. In [22], a piezoelectric actuator was adaptively controlled using a recursive-least-square algorithm. Critically, these two adaptive controllers relied on measurements of piezo-actuator displacement, which is not available in a fuel injection system.

Prior efforts by several of the author’s colleagues and predecessors have resulted in physically-based dynamic models of the injector during multi-pulse [23] and rate shaping [24] operation. Using these models, an output fuel flow estimator for the piezoelectric injector was developed in [25] for cycle-to-cycle control of closely-spaced, multi-pulse injection events, and in [26] for rate shaped injection events. The dynamic injector model in [24] was simplified in [26] for control purposes, and a closed-loop fuel flow rate controller was designed and validated in [27].

1.2.2 Cylinder Deactivation

While CDA is used commonly in the literature, the majority of its applications are for spark-ignited (SI) engines. Specific implementations of CDA will be highlighted in the following paragraphs.

Falkowski et al [28] implemented CDA on a V8, gasoline-powered, SI, Daimler-Chrysler 5.7 L HEMI[®] Engine. In this application, the implementation of CDA was tested in a full-vehicle environment with practical considerations such as NVH, maintenance intervals, and reliability taken into account. Specifically, the use of CDA was required to be completely transparent from the driver’s point of view. This was accomplished by incorporating CDA-capability into the vehicle’s design from concept to completion, which allowed for maximum design flexibility. One of the key design considerations was the inclusion of a torque controller to maintain a smooth transition

between CDA and normal engine operation. Additionally, a fired recharge strategy was used to prevent in-cylinder oil accumulation, though the specifics of the strategy such as its recharge interval were not specified.

Leone et al [11] implemented CDA on several dyno-tested engines of various sizes and studied fuel economy benefits while each engine was subject to different operating constraints. For example, the fuel economy benefit of CDA was tested during conditions of engine warm-up, low speed, and different drive cycles (US EPA, Japanese, European, etc). The tests found that CDA yielded fuel economy benefits in the range of 6-14%, with specific improvements depending greatly on which condition was constraining the engine's operation.

Boretti et al [29] proposed a CDA mechanism that disables piston movement in addition to the disabling of valves and fuel injectors. The goal of this effort was to reduce the friction losses that are still problematic during CDA due to piston movement, even with the pumping loss reduction that is present when the valves and fueling are deactivated. While this novel piston deactivation mechanism was only studied in a simulation of a V8 engine, the reduction in friction losses was concluded to be significant.

In-Cylinder Oil Accumulation

In this thesis, the effect of oil accumulation in deactivated cylinders is outlined, and there are a few other instances of this in the literature. Ma [30] studied the effect of oil transport via piston rings in deactivated cylinders. The accumulation of oil via this transport mechanism was deemed significant, and several piston ring design changes were suggested to reduce this oil accumulation. These changes included alterations to the piston ring/groove clearances and ring gap and drain hole sizes, reducing cylinder bore distortion, and improving the piston-land and oil drain hole structures to reduce upward oil flow.

Yilmaz et al [31] studied oil consumption in a 4-cylinder SI engine that was equipped with instrumentation which enabled real-time oil consumption rate measurements. Yilmaz et al considered three sources of oil consumption: evaporation, oil entrained in blowby gas flow, and oil flow through piston rings and valve guides in the combustion chambers. They concluded that at low loads (i.e. loads of less than 50% of the maximum, which are the primary focus of this thesis), oil consumption via oil transport past the piston rings into the combustion chambers was responsible for approximately 90% of total oil consumption, and this consumption rate increased as load decreased.

Froelund et al [32] investigated the effect of oil consumption on diesel particulate filter (DPF) deterioration, and found that this deterioration could be mitigated with both engine and oil design changes. Since the DPF is one of the most ubiquitous emissions reduction systems in modern diesel engines, its deterioration is very undesirable. Engine-design-related and oil-design-related suggestions to reduce oil-based PM emissions were discussed, and these are of great relevance to this thesis since future work on the test engine at Purdue will likely seek to minimize in-cylinder oil accumulation and consumption.

1.3 Experimental Hardware

Since two completely separate experimental setups were used in this thesis, they will be described independently in this section.

1.3.1 Piezoelectric Fuel Injector Experimental Setup

The off-engine injector experimental setup at Purdue is shown in Fig. 1.3. This setup allows a single piezoelectric fuel injector to be tested while measuring rail pressure, line pressure, stack voltage, and output fuel flow rate. Particularly noteworthy is the measurement of output fuel flow rate, which is not measurable on-engine. This measurement is performed using the Bosch-type technique [33], and was used by the

author and his colleagues for model-based estimation and controller validation purposes. A photograph of the entire experimental setup illustrated in Fig. 1.3 is shown

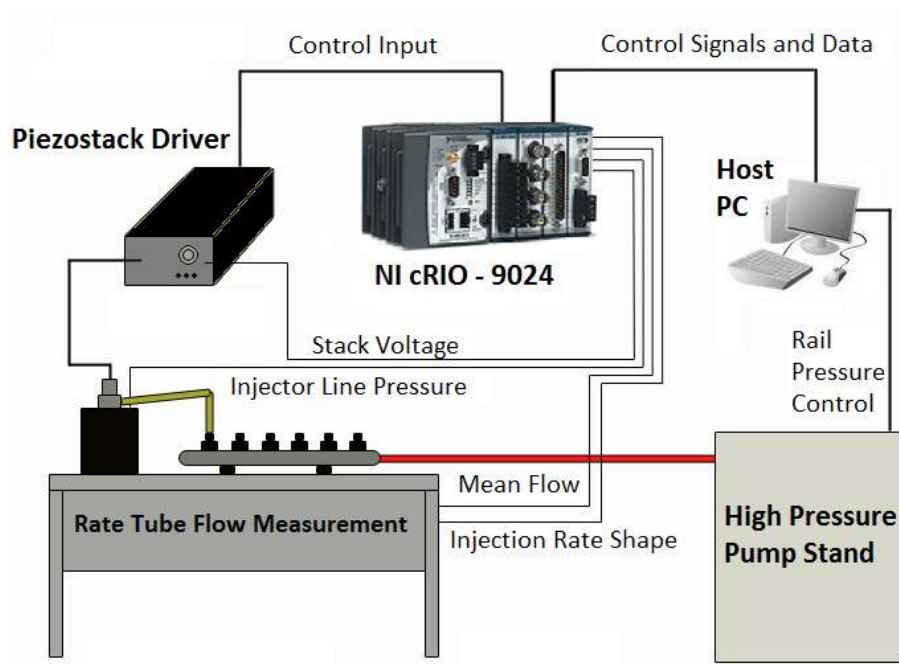


Figure 1.3. Schematic of Off-Engine Injector Experimental Setup

in Fig. 1.4

Several additional pieces of hardware are used in the setup for control and measurement. Perhaps most critical is the NI CompactRIO FPGA, which sends a control signal to the piezostack driver while also reading measurements of stack voltage, line pressure, and output fuel flow rate. Additionally, the FPGA executes an implementation of the model-based estimation [26] and fuel flow control [27] algorithms designed for this injector. These algorithms are coded in LabVIEW and then compiled into low-level FPGA code using the LabVIEW FPGA module.

The data acquisition (DAQ) capabilities of the FPGA run at a frequency of 500 kHz, while the KROHN-HITE anti-aliasing filter operates at a frequency of 200 kHz. The Qortek piezostack driver sends out a control signal at a frequency of 100 kHz.

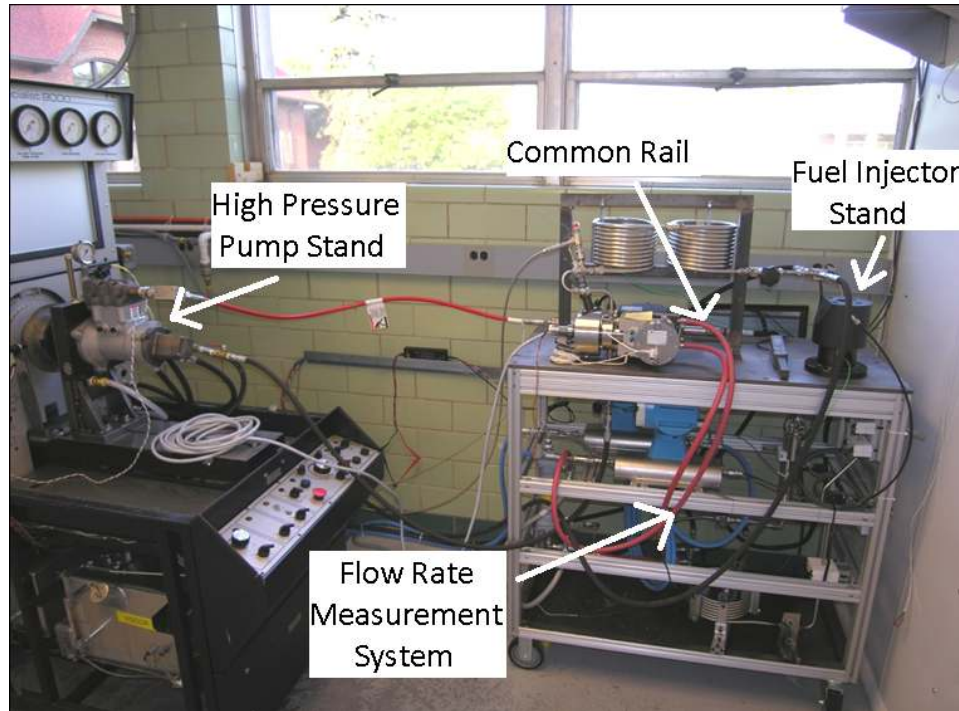


Figure 1.4. Photograph of Off-Engine Injector Experimental Setup

All of these devices, as well as the power supply for the FPGA, are photographed in Fig. 1.5.

1.3.2 CDA and Oil Accumulation Experimental Setup

The experimental setup used in the CDA fired recharge and oil accumulation study is shown in a schematic in Fig. 1.6 and a photograph in Fig. 1.7. The engine used is a 6 cylinder diesel engine with high pressure cooled EGR which is regulated using an electronically-controlled EGR valve, a nozzle-type variable geometry turbocharger (VGT), a charge air cooler, and a common rail fuel injection system. Several nominal parameters of this engine are specified in Table 1.1. The engine lubricating oil used in this engine is Valvoline 15W-40 oil for heavy duty diesel engines, and the age of the engine during the experiments described in this thesis was approximately 2600 hours.

Table 1.1. Nominal engine parameters.

Parameter	Value	Units
No. of Cylinders	6	—
Valves per Cylinder	4	—
Firing Order	1,5,3,6,2,4	—
Maximum Injection Pressure	1800	bar
Bore Diameter	107	mm
Stroke	124	mm
Connecting Rod Length	192	mm
Static Geometric Compression Ratio	17.3	mm
Intake Valve Opening	340 aTDC	CAD
Intake Valve Closing	565 aTDC	CAD
Exhaust Valve Opening	565 aTDC	CAD
Exhaust Valve Closing	380 aTDC	CAD
Exhaust Valve Closing	380 aTDC	CAD
Intake Valve Diameter	29.27	mm
Exhaust Valve Diameter	29.4	mm

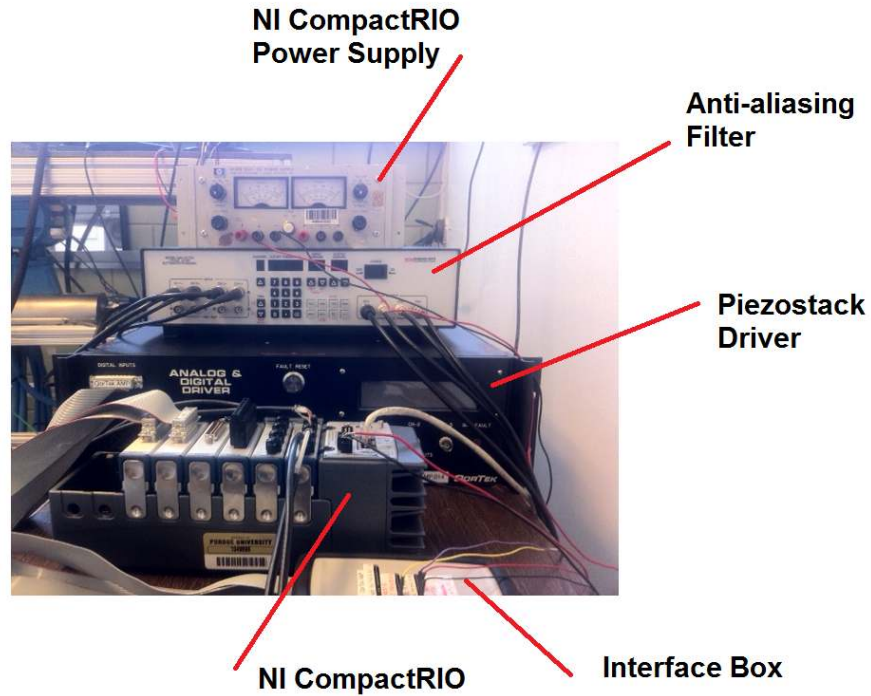


Figure 1.5. Photograph of Off-Engine Injector Control and Measurement Hardware

The most unique feature of this setup is its variable valve actuation (VVA) capability. All six cylinders make use of an electro-hydraulic VVA system which enables cycle-to-cycle control of both intake and exhaust valve events. Specifically, the VVA system can modulate the timings of valve opening and closing, as well as valve lift, ramp rate and velocity. This flexibility is used in this study to disable both the intake and exhaust valves of three of the engine's six cylinders during the transition into CDA mode. Furthermore, the cylinder recharging algorithm presented in this study uses the VVA system to resume normal valve events during a recharge event for a single engine cycle. A schematic diagram of the electro-hydraulic VVA system is shown in Fig. 1.8.

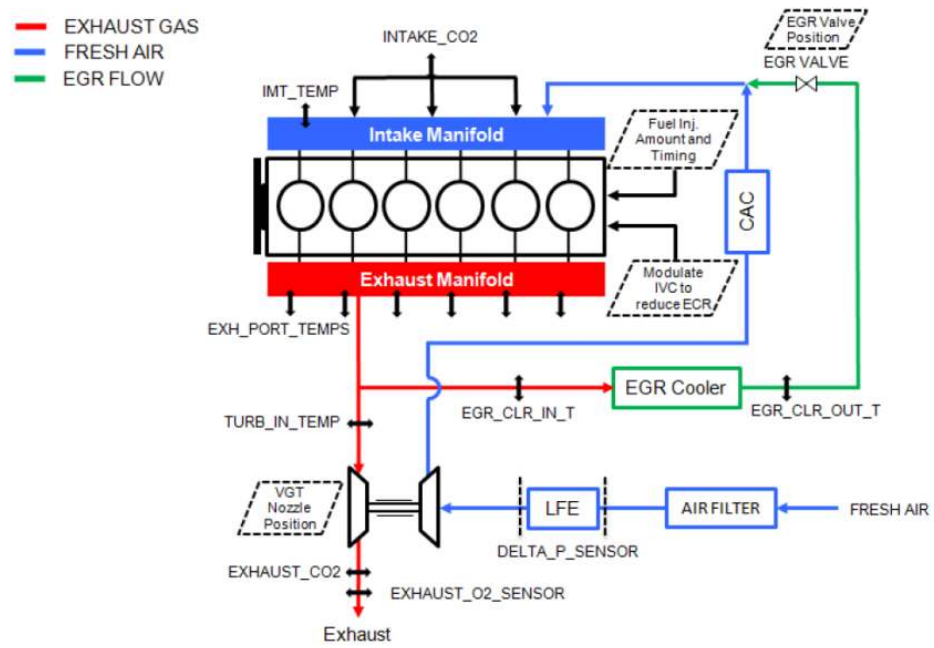


Figure 1.6. Schematic of engine testbed.



Figure 1.7. Experimental testbed with VVA.

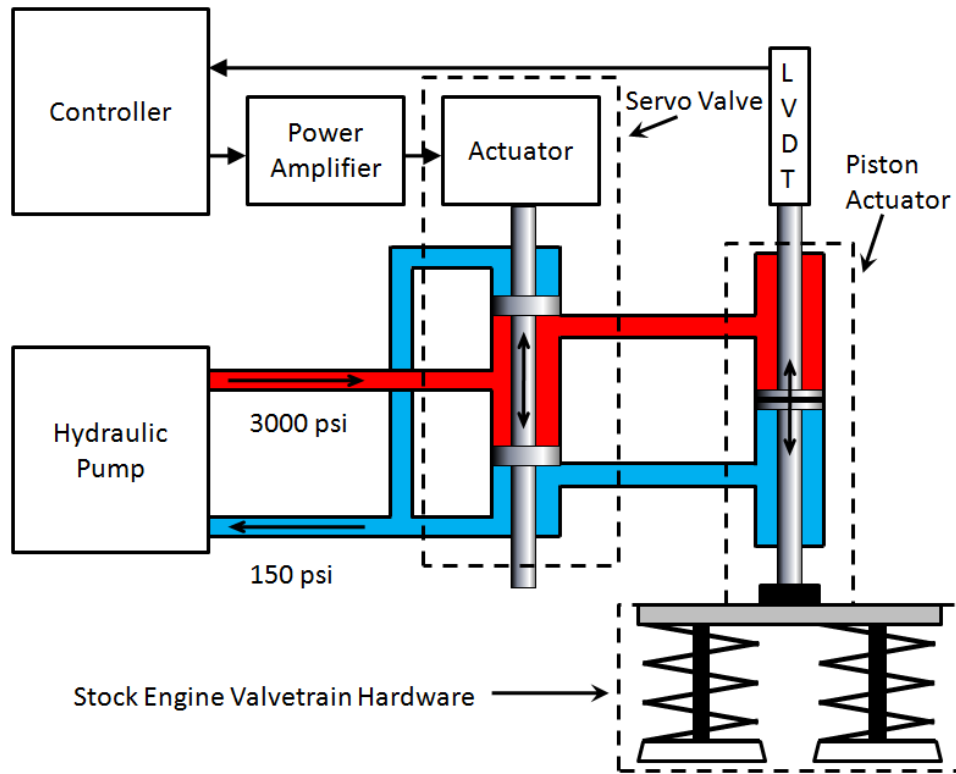


Figure 1.8. Schematic of fully flexible electro-hydraulic VVA actuator.

1.4 Contributions

1.4.1 LabVIEW FPGA Code Optimization

Together with his colleague Dr. Dat Le, the author optimized pre-existing LabVIEW FPGA code in order to fit the closed-loop fuel flow rate controller code onto the FPGA [27,34]. The primary contribution of the author was in the optimization of the subsection of the LabVIEW program that modeled piezostack hysteresis. By converting the pre-existing LabVIEW code into a form that was more FPGA-amenable, the FPGA processing power consumed by the hysteresis portion of the LabVIEW code was significantly reduced. This ultimately freed up enough FPGA resources to enable the closed-loop controller to be implemented and validated. This effort is not described in this thesis, but is described in [27].

1.4.2 Model-Based Estimation of Piezoelectric Fuel Injector Parameters

This effort, led by the author, resulted in an online parameter estimation technique for a piezoelectric fuel injector that is capable of estimating the relationship between the injector's needle seat area vs. needle lift on-engine. While previous efforts by the author's colleagues [24] were made to determine the injector model's parameters using off-engine experiments, this study improves upon those efforts by correcting for parameter error that may be introduced during injector manufacturing and aging. This effort is described in this thesis, and is also outlined in [35].

1.4.3 Oil Accumulation Measurement and Analysis

This study, conducted by the author, assessed the effect of extended periods of CDA-only operation on engine oil accumulation in the deactivated cylinders of a CI engine operating in CDA mode. A heat-release-based analysis was used to quantify the mass of accumulated oil, and experiments are conducted at various engine speeds, loads, and recharge intervals. This study is presented in this thesis.

1.4.4 First-Fire Readiness Analysis

This study, conducted by the author, characterized first-fire readiness in CI engines utilizing CDA. The heat release rate during combustion was used to study first-fire readiness, and test plans were developed and executed at various engine speeds, loads, and recharge intervals. The results of this study are presented in this thesis.

1.4.5 Fired Recharge Algorithm Development and Validation for a Diesel Engine Utilizing CDA

Conducted by the author, this effort involved the implementation of a fired recharge algorithm for a diesel engine utilizing CDA. When the engine is operating in CDA mode, this algorithm reactivates each deactivated cylinder for a single engine cycle

at user-specified intervals of time. Additional effort was made to maintain a constant brake torque during the fired recharge. Using SIMULINK software, this algorithm was implemented on DSpace hardware and validated at different engine speed and load conditions. The results of this effort and its validation are presented in this thesis.

CHAPTER 2: MODEL-BASED ESTIMATION OF PIEZOELECTRIC FUEL INJECTOR PARAMETERS

This Chapter presents the model-based parameter estimation strategy that was developed for a piezoelectric fuel injector.

2.1 Injector System and Parameters of Interest

In this section, the piezoelectric injector system will be briefly illustrated and the parameters in need of online estimation will be described.

2.1.1 Injector System

A schematic diagram of the piezoelectric fuel injector used in this study is shown in Fig. 2.1. In this type of injector, the piezostack serves as the actuator which expands when a voltage V_s is supplied by the driver. When V_s is positive, the piezostack expands and exerts a downward force on the upper plunger. Through the action of the hydraulic circuit created by the body, control, and trapped volumes, the needle is ultimately lifted. This opens the nozzle, causing fuel to flow out of the injector. In order to close the nozzle and stop fuel flow at the end of an injection event, V_s is reduced to 0, the piezostack contracts, and the springs $s_1 - s_5$ force the plungers and needle to return to their initial positions.

An expanded view of the injector's needle seat is shown in Fig. 2.2, where R_{need} is the resistance of the needle seat, R_{sh} is the resistance of the spray holes, A_2 is area of the spray holes, ρ is the density of the fuel in the injector, and P_{bv} , P_{sac} , and P_{cyl} are the pressures in the body volume, sac volume, and cylinder, respectively. In the expanded view of the needle seat it is apparent that as the needle lift (x_2) increases, the effective area of the needle seat (A_1) increases. The exact relationship

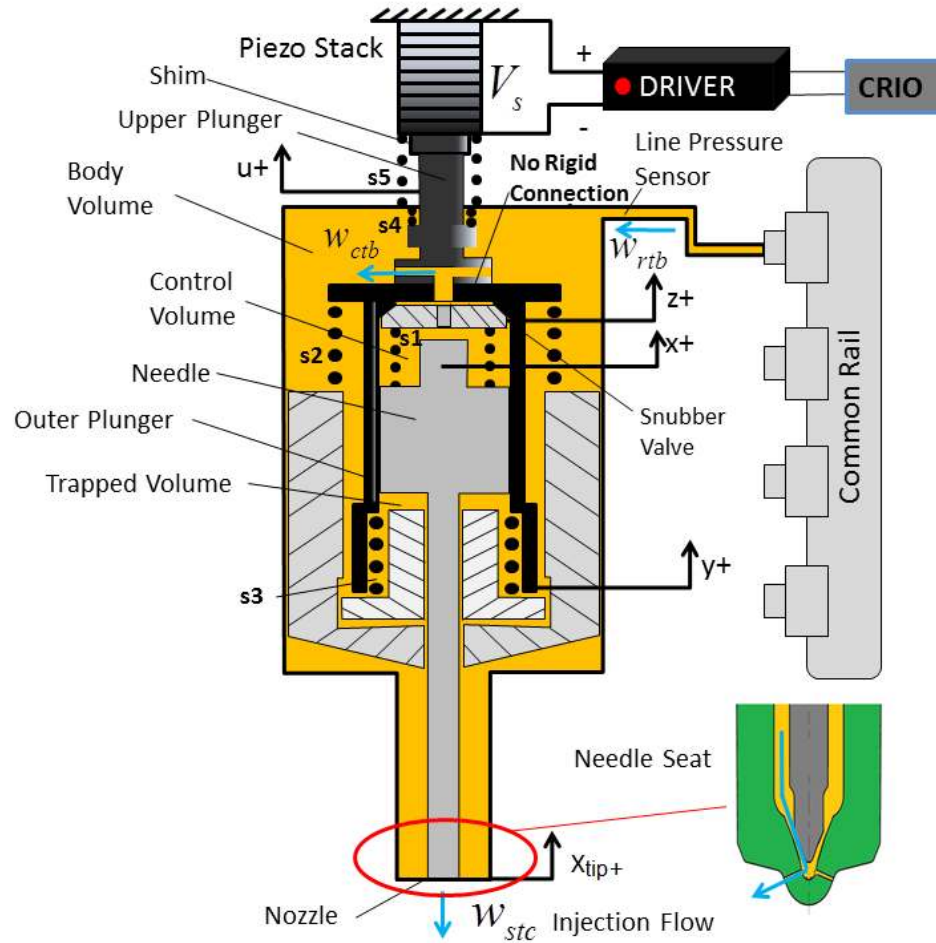


Figure 2.1. Piezoelectric Fuel Injector Schematic Diagram

between A_1 and x_2 is expected to vary from injector-to-injector due to manufacturing differences. Additionally, $A_1(x_2)$ may change over the life of an injector if the needle incurs cavitation damage as it ages.

In [24], $A_1(x_2)$ was determined by performing a series of experiments on a single injector. These experiments were conducted in an off-engine injector test rig (where a measurement of output fuel injection mass flow rate is available), and the resulting $A_1(x_2) = A_{1,0}$ curve was assumed to be accurate for all injectors. Since A_1 essentially quantifies how open or closed the nozzle is, it plays a critical role in determining the flow rate of fuel spraying out of the injector (especially during the toe, when the

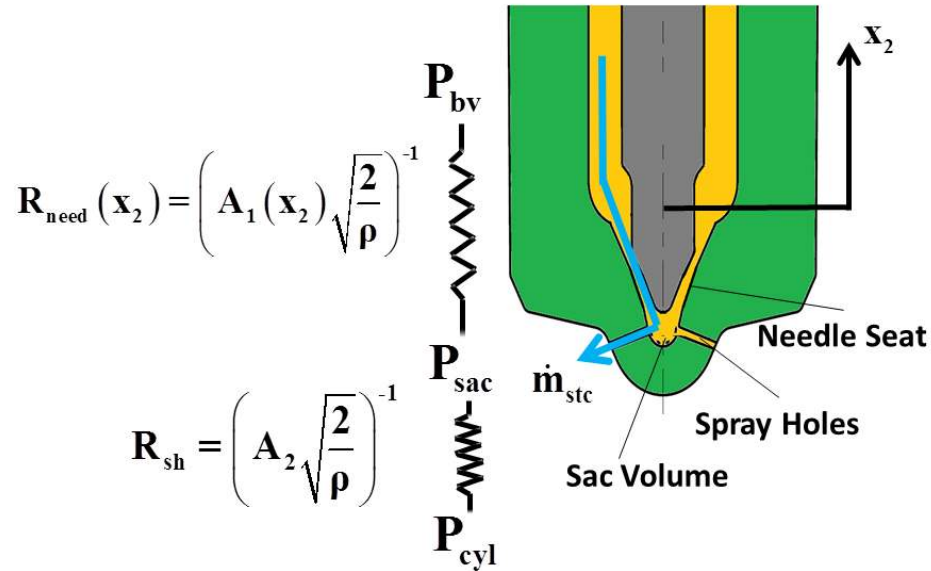


Figure 2.2. Expanded view of injector needle seat

model is particularly sensitive [24]). As such, it would be beneficial to determine the $A_1(x_2)$ relationship for any given injector on-engine (where no measurement of output fuel injection flow rate is available).

Other parameters that are expected to vary on an injector-to-injector basis are piezostack properties (which could also vary over the life of an injector) and various leakage rates of fuel between volumes inside the injector. While these parameters are undoubtedly important for model accuracy, this thesis will focus only on the online estimation of the needle seat area $A_1(x_2)$.

2.1.2 Available Measurements

Before proceeding with the parameter estimation strategy, the measurements that are available on-engine will be outlined here. The stack voltage V_s , line pressure P_{line} (used as a proxy for the body pressure), and total injected fuel per injection event are measurable on-engine. Additionally, the instantaneous fuel flow rate w_{stc} is

measurable in the injector test rig at Purdue, but is useful only for model validation purposes. With this in mind, the state estimator in [26] was used to provide virtual measurements of all the states as well as output fuel flow rate w_{stc} . The lack of true measurements available on-engine makes control design and parameter estimation particularly difficult, as demonstrated later in this Chapter.

2.2 Parameter Estimation

The estimation of parameters for the dynamic system that describes the piezoelectric fuel injector is made extremely difficult by the lack of measurements that are available. Since many traditional parameter estimation techniques such as the recursive least squares (RLS) algorithm and model reference adaptive control (MRAC) rely on input and output measurements, using them to estimate $A_1(x_2)$ is not straightforward. Furthermore, $A_1(x_2)$ is not a constant parameter since it is a function of the state x_2 , whose values range from zero to saturation over the course of a single boot-shaped injection event. The parameter estimation strategy used to estimate $A_1(x_2)$ was designed with two “tools” in mind: the total injected fuel per cycle measurement, and the state estimator from [26]. The complete strategy is illustrated in Fig. 2.3, and each block therein will be described individually.

2.2.1 Injector Simulation Model

The dynamic injector model described and validated in [24] was used in the “Injector Simulation Model” block to simulate a real injector. This model contains eleven states and its outputs to the rest of the strategy are the total injected fuel per injection and the body pressure (which would be referred to as the line pressure on a real injector).

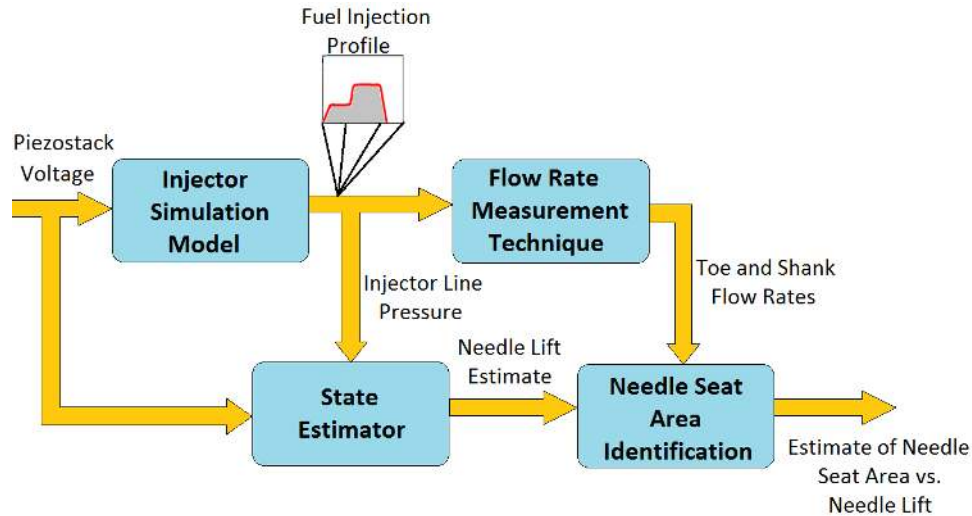


Figure 2.3. Parameter Estimation Strategy

2.2.2 State Estimator

The state estimator, previously designed in [26], is used here to provide an estimate of the needle lift x_2 . The estimator is based on a simplified version of the injector simulation model in [24], and contains six states as well as simplifying assumptions about the bulk modulus and density of the fuel in the injector.

2.2.3 Flow Rate Measurement Technique

This block accepts the total injected fuel per injection as input. On-engine, the total injected fuel is calculated by some pre-existing estimation algorithm while in simulation it is calculated by integrating the output fuel flow rate over the course of an injection. In order to use this input to calculate the average flow rates during the toe and shank of a boot-shaped injection, a few assumptions are required.

Fig. 2.4 illustrates the quantities that must be known in order to calculate the toe and shank average flow rates for a given injection. The total injected fuel measurement ($Area_{total}$) is the sum of the blue and green areas ($Area_{toe}$ and $Area_{shank}$, respectively)

in Fig. 2.4. The first assumption is that the blue and green areas are rectangular. In reality this is not the case, but the sloped parts of the injection (e.g. between the toe and shank) are steep enough to justify this assumption. Assuming rectangular

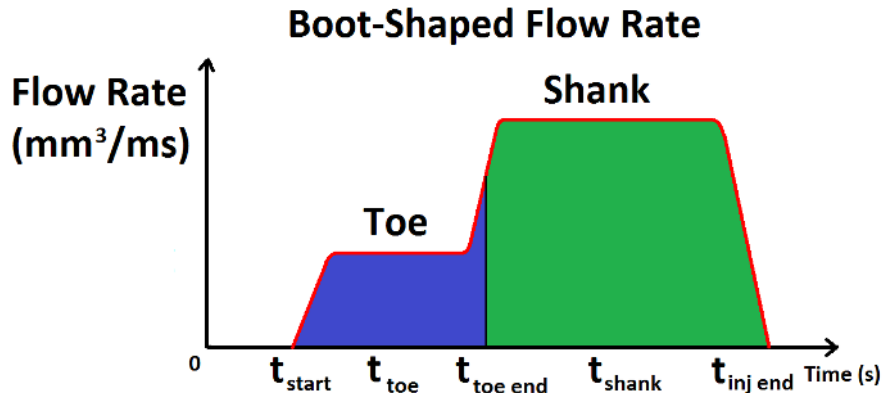


Figure 2.4. Flow Rate Measurement Technique

blue and green areas, all that must be known in order to calculate toe and shank flow rates are the injection start time, toe end time, and injection end time. These are assumed to coincide with the corresponding times in the stack voltage profile, which is measurable. The final assumption that must be made is that the shank represents a state of flow saturation. Thus, for a given rail pressure, the shank flow (w_{shank}) is assumed to be constant. In this fashion, w_{shank} is not actually “calculated.” Rather, its value is assumed based on the commanded rail pressure for a given injection event.

According to the above assumptions, the following quantities are considered known in the “Flow Rate Measurement Technique” block of Fig. 2.3: t_{start} , t_{toeend} , t_{injend} , w_{shank} , and $Area_{shank}$. Using these quantities, the toe flow rate (w_{toe}) is calculated as

$$w_{toe} = (Area_{total} - Area_{shank}) / (t_{toeend} - t_{start}) \quad (2.1)$$

where

$$Area_{shank} = w_{shank}(t_{injend} - t_{toeend}) \quad (2.2)$$

The two other times labeled in Fig. 2.4, t_{toe} and t_{shank} , must be calculated and fed into the state estimator so that the appropriate values for needle lift are given to the “Needle Seat Area Identification” block in Fig. 2.3. t_{toe} and t_{shank} are calculated as

$$t_{toe} = (t_{start} + t_{toeend})/2 \quad (2.3)$$

and

$$t_{shank} = (t_{toeend} + t_{injend})/2 \quad (2.4)$$

The estimates of x_2 at t_{toe} and t_{shank} are used in the estimation of the needle seat area.

The piezostack voltage for a typical boot-shaped injection is shown in Fig. 2.5 with the vertical lines illustrating the times t_{start} , t_{toe} , t_{toeend} , t_{shank} , and t_{injend} . The corresponding flow rate predicted by the simulation model is shown in Fig. 2.6, with the same times shown by vertical lines and the calculated average flow rates shown by horizontal lines. The assumptions made by this measurement technique significantly impact the accuracy of the w_{toe} calculation, and this will be addressed later in the thesis.

2.2.4 Needle Seat Area Identification

In this block, the output equation of the injector model

$$w_{stc} = \frac{A_1(x_2)A_2}{\rho_{cyl}} \sqrt{\frac{2\rho(P_{bv} - P_{cyl})}{A_1^2(x_2) + A_2^2}} \quad (2.5)$$

is used to calculate the values of A_1 during the toe and shank since all other variables are known. Specifically, the needle position, x_2 , during the steady state toe and shank

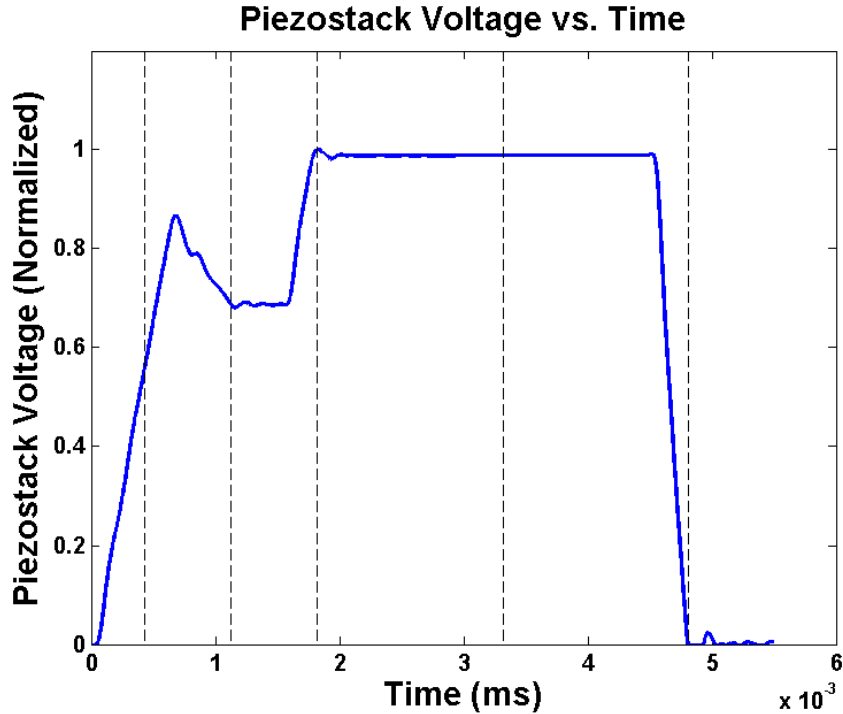


Figure 2.5. Piezostack Voltage for Typical Boot-Shaped Injection

portions of the boot profile are estimated by the state estimator, as shown in Fig. 2.3. Rearranging Eqn. (2.5) gives

$$A_1(x_2) = \left(\frac{2\rho(P_{bw} - P_{cyl})}{w_{stc}^2 \rho_{cyl}^2} - \frac{1}{A_2^2} \right)^{-1/2} \quad (2.6)$$

By substituting w_{toe} and w_{shank} into Eqn. (2.6) for w_{stc} , two values of $A_1(x_2)$ are estimated per injection. In other words, for a variety of boot-shaped injections with different toe heights and rail pressures, a variety of x_2 and A_1 combinations can be determined, enabling an estimation of A_1 as a function of x_2 . As the engine continues to run, the accuracy of the $A_1(x_2)$ estimate ideally improves.

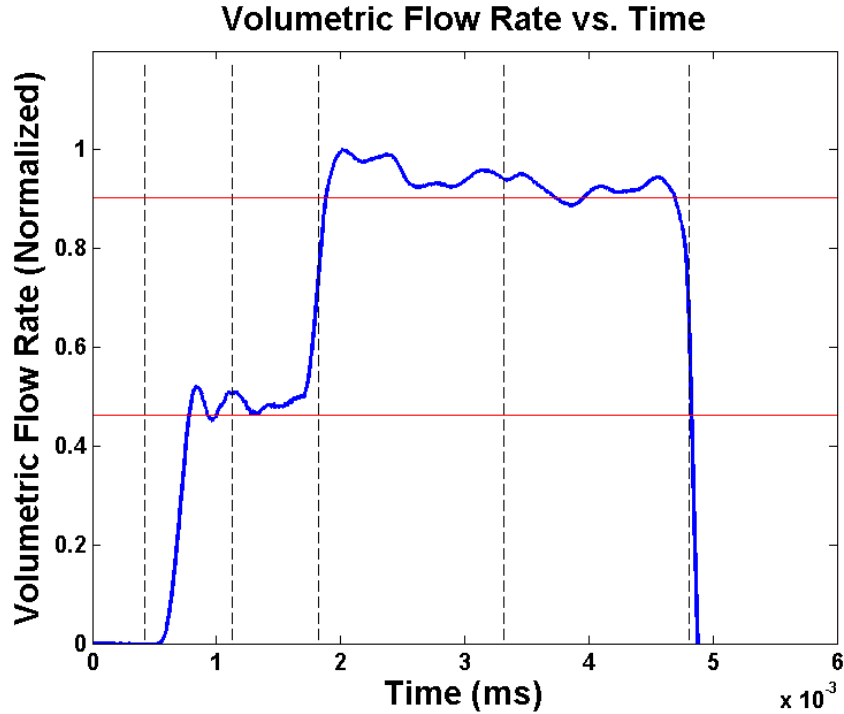


Figure 2.6. Flow Rate for Typical Boot-Shaped Injection

2.3 Simulation Results

In this section, the parameter estimation strategy will be validated and it will be demonstrated that using the estimated needle seat effective area vs. needle lift values in the state estimator improves estimates of fuel flow rate.

2.3.1 Parameter Estimation Simulation

The validation of this parameter estimation strategy involves demonstrating that the estimated $A_1(x_2)$ values, $\hat{A}_1(x_2)$, obtained on a cycle-to-cycle basis are close to those used in the injector simulation model (i.e. the “truth reference,” per Fig. 2.3). Accordingly, the following simulation approach was used. In the injector simulation model, $A_1(x_2)$ was set equal to $A_{1,0}$. Thus, $A_{1,0}$ becomes the “true” relationship $A_1(x_2)$ in these simulations, and it will henceforth be referred to as $A_{1,true}$. In the

estimator, some initial choice of $A_{1,estimator}$ must be used. For the sake of simplicity, $A_{1,estimator}$ is chosen to be

$$A_{1,estimator} = \alpha A_{1,true} \quad (2.7)$$

where α is a positive constant. Whether or not Eqn. (2.7) actually represents the way in which $A_1(x_2)$ varies from injector-to-injector is unknown, but this choice remains useful for simulation purposes.

Simulating fifteen boot-shaped injection events of varying toe heights and rail pressures yields the results shown in Figs. 2.7 and 2.8 for $\alpha = 0.75$ and $\alpha = 1.25$, respectively.

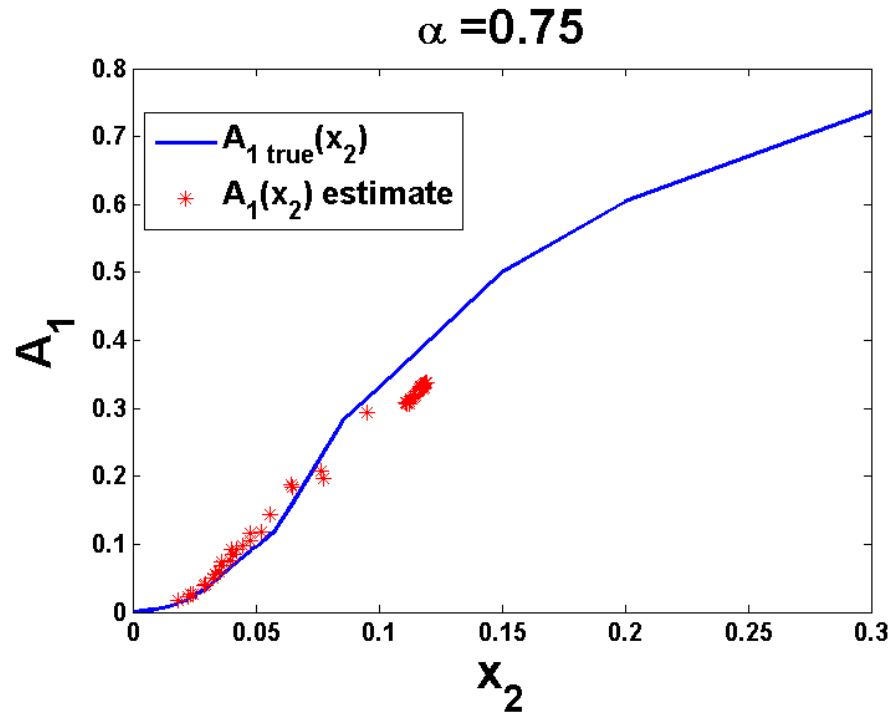


Figure 2.7. Parameter Estimator Simulation Results for $\alpha = 0.75$

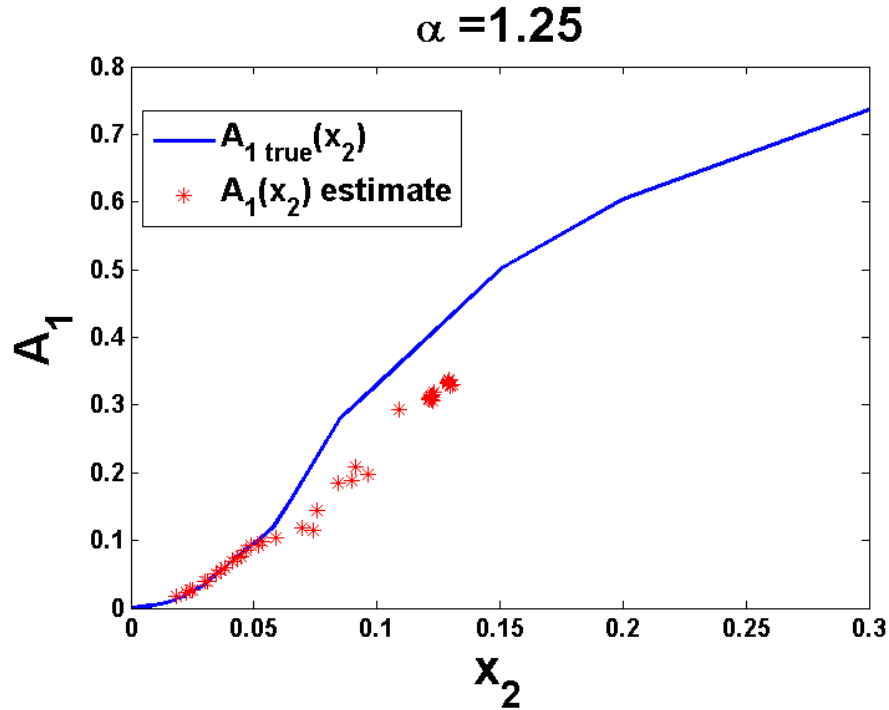


Figure 2.8. Parameter Estimator Simulation Results for $\alpha = 1.25$

2.3.2 State Estimator Simulation

The ultimate goal of this parameter estimation strategy is to use the estimate $\hat{A}_1(x_2)$ to improve the accuracy of the state estimator flow rate prediction [26]. Ideally, a new value of $\hat{A}_1(x_2)$ is available after every boot-shaped injection event. As such, some parameter update law that determines how to most effectively utilize new data points in the state estimator should be designed. However, the design of such an update law is out of the scope of this paper. What will be shown is the effect of simply replacing the data points used in $A_{1,estimator}$ with those obtained after the fifteen boot-shaped injection events used to obtain the $\hat{A}_1(x_2)$ values shown in Figs. 2.7 and 2.8. In other words, $\alpha A_{1,true}$ is replaced by the red points in Figs. 2.7 and 2.8 after fifteen injections.

Using this very simple parameter update strategy, the state estimator is simulated. Simulation results for boot-shaped injections of varying toe heights and α values are shown in Figs. 2.9 - 2.12

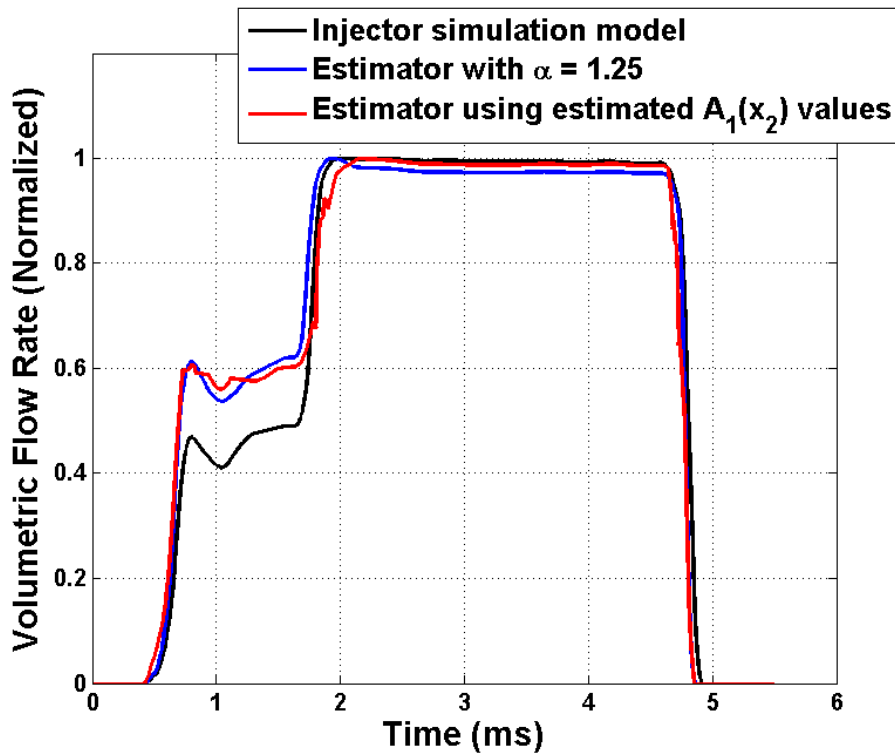


Figure 2.9. State Estimator Simulation Results for $\alpha = 1.25$, 40% Toe Height

In Figs. 2.9 - 2.12, the black lines represent the output fuel flow rate of the injector simulation model (the “truth reference”). This is the flow rate that the state estimator strives to reproduce. The blue lines represent the output fuel flow rate of the state estimator while using an erroneous initial “guess” of $A_1(x_2)$, of the form in Eqn. (2.7). The red lines represent the performance of the estimator after $A_{1,estimator}$ has been updated with the red points obtained from fifteen boot-shaped injections. For example, in Fig. 2.10 the initial guess for $A_{1,estimator}$ was

$$A_{1,estimator} = 1.25A_{1,true} \quad (2.8)$$

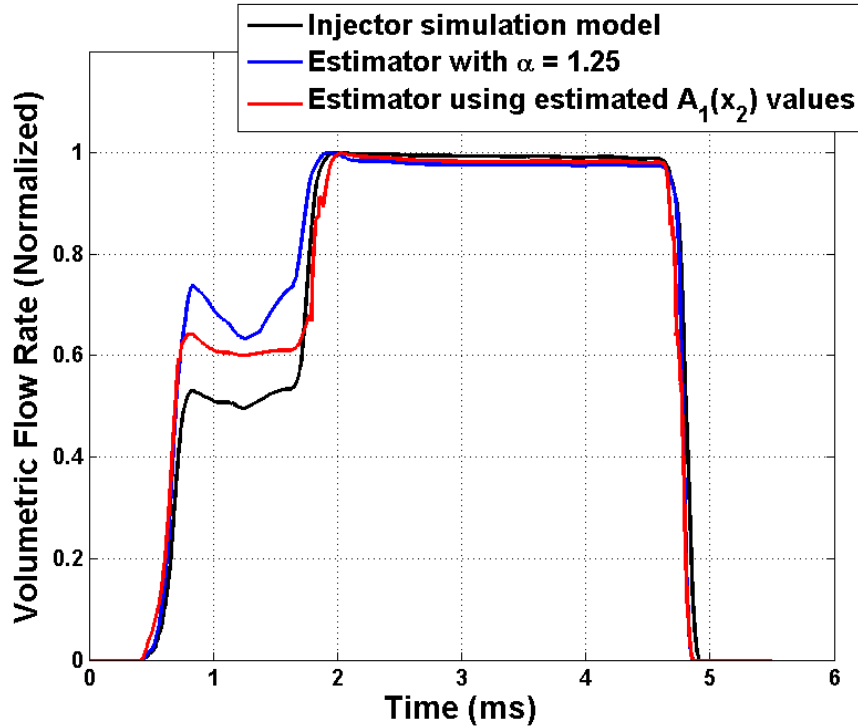


Figure 2.10. State Estimator Simulation Results for $\alpha = 1.25$, 50% Toe Height

After fifteen injections, this initial guess of $1.25A_{1,true}$ was completely replaced by the red points from Fig. 2.8. This resulted in the improved estimator performance that is visually apparent in Fig. 2.10.

In order to quantify this improvement in state estimator performance, the percent error in the total injected fueling quantity predicted by the injector simulation model and the state estimator both before and after updating $A_{1,estimator}$ was calculated. Table 2.1 shows these percent error values. The fueling quantities in this table were calculated by simply integrating the volumetric flow rate curves shown in Figs. 2.9 - 2.12 (results for flow rates not shown here were also included in the table), with the end of the toe said to be the time at which the normalized flow rate reached half-way between the nominal toe and shank flow rate.

Table 2.1. Injected Fuel Quantity Error

Injection Profile	Before/After Parameter Update	Toe Fueling Quantity Error (%)	Total Fueling Quantity Error (%)
$\alpha = 1.25$, 50% TH	Before	26.63	9.25
$\alpha = 1.25$, 50% TH	After	25.41	0.26
$\alpha = 0.75$, 50% TH	Before	22.76	15.35
$\alpha = 0.75$, 50% TH	After	9.15	17.07
$\alpha = 1.25$, 40% TH	Before	28.73	8.53
$\alpha = 1.25$, 40% TH	After	34.62	1.43
$\alpha = 0.75$, 40% TH	Before	23.30	14.96
$\alpha = 0.75$, 40% TH	After	8.60	16.72
$\alpha = 1.25$, 30% TH	Before	38.78	9.04
$\alpha = 1.25$, 30% TH	After	40.72	2.36
$\alpha = 0.75$, 30% TH	Before	21.33	14.18
$\alpha = 0.75$, 30% TH	After	1.94	16.00
$\alpha = 1.25$, 20% TH	Before	52.68	9.45
$\alpha = 1.25$, 20% TH	After	60.71	3.08
$\alpha = 0.75$, 20% TH	Before	10.27	12.20
$\alpha = 0.75$, 20% TH	After	5.80	15.72

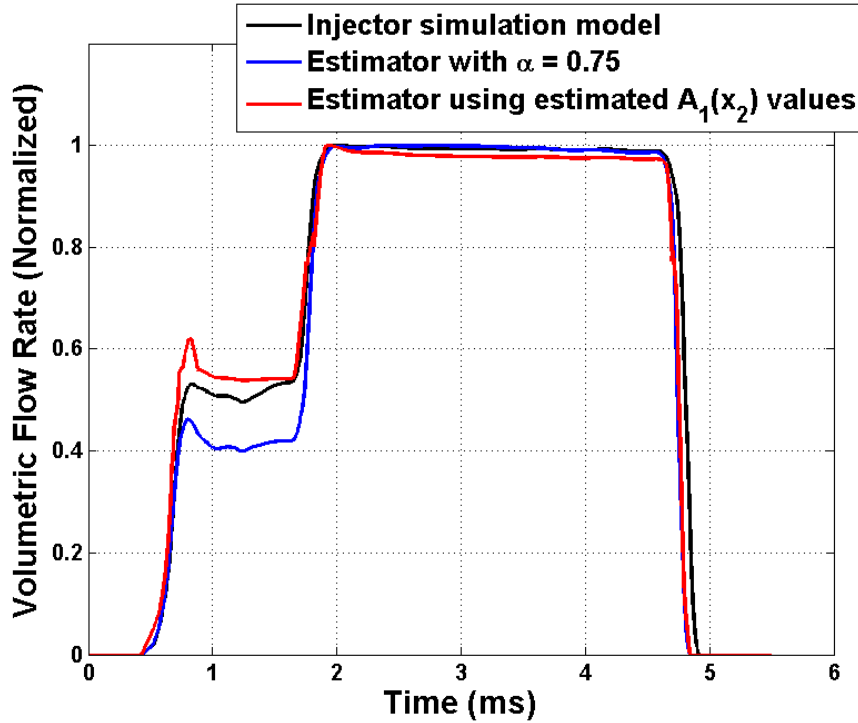


Figure 2.11. State Estimator Simulation Results for $\alpha = 0.75$, 50% Toe Height

According to Table 2.1, the parameter estimation strategy outlined in this paper largely resulted in improvement in the toe fueling quantity prediction (where the model is most sensitive) after $A_{1,estimator}$ was updated. However, there are a few cases in which this is not reflected in Table 2.1. Fig. 2.9 is an example of an injection profile that was not improved by a parameter update. Exactly why this is the case is unknown, but the parameter estimation strategy in this paper generally seemed to be more effected for initial errors in $A_{1,estimator}$ that were below its true value.

The error in the total injected fuel prediction also improved after the parameter update for the profiles in which $\alpha = 1.25$, but was actually made slightly worse for the $\alpha = 0.75$ profiles. Visually inspecting Figs. 2.9 - 2.12, it is clear that the flow rate from the simulation model “truth reference” (the black line) takes slightly more time to reach zero at the end of injection than do both of the estimated flow rates.

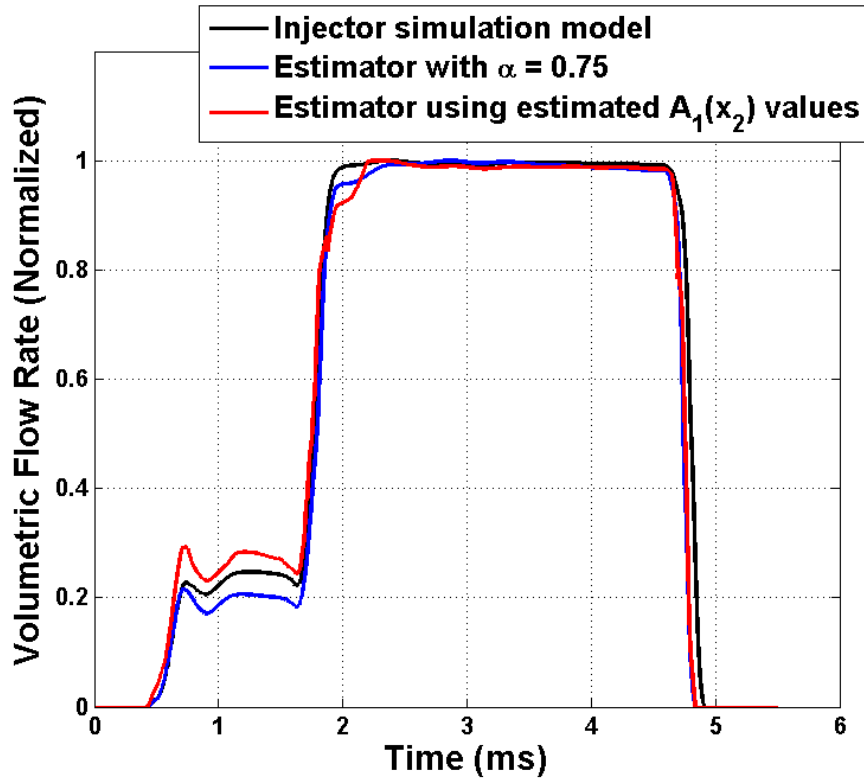


Figure 2.12. State Estimator Simulation Results for $\alpha = 0.75$, 20% Toe Height

This could influence the error in total injected fueling quantity that is apparent in Table 2.1.

2.4 Discussion and Conclusion

Figs. 2.7 and 2.8 demonstrate that $\hat{A}_1(x_2)$ lies near $A_{1,true}$. There are two main issues with this estimation strategy that need to be addressed. First, the accuracy of toe and shank flow rate measurements that are provided on a cycle-to-cycle basis by the “Flow Rate Measurement Technique” block depends very strongly on the assumptions made about saturation flow rate during the shank and the start and end times of the toe duration. Second, while the state estimator was experimentally validated in [26], the $A_1(x_2)$ used therein was one that was determined using off-

engine experiments. Thus, the x_2 estimate supplied by the state estimator must at least initially be assumed to contain some error since it is being calculated using presumably inaccurate values of $A_1(x_2)$.

The first issue can be dealt with in a relatively straightforward manner. Improving the confidence with which the measurement technique's assumptions are made would improve the technique's accuracy. The second issue is somewhat more difficult. *A priori*, there is no guarantee that $\hat{A}_1(x_2)$ will converge to its true value when the initial value of $A_1(x_2)$ used in the estimator contains some error. However, results in section 2.3.1 illustrate that this parameter estimation strategy is reasonably accurate.

The results in section 2.3.2 demonstrate that the parameter estimator in this paper results in improved state estimator performance, especially for initial guesses of $A_{1,estimator}$ in which $\alpha = 1.25$. Perhaps most importantly, the prediction of the fuel flow rate during the toe exhibited improvement in most cases after the parameter update, even though the toe is when the injector model is most sensitive.

2.5 Summary

The effort in this Chapter resulted in a parameter estimation strategy that improved the model-based estimate of the injector's output fuel flow rate in the presence of initial parameter error.

1. The parameter of interest is the needle seat area as a function of needle lift ($A_1(x_2)$)
2. This parameter is expected to vary from injector-to-injector due to imperfections introduced in the injector manufacturing process.
3. This parameter is also expected to vary over the life of an injector due to cavitation damage.

4. Using the state estimator in [26] and an estimate of total injected fuel per cycle, the injector model's output equation is used to yield an online estimate of $A_1(x_2)$.
5. In the presence of a 25% initial error in $A_1(x_2)$, the parameter estimator improves the fuel flow rate estimate by approximately 10% after the injector has operated for several injection events.

CHAPTER 3: OIL ACCUMULATION MEASUREMENT AND ANALYSIS

This Chapter presents a technique to analyze the amount of engine lubricating oil that has accumulated in deactivated cylinders during prolonged CDA engine operation. While no direct measurement of in-cylinder oil accumulation is available, a heat-release-based analysis is presented which uses the total heat released during a combustion event, combined with the lower heating value of engine oil, to calculate a mass of accumulated oil burned after the engine transitions from CDA to six cylinder mode. Oil accumulation is studied experimentally for varying lengths of time spent in CDA mode. This Chapter concludes with accumulated oil mass values, which show that accumulated oil mass generally increased as the duration of CDA operation increased, although a few cylinder-to-cylinder and day-to-day variations were also observed.

3.1 Heat-Release-Based Analysis of Oil Accumulation

In this study, engine oil accumulation in deactivated cylinders is studied by performing experiments with varying lengths of CDA operation (henceforth referred to as “CDA time”). In this analysis, CDA mode always refers to valve motion and fuel injection deactivation for three of the engine’s six cylinders. Two combinations of cylinders are deactivated in this analysis: 1, 2, and 3 or 4, 5, and 6. These combinations are chosen due to the cylinder firing order, and this CDA strategy cuts the total engine displacement in half. Engine lubricating oil is expected to accumulate in deactivated cylinders because of the low in-cylinder pressures that occur after long periods of deactivation. These low pressures enable the transport of engine oil from the crankcase into the combustion chambers via the imperfect seal created by the piston rings. It is expected that longer CDA times yield more oil accumulation, and this

is what the results generally demonstrate. By analyzing heat release data during the transition from CDA to six cylinder mode, an analytical method was developed which allows for the calculation of the mass of oil that burned in each newly reactivated cylinder.

It was assumed that any deviation in a cylinder's heat release from its normal value immediately following the transition to six cylinder mode is due entirely to the combustion of accumulated oil. Thus, the oil mass values presented in this Chapter represent lower bounds on accumulated oil mass since it is possible that some portion of the oil and fuel mixture does not completely burn after resuming six cylinder mode. Fig. 3.1 illustrates this idea for 0.5, 5, 10, and 20 minute CDA times. As shown in this figure, the cumulative heat release following the transition to six cylinder mode differs from an active cylinder's heat release as CDA time increases to 20 minutes. The grey line represents cylinder 1's heat release while it is active, and this is assumed to represent its heat release in the presence of no oil accumulation.

The fundamental equation that describes the combustion of accumulated oil and injected fuel is

$$\int \frac{dQ_{gross}}{d\theta} d\theta = Q_{gross} = m_{fuel}LHV_{fuel} + m_{oil}LHV_{oil} \quad (3.1)$$

where $dQ_{gross}/d\theta$ is the gross heat release rate, Q_{gross} is the cumulative gross heat release, m_{fuel} and m_{oil} are the masses of fuel and oil combusted after the transition to six cylinder mode, LHV_{fuel} and LHV_{oil} are the lower heating values of diesel fuel and engine lubricating oil, respectively, and θ is the cylinder's crank angle degree. The diesel fuel used in this study has a lower heating value of $LHV_{fuel} = 42.965$ MJ/kg. While the exact lower heating value of the engine oil used in this study is not known, it can be approximated as $LHV_{oil} = 40.2$ MJ/kg, [36]. The gross heat release rate is calculated as

$$\frac{dQ_{gross}}{d\theta} = \frac{dQ_{net}}{d\theta} + \frac{dQ_{wall}}{d\theta} \quad (3.2)$$

where $dQ_{net}/d\theta$ is the net heat release rate and $dQ_{wall}/d\theta$ is the rate of heat transfer through the cylinder walls. In the literature, all three of these heat release rates are

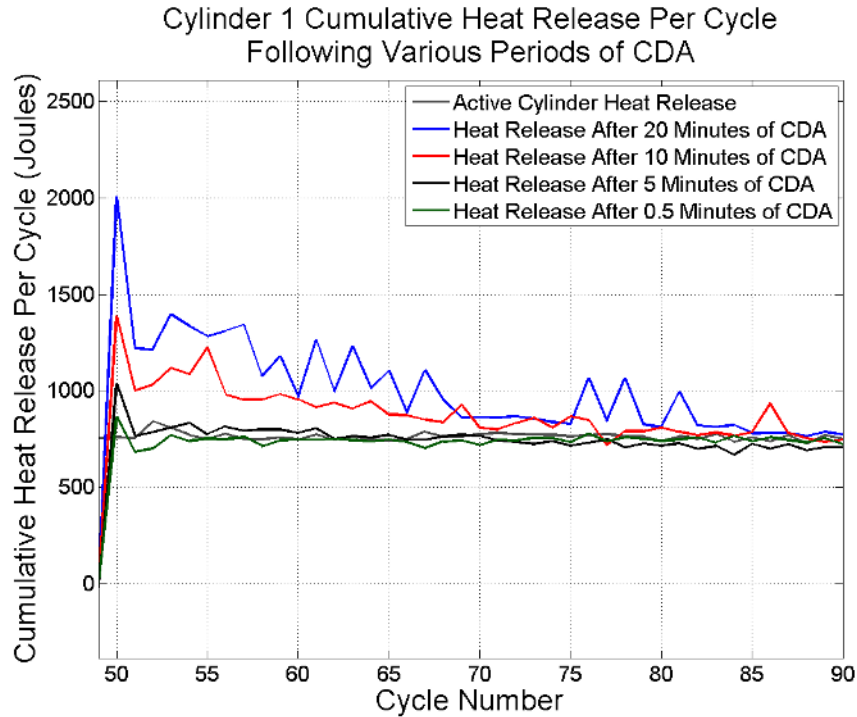


Figure 3.1. Cumulative heat release in cylinder 1 for 0.5, 5, 10, and 20 minute CDA times. Active cylinder cumulative heat release shown for comparison.

often referred to as “apparent,” but that is only because they are based on in-cylinder pressure measurements as opposed to some other measurement of energy transfer. In this analysis, the term “apparent” will be omitted with regards to these three heat release rates for the sake of brevity.

The cumulative heat releases shown in Fig. 3.1 take into account the effects of both the energy transfer to the piston and the heat transfer between the contents of the cylinder and the cylinder walls. In these cumulative heat release calculations, a cylinder-pressure-based model of the heat transfer rate, $dQ_{wall}/d\theta$ must be used in order to accurately calculate m_{oil} .

The equation used to calculate the rate of heat transfer through the cylinder walls is

$$\frac{dQ_{wall}}{d\theta} = A(\theta)h(\theta)(T - T_{wall}) \quad (3.3)$$

where $A(\theta)$ is the inside surface area of the cylinder as a function of crank angle, $h(\theta)$ is the instantaneous heat transfer coefficient, T is the bulk temperature of the contents of the cylinder, and T_{wall} is the temperature of the cylinder walls. In this study, Heywood's approximation [37] for cylinder surface area is used:

$$A(\theta) = \frac{\pi B^2}{2} + \frac{\pi B L_{stroke}}{2} [r + 1 - \cos(\theta) - (r^2 - \sin^2(\theta))^{1/2}] \quad (3.4)$$

where B is the cylinder bore in meters, L_{stroke} is the piston stroke length in meters, and r is the connecting rod length in meters. The cylinder wall temperature is taken to be the mean of the engine coolant temperature and the exhaust manifold temperature [38]. The bulk temperature of the cylinder contents, T , is calculated using the idea gas law. Finally, the instantaneous heat transfer coefficient, $h(\theta)$, is calculated using the Woschni model [39]:

$$h(\theta) = \beta B^{-0.2} P(\theta)^{0.8} T(\theta)^{-0.55} w(\theta)^{0.8} \quad (3.5)$$

where B is the cylinder bore in meters, $P(\theta)$ is the in-cylinder pressure in kPa, $T(\theta)$ is the in-cylinder temperature in Kelvin, $w(\theta)$ is the average in-cylinder gas velocity, and β is a tunable parameter used to match this coefficient to a specific engine geometry. The in-cylinder gas velocity, $w(\theta)$, is defined as

$$w(\theta) = c_1 \bar{s}_p + c_2 \frac{V_d T_r}{P_r V_r} (P - P_{mot}) \quad (3.6)$$

where P_{mot} is the motored cylinder pressure, defined as

$$P_{mot} = P_r \left(\frac{V_r}{V} \right)^\gamma \quad (3.7)$$

γ in Eqn. (3.7) is the specific heats ratio. In Eqn. (3.6), \bar{s}_p is the mean piston speed in meters per second and T_r , P_r , and V_r are the temperature, pressure, and volume

of the cylinder at some reference condition (intake valve closing in this case). Finally, the constants c_1 and c_2 depend on which stroke the cylinder is experiencing. Since combustion happens during the closed portion of the engine cycle [37],

$$c_1 = 2.28 \quad (3.8)$$

and

$$c_2 = 3.24 \times 10^{-3} \quad (3.9)$$

Both of the terms on the right-hand-side of Eqn. (3.2) can be calculated based on in-cylinder pressure measurements. $dQ_{net}/d\theta$ is automatically calculated using AVL Indicom combustion analysis software every time engine data is collected, and $dQ_{wall}/d\theta$ is calculated according to the Woschni correlation. $dQ_{gross}/d\theta$ is then sum of these two terms. For a fired recharge in cylinder 6, all three heat release rate terms are plotted in Fig. 3.2.

Now that dQ_{gross} can be calculated, the tunable constant β in Eqn. (3.5) must be calculated for each cylinder. This is done by calculating dQ_{gross} for cases in which it is assumed that no oil has accumulated in-cylinder (i.e. a cylinder that has been active for a long time), and then calculating an amount of fuel burned during combustion using Eqn. (3.1). Rearranging Eqn. (3.1) and solving for m_{fuel} in the case of $m_{oil} = 0$ gives

$$m_{fuel} = \frac{Q_{gross}}{LHV_{fuel}} \quad (3.10)$$

Values of m_{fuel} calculated according to Eqn. (3.10) can be compared to the ECM total fueling command as well as the total fuel injected per cycle calculated by the fuel scale in the test cell. While the fuel scale reading cannot be used to measure the total fuel injected during a fired recharge due to the long time required to take a fuel reading, the ECM total fueling command can be compared to the m_{fuel} values calculated according to Eqn. (3.10). Averaging m_{fuel} calculations for many engine cycles and comparing with the ECM total fueling command, values of the tunable

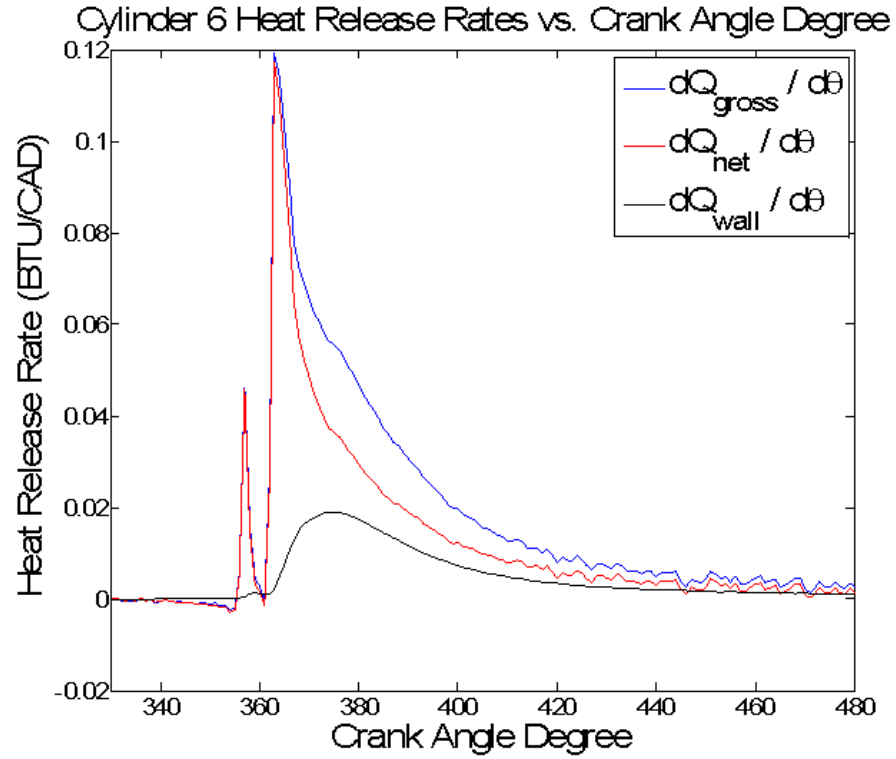


Figure 3.2. Gross, net, and wall heat transfer rates for a fired recharge in cylinder 6

Table 3.1. Waschni heat transfer model tuning constant for each cylinder.

Cylinder Number	β
1	0.85
2	1.10
3	0.98
4	1.33
5	0.86
6	1.41

parameter β in Eqn. (3.5) for each cylinder are shown in Table 3.1 for the engine used in this study.

Since the heat transfer rate can now be calculated accurately after this tuning process, Eqn. (3.1) can be rearranged in order to calculate values of m_{oil} for combustion events in recently reactivated:

$$m_{oil} = \frac{Q_{gross} - m_{fuel}LHV_{fuel}}{LHV_{oil}} \quad (3.11)$$

There are several sources of error that contribute to oil mass calculation errors when using Eqn. (3.11). The first source of error results from differences in each cylinder's pressure transducers. The pressure transducers are piezoelectric, and must be calibrated to yield accurate pressure measurements. Due to the sensitivity of this calculation, each cylinder's pressure readings may be slightly different. Since all of the heat release data (gross, net, and heat transfer) presented in this study is calculated based on in-cylinder pressure measurements, imperfectly calibrated pressure transducers result in cylinder-to-cylinder variation in calculated heat release. The second major source of error that arises when calculating oil mass using Eqn. (3.11) stems from the assumption that m_{fuel} is equal to its ECM-commanded value. If an overestimate of m_{fuel} is used, Eqn. (3.11) can yield a negative value of m_{oil} , which is obviously not realistic. Even though the ECM can be trusted to deliver similar amounts of fuel to each cylinder, the experiments outlined in the next section eliminate this problem entirely.

3.2 Test Plan for the Experimental Analysis of Oil Accumulation

At this point, some experimental test plan is needed to acquire "baseline" heat release data for each cylinder to eliminate the effects of the two major sources of error in Eqn. (3.11). If each cylinder's cumulative heat release during a case of no oil accumulation is known, m_{oil} can be calculated as

$$m_{oil} = \frac{Q_{gross,deactive} - Q_{gross,baseline}}{LHV_{oil}} \quad (3.12)$$

In this equation, $Q_{gross,deactive}$ is the cumulative gross heat release for a given cylinder while it is assumed that oil and fuel are burning, and $Q_{gross,baseline}$ is the cumulative heat release for that same cylinder under the same conditions, but while the cylinder has been active for an extended period. As such, $Q_{gross,baseline}$ represents a cylinder's cumulative heat release in a case of no oil accumulation, and it is referred to as the baseline heat release for that cylinder.


If oil combustion is evident in more than one cycle, the total mass of oil burned after a cylinder's reaction is given by

$$m_{oil} = \frac{1}{LHV_{oil}} \sum_{i=1}^n (Q_{gross,deactive,i} - Q_{gross,baseline,i}) \quad (3.13)$$


where i is the cycle number after reactivation and n is the number of cycles in which oil combustion is evident.

The acquisition of baseline heat release data for each cylinder is performed using the experimental procedure illustrated in Figure 3.3. At the beginning of an exper-

Cylinder	1	2	3	4	5	6	Notes:
	0	0	0	2x	2x	2x	Cylinders 1,2,3 in CDA for N minutes
	x	x	x	x	x	x	6 cylinder mode (2 minutes)
Total Fuel Amount:	2x	2x	2x	0	0	0	Cylinders 4,5,6 in CDA for N minutes
	x	x	x	x	x	x	6 cylinder mode (2 minutes)



Take 100 cycles of data during this transition



Take 100 cycles of data during this transition

Figure 3.3. Test plan used to study oil accumulation

iment, cylinders 1, 2, and 3 are deactivated, and a CDA duration of N minutes is commanded. Next, the ECM total fueling command is set to some value, $2X$ mg per cycle. After N minutes of CDA have elapsed, six cylinder mode is resumed, and the total fueling command is automatically cut in half (i.e. commanded to X

mg per cycle) to maintain a constant torque. During the transition from CDA to six cylinder mode, 100 cycles of in-cylinder pressure data are recorded. This data is used to calculate $Q_{gross,baseline}$ (i.e. baseline heat release) for cylinders 4, 5, and 6, as well as $Q_{gross,deactive}$ for cylinders 1, 2, and 3. Next, the engine is left to run in steady-state six cylinder mode for approximately two minutes in order to ensure that all accumulated oil has been eliminated from the recharging cylinders. After this is complete, cylinders 4, 5, and 6 are deactivated and the total fueling command is doubled to maintain approximately constant torque. After N minutes of CDA, another 100 cycles of in-cylinder pressure data are recorded which capture the transition to six cylinder mode, but this time the data used to calculate $Q_{gross,baseline}$ for cylinders 1, 2, and 3, and $Q_{gross,deactive}$ for cylinders 4, 5, and 6. Now, Eqn. (3.12) can be used to calculate m_{oil} with the effects of pressure transducer and fuel injector uncertainty reduced.

3.3 Results and Discussion

Engine Operating Condition

Using the test plan outlined in Section 3.2, data was recorded at an engine operating condition of 800 rpm with a brake mean effective pressure (BMEP) of 2.54 bar. CDA times of $N = 20$ minutes, $N = 10$ minutes, $N = 5$ minutes, and $N = 0.5$ minutes were studied. The engine operating condition of 800 rpm and 2.54 bar BMEP is referred to as “loaded idle.” Loaded idle (as opposed to “unloaded” idle, which has a BMEP of 0.26 bar) is experienced by an engine that is providing auxiliary power to a vehicle that is not moving. For example, utility vehicles which utilize a power take off system commonly operate at loaded idle. Due to its low exhaust gas temperatures (which are not ideal for after-treatment system effectiveness) and the significant amounts of time spent at it [40], the loaded idle engine condition is the focus of this study.

Results

This test plan was executed two times, several days apart, and the data were analyzed using the following approach.

First, for a given data point, $Q_{gross,baseline}$ and $Q_{gross,deactive}$ were calculated as in Section 3.1 for all 100 cycles of in-cylinder pressure data. An example of a result for cylinder 1 after 20 minutes of CDA is shown in Fig. 3.4. The gray line in Fig.

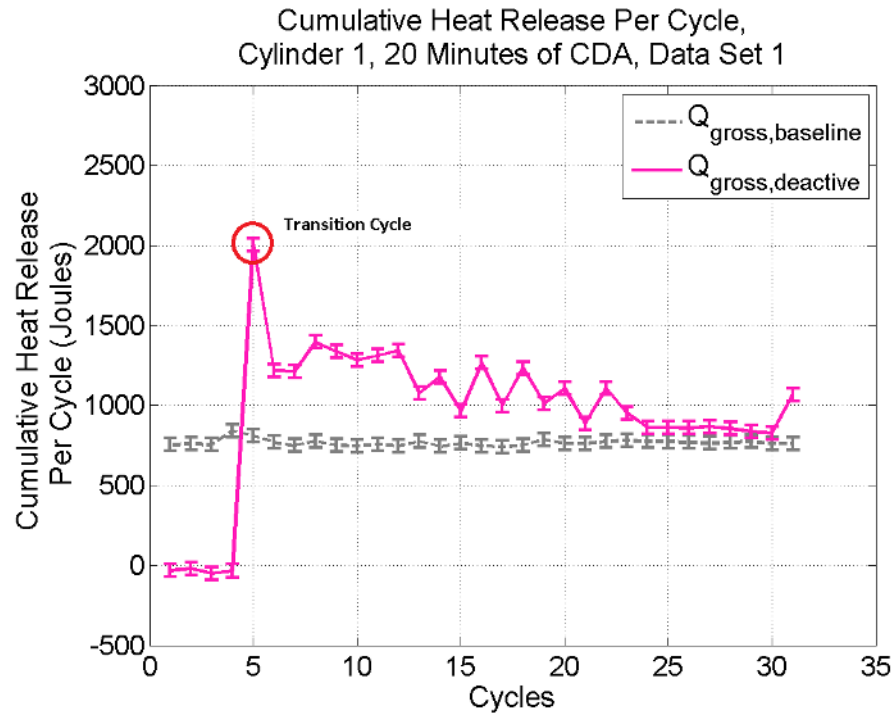


Figure 3.4. Cumulative heat release per cycle in cylinder 1 after 20 minutes of CDA.

3.4 represents cylinder 1's baseline cumulative heat release per cycle, and it is fairly constant during the transition from CDA to six cylinder mode, which happens in cycle 5. The pink line is the cumulative heat release per cycle in cylinder 1 as it is being reactivated. Clearly, the heat released by combustion in the first cycle after reactivation is markedly higher than the baseline case. Since the ECM-commanded

total fueling is identical for the baseline and reactivating cases, the difference between the pink and gray lines is caused solely by the combustion of accumulated oil.

In Fig. 3.4, $Q_{gross,deactive}$ is significantly greater than $Q_{gross,baseline}$ for several cycles after the transition to six cylinder mode. This yields two key conclusions regarding accumulated oil: that it does not combust entirely in the first cycle of six cylinder mode, and that the uncombusted portion does not all escape via the exhaust valve opening after some of it has indeed burned. In this analysis, oil combustion is assumed to be complete as soon as the error bars of $Q_{gross,deactive}$ and $Q_{gross,baseline}$ first overlap. For example, the oil combustion shown in Fig. 3.4 ends in cycle 24, which is $n = 19$ cycles after the transition to six cylinder mode which occurred in cycle 5.

The error bars in Fig. 3.4 represent two standard deviations of a 30-cycle mean of $Q_{gross,baseline}$. Data sets 1 and 2 refer to the results of the test plan that were gathered on two separate days, spaced several days apart. Tables 3.2 and 3.3 give the magnitude of the error bars for each cylinder in data sets 1 and 2, respectively. The oil mass error bars that correspond to each cumulative heat release error bar are also given. These oil mass error bars are simply calculated as the heat release error bar magnitudes divided by LHV_{oil} .

Table 3.2. Magnitudes of error bars for each cylinders cumulative heat release and accumulated oil mass in data set 1.

Cylinder Number	Heat Release Error Bar Magnitude (Joules)	Oil Mass Error Bar Magnitude (mg)
1	40.15	1.00
2	67.17	1.67
3	138.16	3.44
4	39.63	0.99
5	42.49	1.06
6	263.33	6.55

Table 3.3. Magnitudes of error bars for each cylinders cumulative heat release and accumulated oil mass in data set 2.

Cylinder Number	Heat Release Error Bar Magnitude (Joules)	Oil Mass Error Bar Magnitude (mg)
1	35.18	0.88
2	64.05	1.59
3	206.61	5.14
4	39.83	0.99
5	65.87	1.64
6	284.39	7.08

Now that the number of oil combustion cycles, n , has been defined, oil mass values can be calculated according to Eqn. (3.13).

The shaded area in Fig. 3.5 illustrates the sum in Eqn. (3.13) for cylinder 1 after 20 minutes of CDA. Dividing this shaded area by LHV_{oil} gives an oil mass of $m_{oil} = 219.35$ mg, which is approximately 10 times greater than the ECM-commanded total injected fuel of 22.75 mg for a given cycle for cylinder 1.

Continuing the analysis for cylinder 1, the result shown in Fig. 3.6 was obtained after a CDA time of 10 minutes. This time, the shaded area is smaller and agrees with the expectation that shorter CDA times yield smaller amounts of accumulated oil. The oil mass calculated for this case is $m_{oil} = 106.89$ mg, which is roughly 5 times greater than the injected fuel mass.

After 5 minutes of CDA in cylinder 1, the result shown in Fig. 3.7 was obtained. This time, the shaded area is smaller yet again and further corroborates the hypothesis that shorter CDA times yield smaller amounts of accumulated oil. The oil mass calculated for this case is $m_{oil} = 7.25$ mg, which is roughly 1/3 the injected fuel mass.

Finally, the result for 0.5 minutes of CDA in cylinder 1 shown in Fig. 3.8 was obtained. This time, there is no shaded area since the two lines' error bars overlap

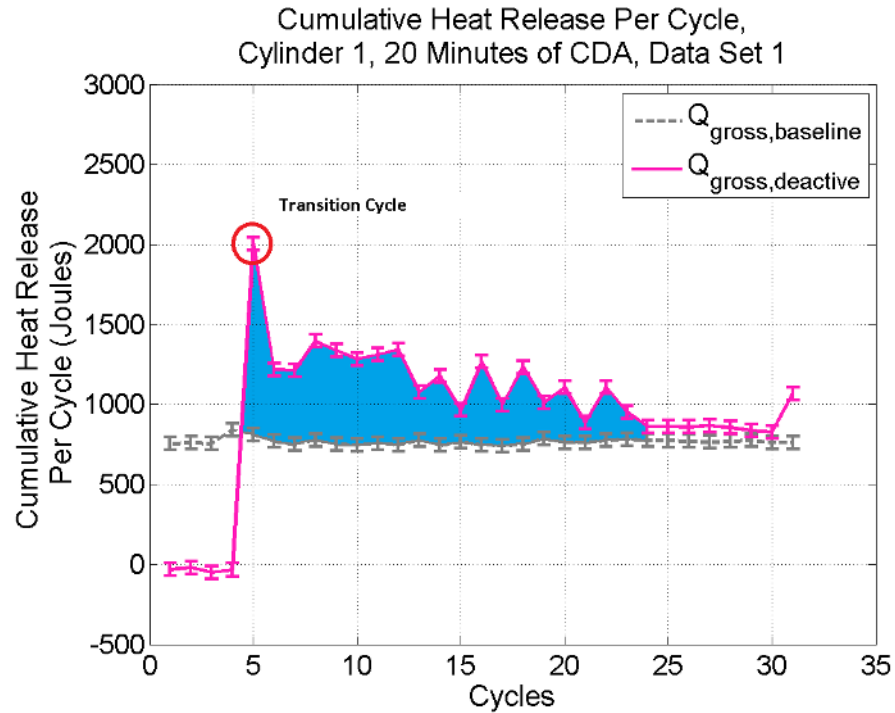


Figure 3.5. Cumulative heat release per cycle in cylinder 1 after 20 minutes of CDA with sum shaded.

immediately after reactivation. While it is possible that some oil does accumulate and burn, this analysis cannot calculate that oil mass with any statistical certainty.

The cumulative heat release values in Figs. 3.5 - 3.8 are the integrals of heat release rate profiles. For the data shown in Fig. 3.5, heat release rate profiles for the first 5 cycles after reactivation are illustrated in Fig. 3.9. Ten cycles worth of baseline heat release rates are also indicated by the light gray lines.

The solid blue line shows the heat release rate during the first cycle after reactivation, and it deviates from baseline over nearly the entire range of crank angles shown in the figure. Over the subsequent 4 engine cycles, the heat release rate settles closer to the baseline, but significant oil combustion is still present. Fig. 3.10 shows a similar plot for 0.5 minutes of CDA in cylinder 1.

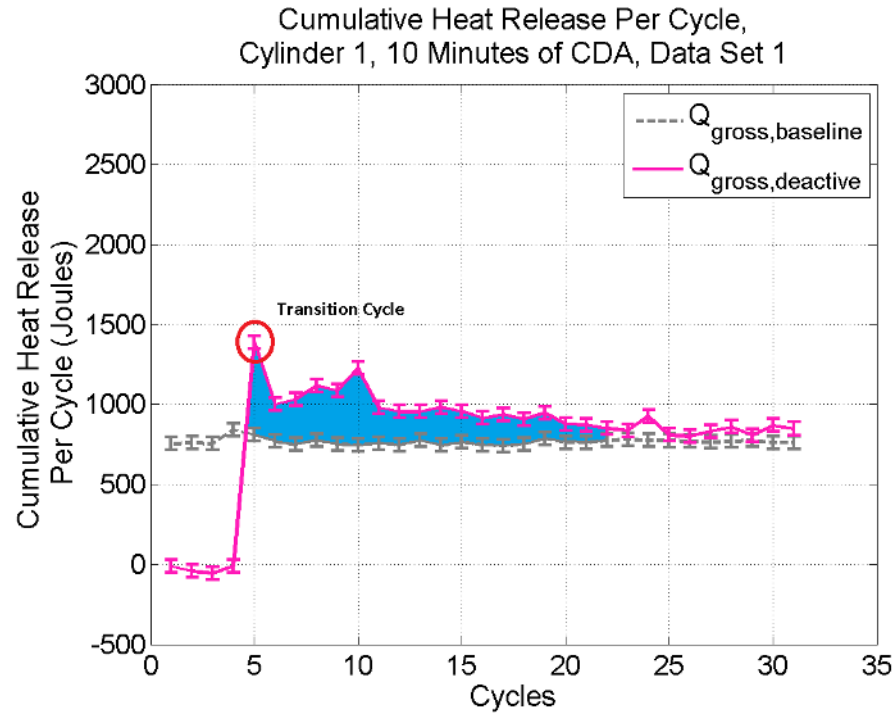


Figure 3.6. Cumulative heat release per cycle in cylinder 1 after 10 minutes of CDA with sum shaded.

While some deviation from baseline is visually apparent in the 5 cycles following reactivation, no statistically significant oil mass can be calculated due to the error bar overlap in cycle 1 that is shown in Fig. 3.8.

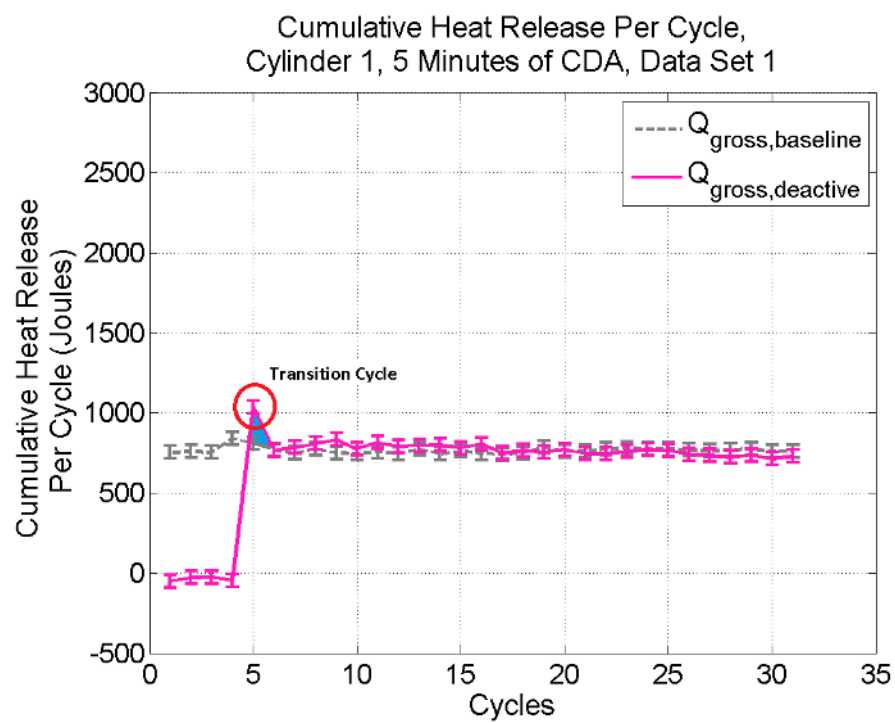


Figure 3.7. Cumulative heat release per cycle in cylinder 1 after 5 minutes of CDA with sum shaded.

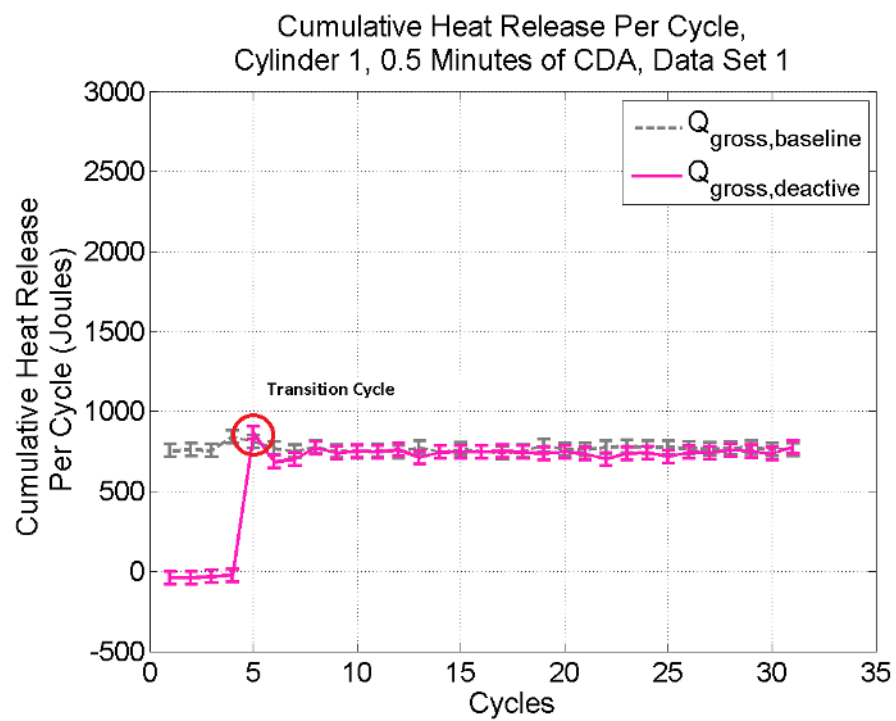


Figure 3.8. Cumulative heat release per cycle in cylinder 1 after 0.5 minutes of CDA with sum shaded.

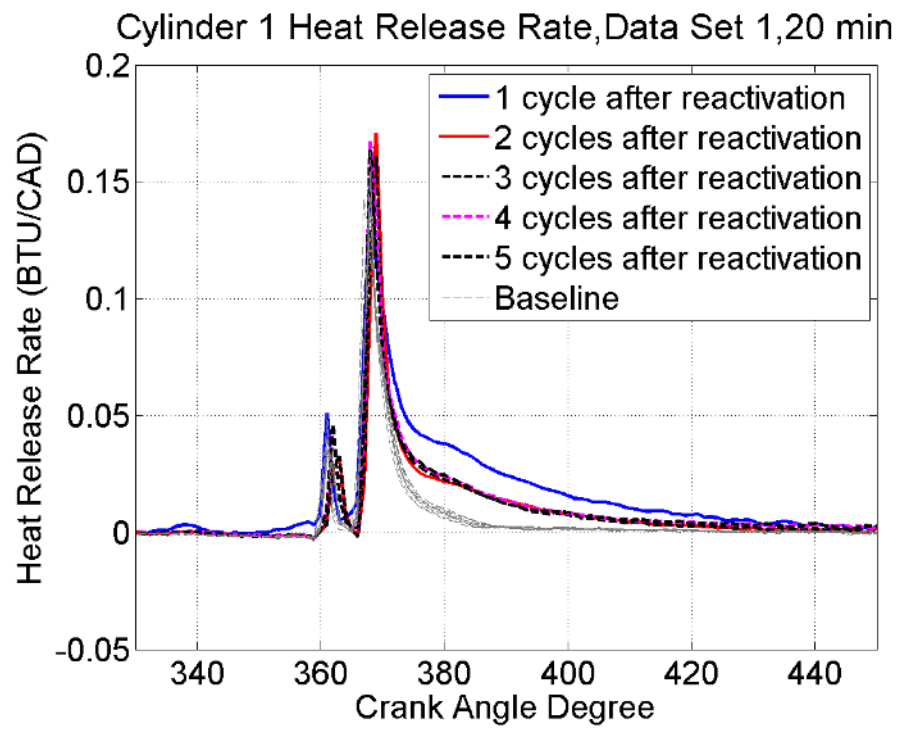


Figure 3.9. Heat release rate as a function of crank angle in cylinder 1 after 20 minutes of CDA.

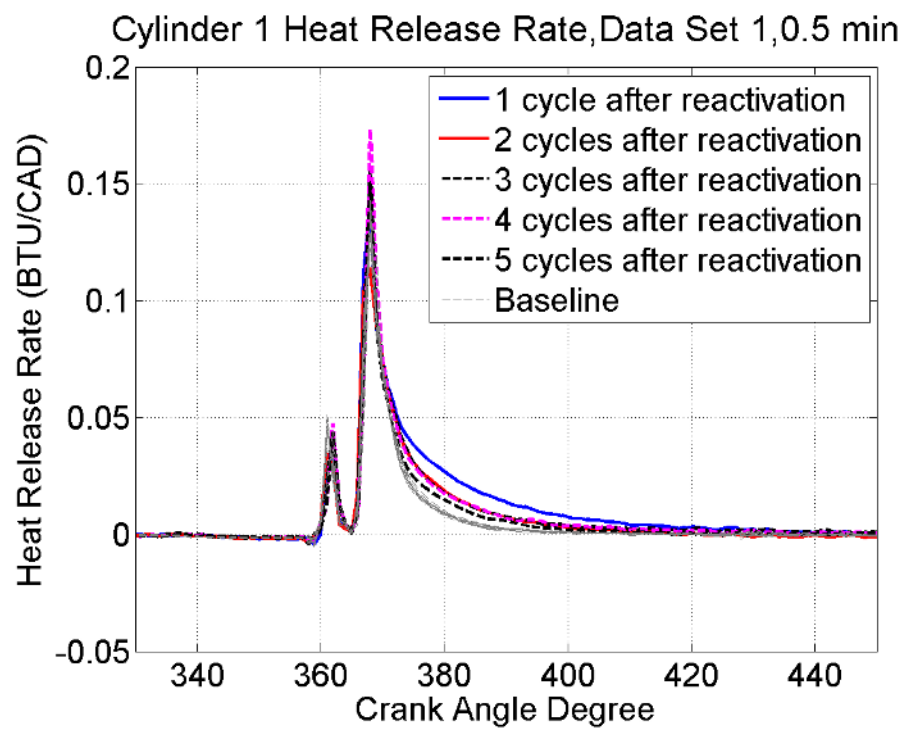


Figure 3.10. Heat release rate as a function of crank angle in cylinder 1 after 0.5 minutes of CDA.

Cylinder 1

The oil mass results for cylinder 1 in data sets 1 and 2 are illustrated in Fig. 3.11. The results are consistent between data sets 1 and 2, and they demonstrate

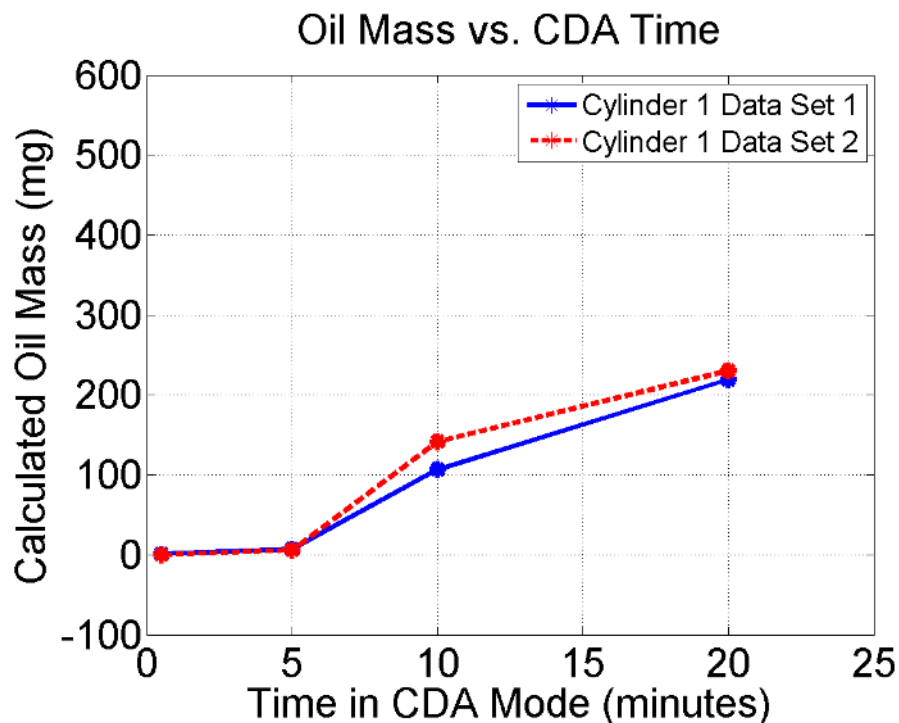


Figure 3.11. Calculated oil masses in cylinder 1 for data sets 1 and 2.

a monotonically increasing trend that supports the hypothesis that increasing CDA times yield increasing masses of oil. However, the monotonic increase in data set 2 is only present after a modification is made to the error bar overlap method of determining n . This modification is necessary due to abnormal combustion that is seen in the 10 minute CDA time data point.

Fig. 3.12 shows the cumulative heat release per cycle in cylinder 1 after 10 minutes of CDA in data set 2. Cylinder 1 is reactivated in cycle 5, which is the same cycle in which the two lines' error bars first overlap. According to the method used so far, this means that $n = 0$ and $m_{oil} = 0$ mg. However, a significant mass of oil does appear to burn in cycles 6-30. Rather than ignore this oil combustion, the analysis of this

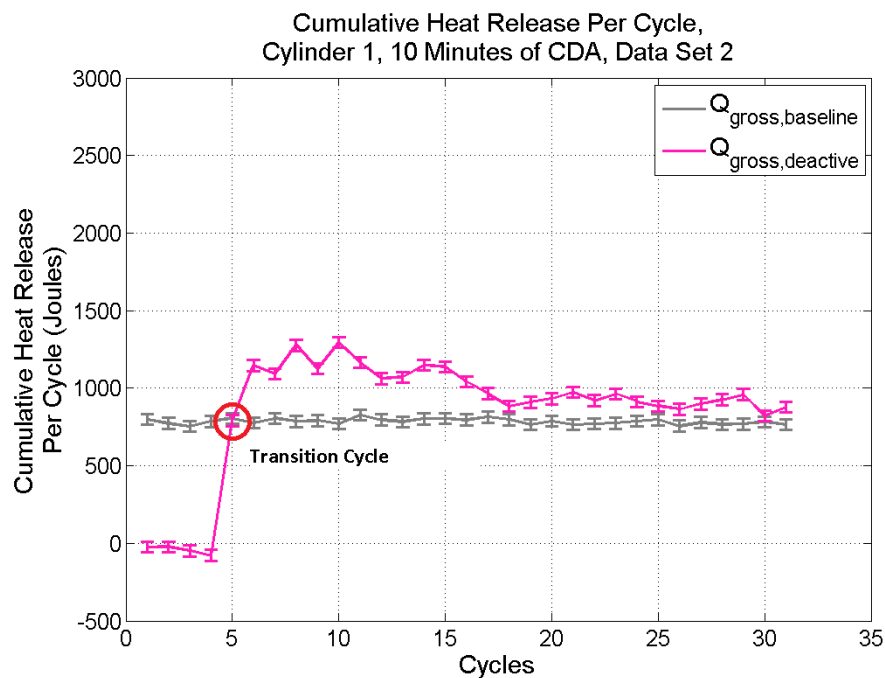


Figure 3.12. Cumulative heat release per cycle in cylinder 1 after 10 minutes of CDA in data set 2.

specific data point was modified such that the first error bar overlap in cycle 6 was ignored, yielding $n = 24$ and $m_{oil} = 141.66$ mg.

Cylinder 2

The oil mass results for cylinder 2 in data sets 1 and 2 are illustrated in Fig. 3.13. Compared to cylinder 1, cylinder 2 shows more oil accumulation at 5 and 10 minute

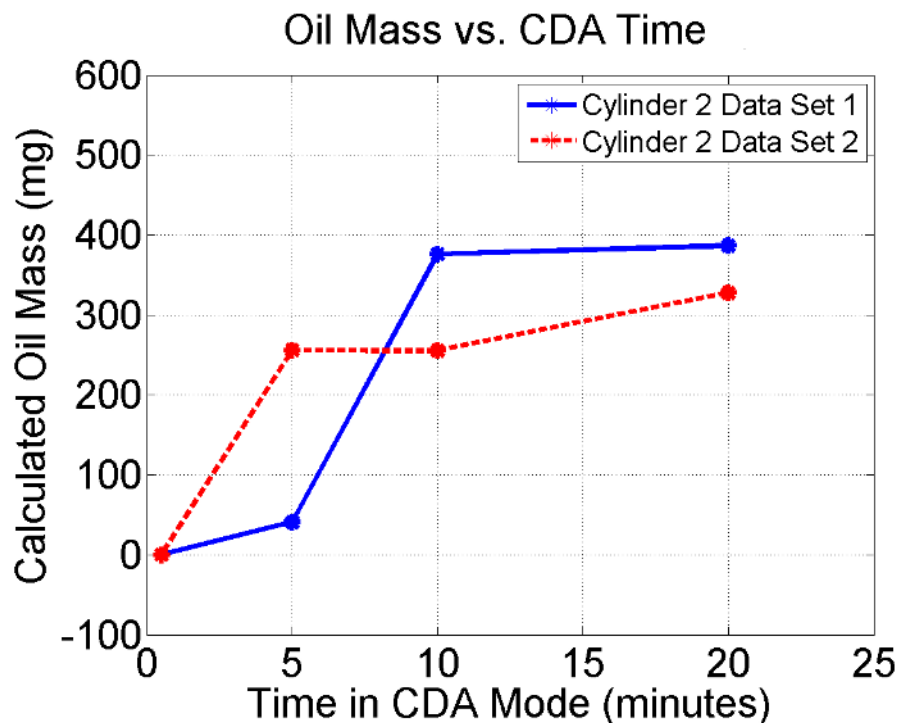


Figure 3.13. Calculated oil masses in cylinder 2 for data sets 1 and 2.

CDA times, more overall oil accumulation at all CDA times greater than 0.5 minutes, and a “leveling-off” behavior as oil accumulation appears to saturate after 10 minutes in data set 1 and 5 minutes in data set 2.

The cumulative heat release per cycle for 10 minutes of CDA in data set 1 is shown in Fig. 3.14. Compared to cylinder 1’s cumulative heat release per cycle after 10 minutes of CDA in data set 1 (Fig. 3.6), cylinder 2’s is significantly higher. Since this type of behavior occurred in data sets 1 and 2, which were conducted several days apart, it can be concluded that oil accumulation is generally more significant in cylinder 2 than cylinder 1. Because the primary means of oil transport into a deactivated cylinder is through piston ring imperfections, greater oil masses could be

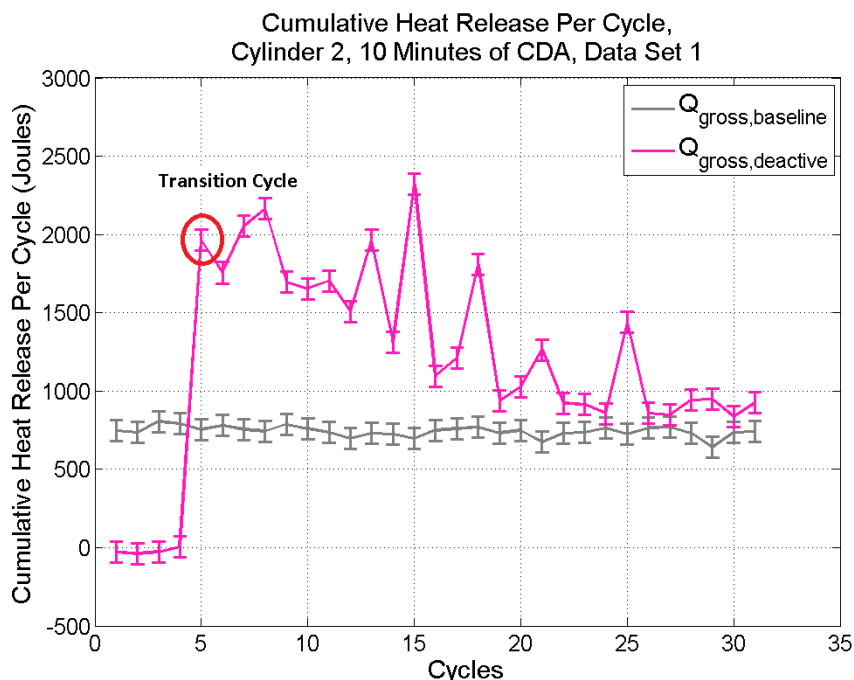


Figure 3.14. Cumulative heat release per cycle in cylinder 2 after 10 minutes of CDA in data set 1.

evidence of a less perfect piston ring seal. While no piston ring analysis was conducted by the author, it is possible that cylinder 2’s piston ring is “leakier” than cylinder 1’s, which explains its greater oil mass values.

Cylinder 3

The oil mass results for cylinder 3 in data sets 1 and 2 are illustrated in Fig. 3.15. While data set 2 shows a non-decreasing trend, the most peculiar aspect of this data is the zero oil mass calculated at 5, 10, and even 20 minute CDA times. This is at least partially explained by referring to Tables 3.2 and 3.3, which indicate that cylinders 3 and 6 are by far the “noisiest” due to their error bars being the largest. Large error bars can significantly affect oil mass calculations by influencing the error bar overlap cycle that determines n . Small n -values by definition yield small m_{oil} values, and Fig. 3.16 demonstrates that this happens in cylinder 3. In Fig. 3.16, reactivation occurs in cycle 5, and so does the first error bar overlap. Also, $Q_{gross,deactive}$ in cycle 5 is less

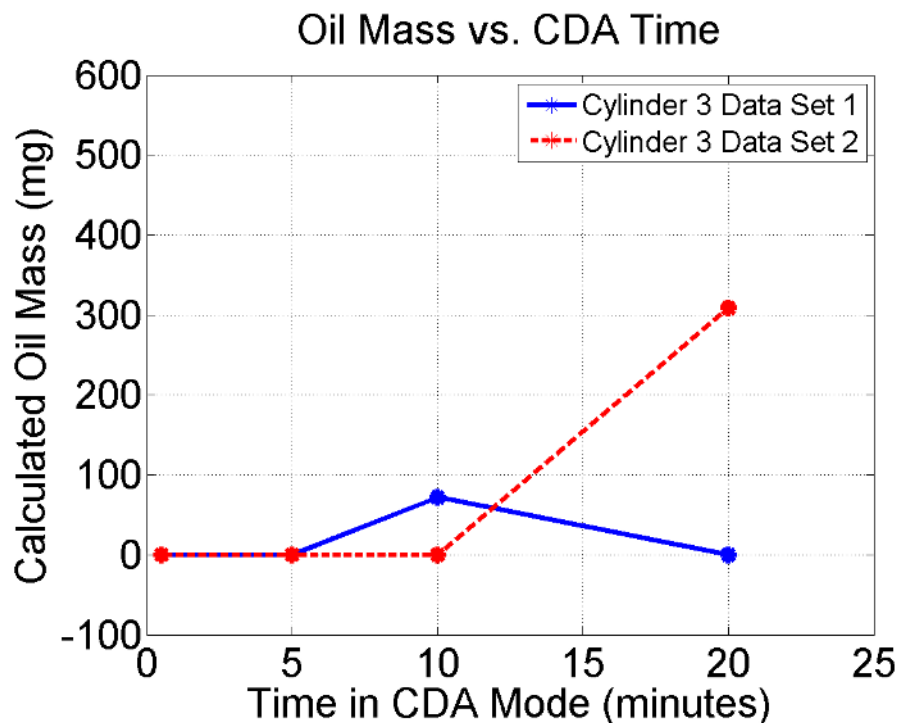


Figure 3.15. Calculated oil masses in cylinder 3 for data sets 1 and 2.

than $Q_{gross,baseline}$. Fig. 3.20 shows the cumulative heat release as a function of crank angle for the first 5 cycles after reactivation for the data in Fig. 3.16. In accordance with Fig. 3.16, the solid blue line in Fig. 3.20 indicates that the cumulative heat release in the first cycle after reactivation was less than baseline. Furthermore, the start of combustion was delayed in the first cycle. Fig. 3.18 provides more insight by showing the heat release rates as a function of crank angle for this data point. Again, the solid blue line demonstrates that the start of combustion was delayed in the first cycle, and that its overall heat release is less than baseline. Interestingly, cycles 2-5 in Figs. 3.16 - 3.18 show that heat release settled near the baseline after the extremely distorted first cycle. A possible explanation for this effect is that after the distorted combustion in the first cycle after reactivation, some of the accumulated oil escaped through the exhaust valve before burning in cycles 2-5. The exact same effect is seen at the 10 minute CDA time data point in data set 2.

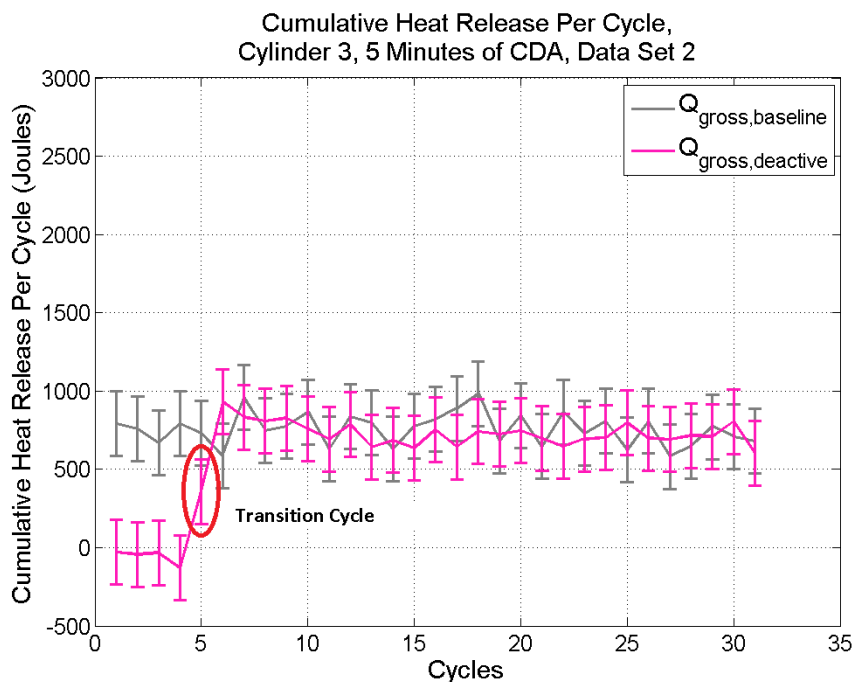


Figure 3.16. Cumulative heat release per cycle in cylinder 3 after 5 minutes of CDA in data set 2.

However, the zero oil mass value calculated for the 20 minute CDA time data point in data set 1 is not due to the same behavior. Inspecting the cumulative heat release per cycle for this data point in Fig. 3.19, the cylinder reactivation in cycle 5 again coincides with the first error bar overlap cycle, yielding zero calculated oil mass. While $Q_{gross,deactive}$ is greater than $Q_{gross,baseline}$ in cycles 5-9, no modification to the analysis can reasonably be made as was done for the cylinder 1, 10 minute data point in Fig. 3.12 since the error bars continue to overlap in this case. Furthermore, Fig. 3.20 shows that no combustion occurred during the pilot injection in the first cycle after reactivation. Since subsequent cycles are not significantly different from the baseline, it is possible that after the distorted combustion in the first cycle, nearly all of the accumulated oil in cylinder 3 was exhausted before burning in later cycles.

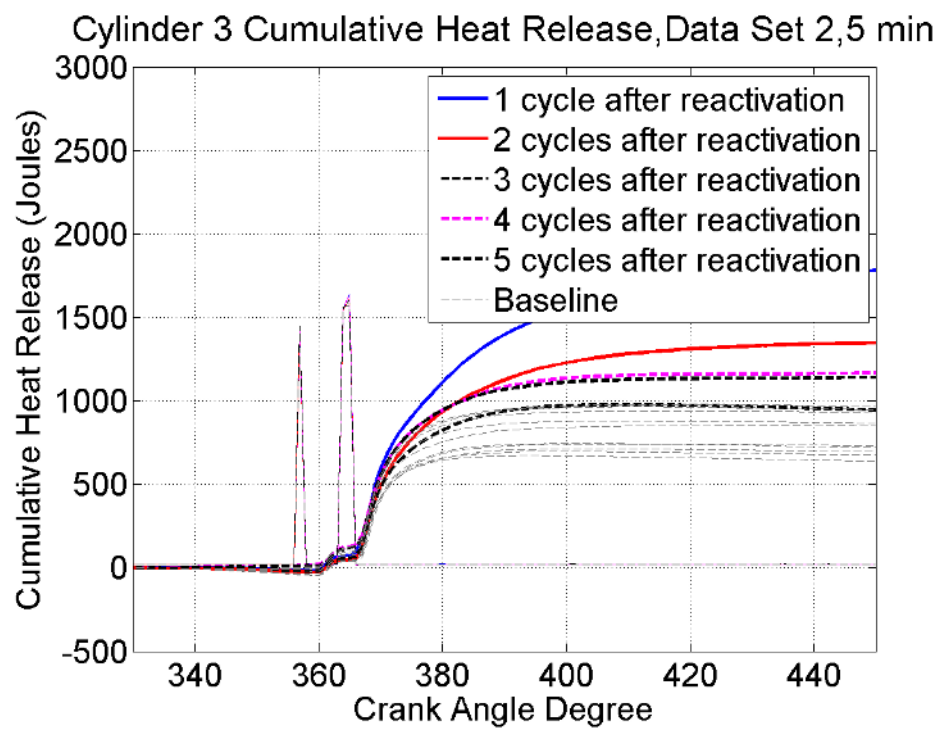


Figure 3.17. Cumulative heat release as a function of crank angle in cylinder 3 after 5 minutes of CDA in data set 2.

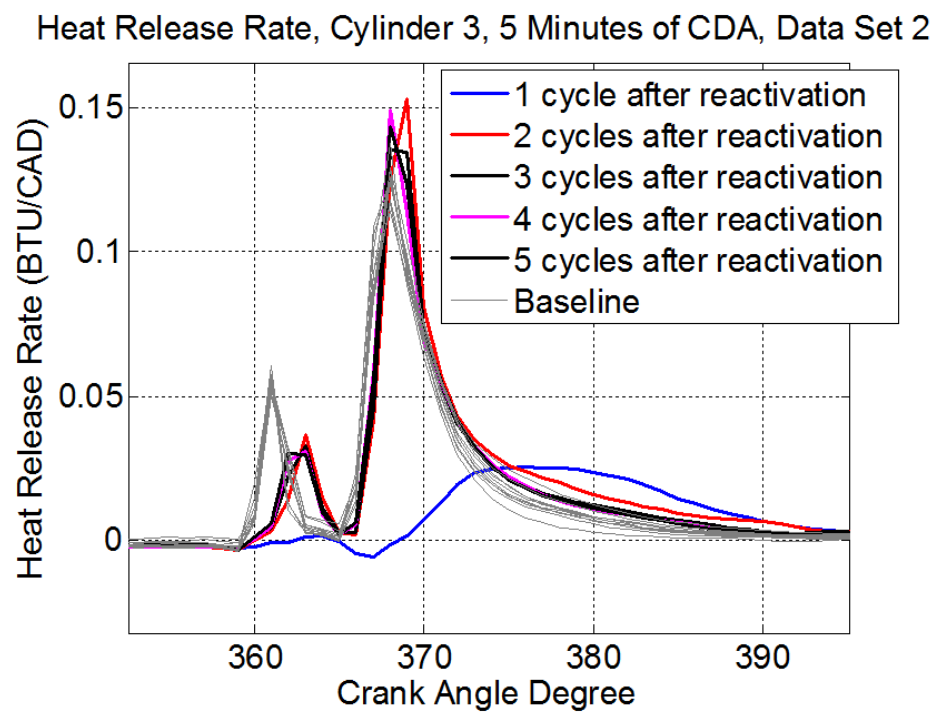


Figure 3.18. Heat release rate as a function of crank angle in cylinder 3 after 5 minutes of CDA in data set 2.

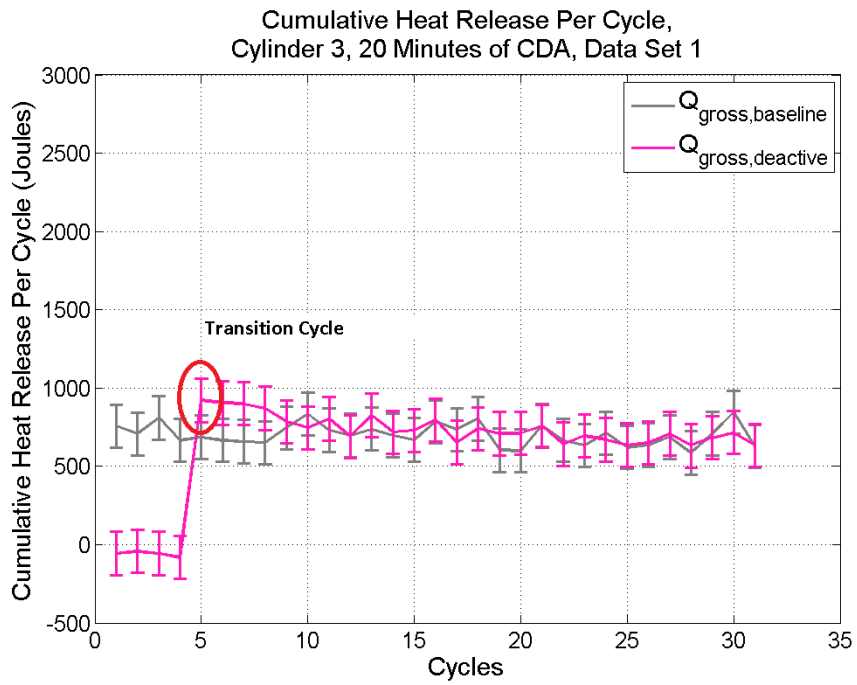


Figure 3.19. Cumulative heat release per cycle in cylinder 3 after 20 minutes of CDA in data set 1.

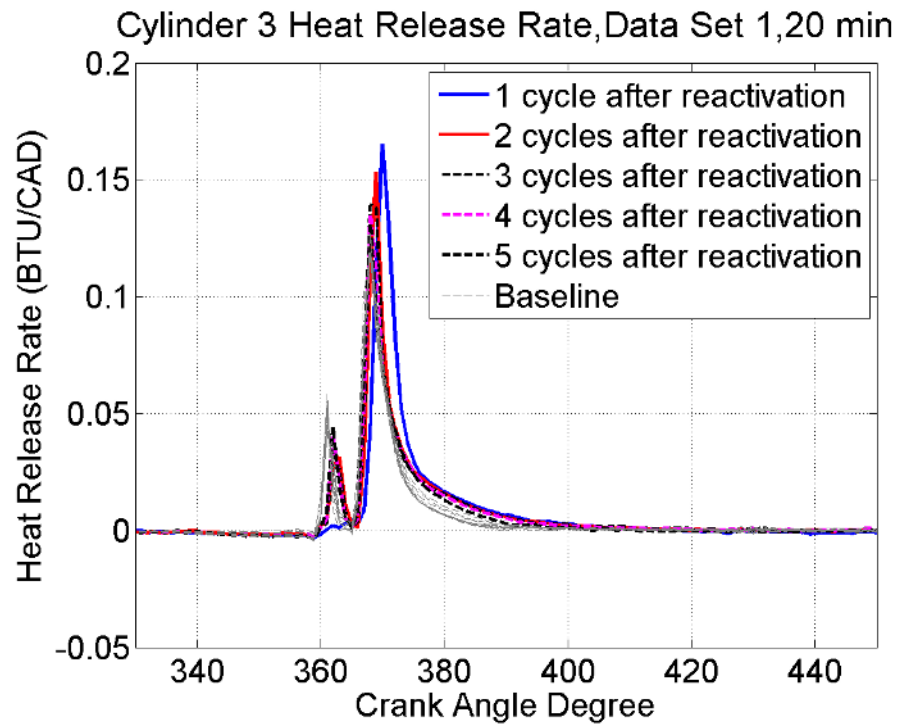


Figure 3.20. Heat release rate as a function of crank angle in cylinder 3 after 20 minutes of CDA in data set 1.

Cylinder 4

The oil mass results for cylinder 4 in data sets 1 and 2 are illustrated in Fig. 3.21. These results demonstrate a monotonic increase in accumulated oil mass that

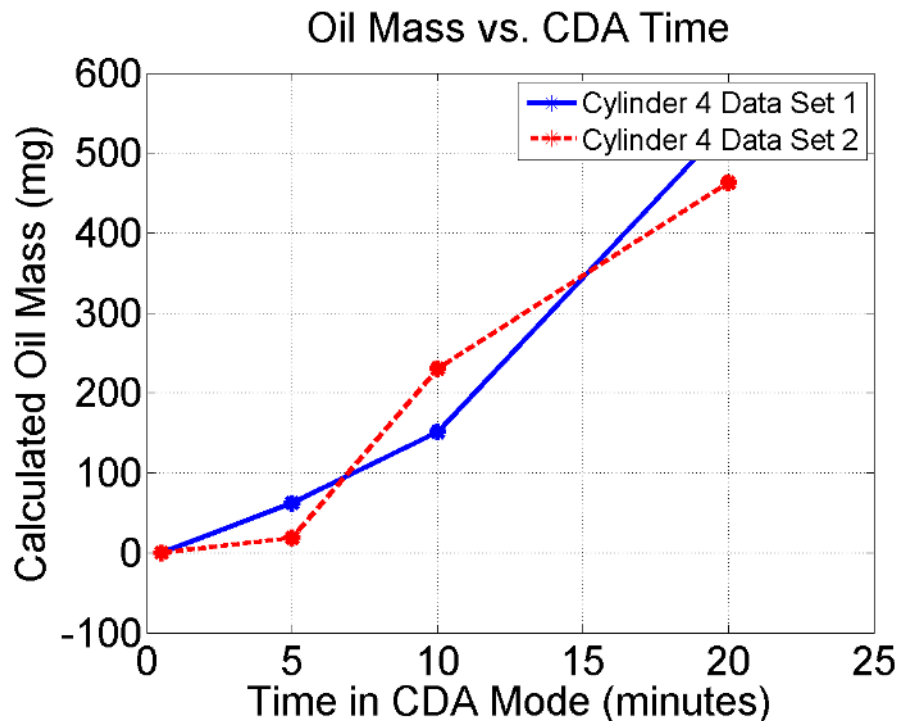


Figure 3.21. Calculated oil masses in cylinder 4 for data sets 1 and 2.

is consistent between both data sets.

Cylinder 5

The oil mass results for cylinder 5 in data sets 1 and 2 are illustrated in Fig. 3.22. While these results generally show a monotonic increase in oil mass, less oil mass was calculated after 20 minutes of CDA in data set 1 than 10 minutes. Fig. 3.23 shows the cumulative heat release per cycle for this data point, and it is noteworthy that $Q_{gross,deactive}$ experiences its maximum value in cycle 9, which is the 5th cycle after the reactivation in cycle 5. This is further illustrated in Fig. 3.24, which shows that not only did the maximum heat release occur 5 cycles after reactivation, but also that no pilot combustion occurred in the first cycle. Fig. 3.25 verifies the lack of pilot

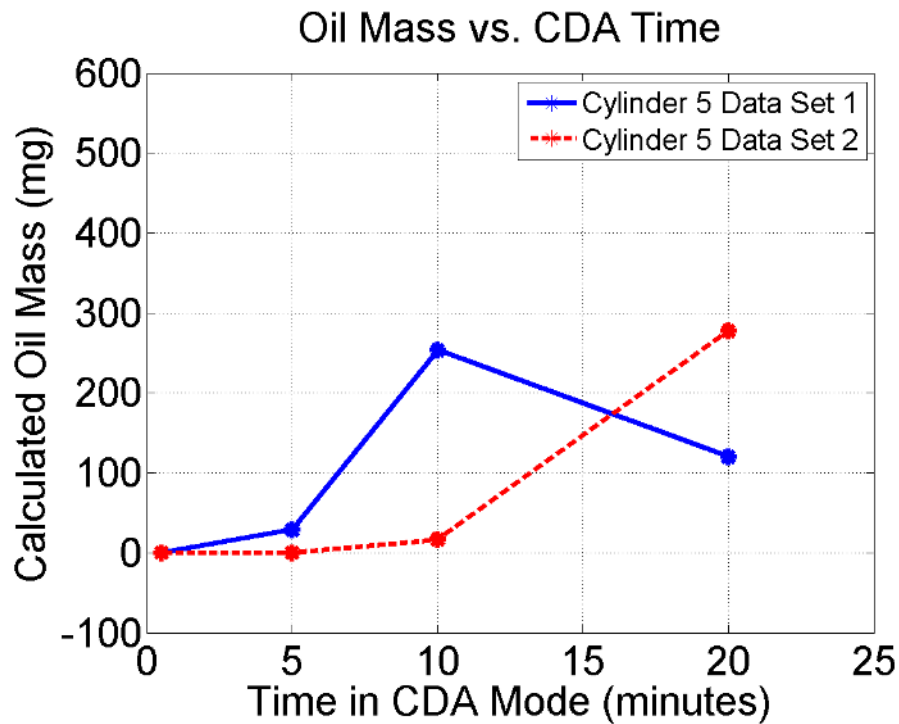


Figure 3.22. Calculated oil masses in cylinder 5 for data sets 1 and 2.

combustion in the first cycle, and also shows that extremely distorted combustion occurred in the fourth and fifth cycles following reactivation. The lower overall oil mass calculated after 20 minutes of CDA than 10 minutes of CDA in data set 1 could have been caused by the same oil exhaust behavior that has been described previously.

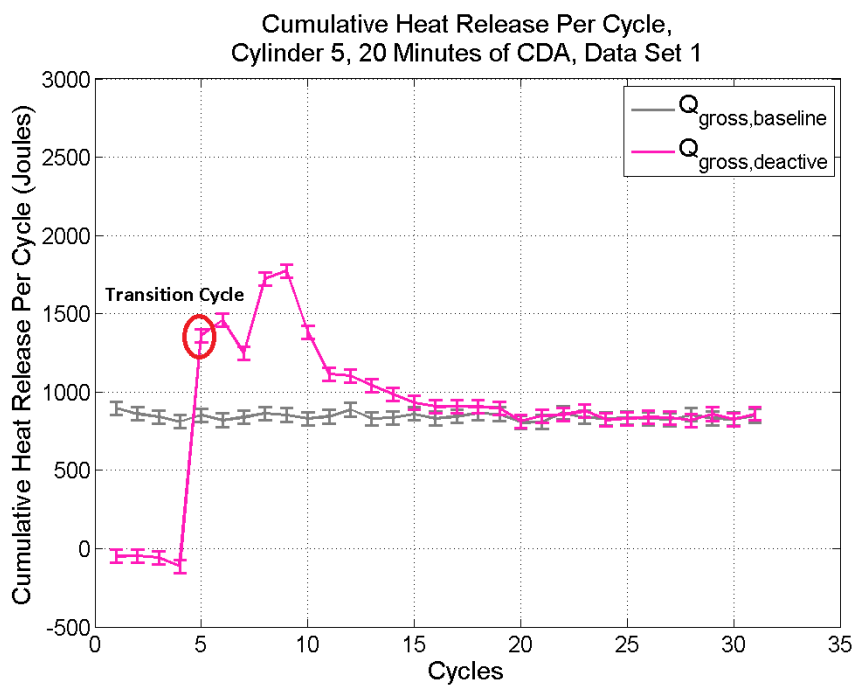


Figure 3.23. Cumulative heat release per cycle in cylinder 5 after 20 minutes of CDA in data set 1.

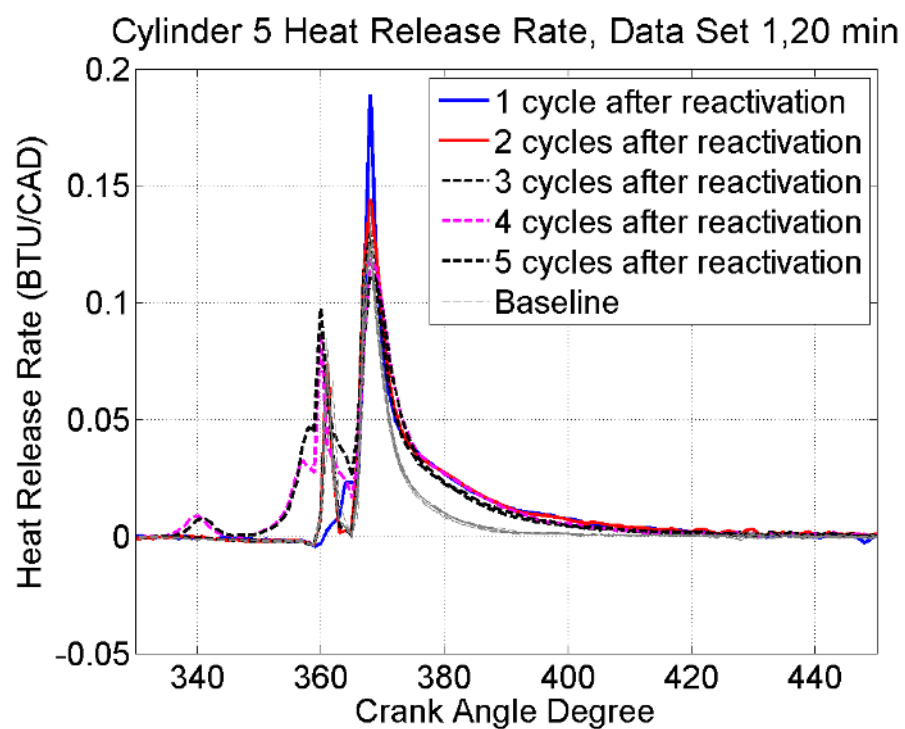


Figure 3.24. Cumulative heat release as a function of crank angle in cylinder 5 after 20 minutes of CDA in data set 1.

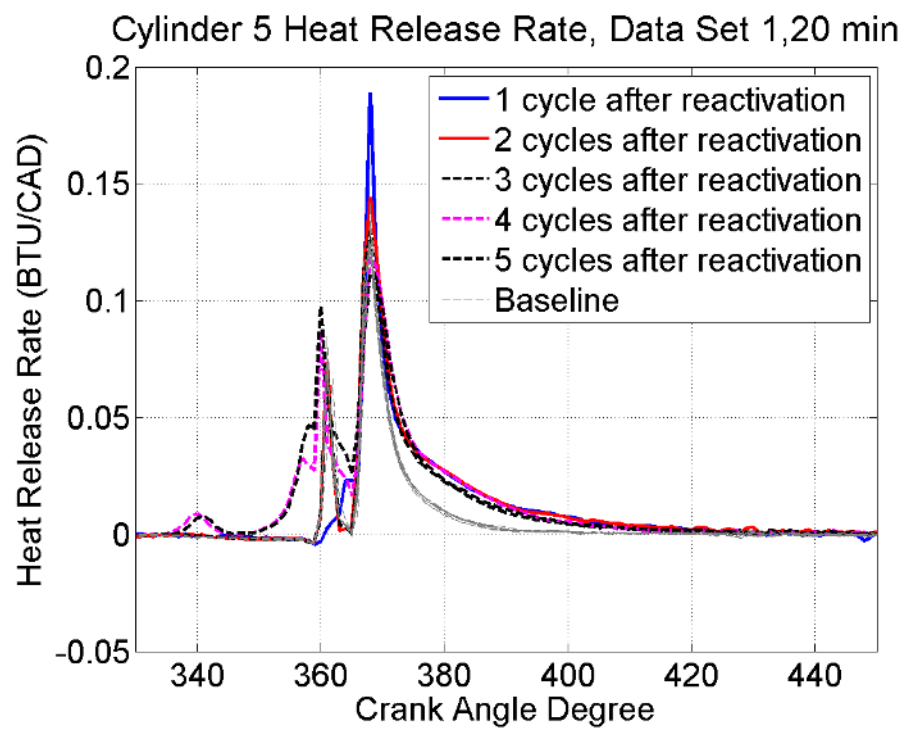


Figure 3.25. Heat release rate as a function of crank angle in cylinder 5 after 20 minutes of CDA in data set 1.

Cylinder 6

The oil mass results for cylinder 6 in data sets 1 and 2 are illustrated in Fig. 3.26. Like cylinders 1 and 4, these results demonstrate a monotonic increase in accumulated

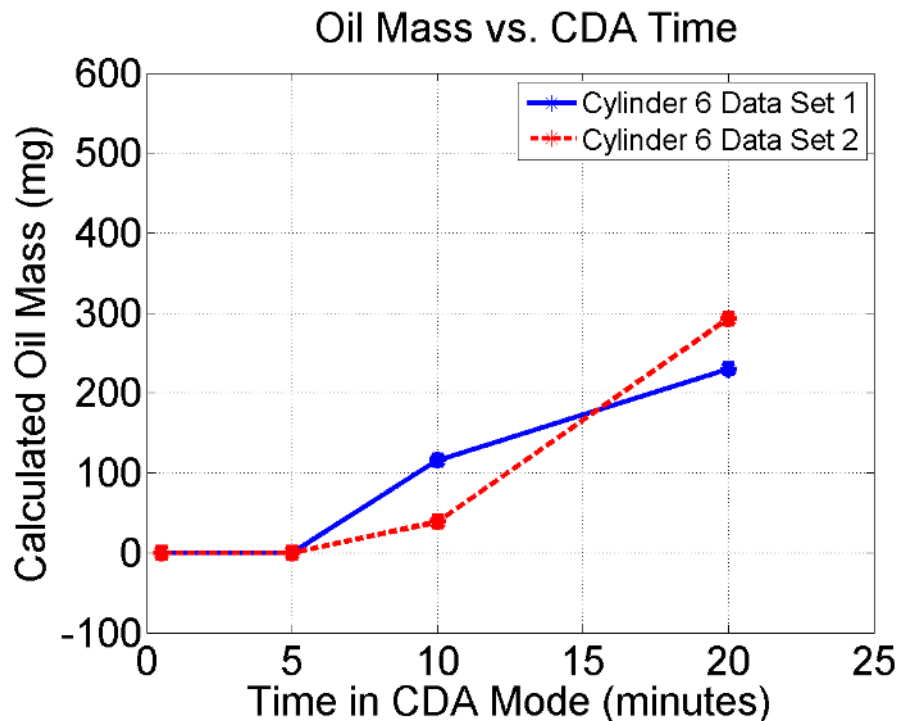


Figure 3.26. Calculated oil masses in cylinder 6 for data sets 1 and 2.

oil mass that is consistent between both data sets.

Complete Data Set 1

For data set 1, the results of all six cylinder's oil mass calculations are shown in Fig. 3.27. Fig. 3.27 indicates that significant oil accumulation occurs in five of the six cylinders at CDA times of 20 minutes, and nonzero oil accumulation occurred in two of the six cylinders at only 5 minute CDA times. Cylinder 3's lack of oil accumulation at 20 minutes was investigated using plots of heat release and it was hypothesized that cylinder 3's particularly large error bars, combined with the possible exhausting of unburned oil after the first cycle, contributed to its zero oil mass calculation. Cylinder 5 is the only other cylinder that did not exhibit a monotonic increase in oil mass,

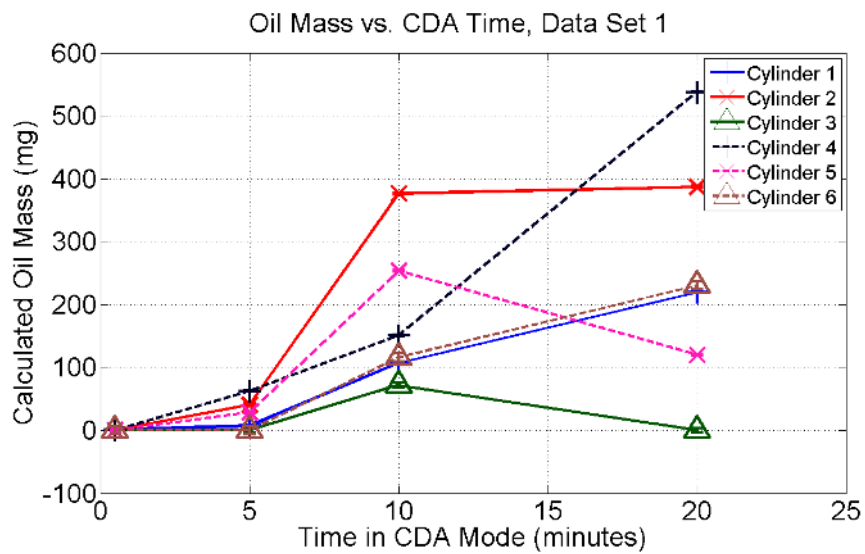


Figure 3.27. Calculated oil masses in all cylinders for data set 1.

and this was also explained by the possible exhausting of unburned oil after quenched combustion in the first cycle after reactivation.

Complete Data Set 2

For data set 2, the results of all six cylinder's oil mass calculations are shown in Fig. 3.28. Fig. 3.28 indicates that all six cylinders experienced significant oil accumulation

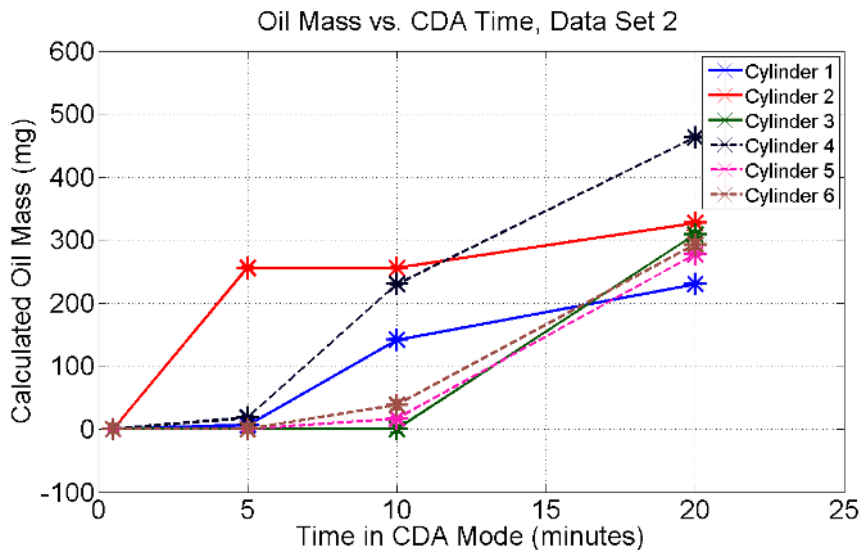


Figure 3.28. Calculated oil masses in all cylinders for data set 2.

at 20 minute CDA times, and that three of the six cylinders experienced significant oil accumulation at 5 minute CDA times.

Overall Figs. 3.27 - 3.28 demonstrate that oil accumulation is generally very significant as the engine is operated in CDA mode for periods of time greater than 5 minutes. Numerical values for the masses of each cylinders' oil accumulation for data sets 1 and 2 are given in Tables 3.4 and 3.5, respectively.

Table 3.4. Accumulated oil masses for data set 1.

CDA Time (min)	Deactivated Cylinders	Cyl. 1 Oil Mass (mg)	Cyl. 2 Oil Mass (mg)	Cyl. 3 Oil Mass (mg)	Cyl. 4 Oil Mass (mg)	Cyl. 5 Oil Mass (mg)	Cyl. 6 Oil Mass (mg)
20	1, 2, 3	219.35	386.61	0.00	-	-	-
20	4, 5, 6	-	-	-	537.70	120.02	229.85
10	1, 2, 3	106.89	376.21	71.60	-	-	-
10	4, 5, 6	-	-	-	151.00	253.38	115.77
5	1, 2, 3	7.25	40.83	0.00	-	-	-
5	4, 5, 6	-	-	-	62.16	28.72	0.00
0.5	1, 2, 3	0.90	0.00	0.00	-	-	-
0.5	4, 5, 6	-	-	-	0.00	0.06	0.00

Table 3.5. Accumulated oil masses for data set 2.

CDA Time (min)	Deactivated Cylinders	Cyl. 1 Oil Mass (mg)	Cyl. 2 Oil Mass (mg)	Cyl. 3 Oil Mass (mg)	Cyl. 4 Oil Mass (mg)	Cyl. 5 Oil Mass (mg)	Cyl. 6 Oil Mass (mg)
20	1, 2, 3	230.13	327.29	308.52	-	-	-
20	4, 5, 6	-	-	-	462.95	277.24	292.94
10	1, 2, 3	141.66	255.51	0.00	-	-	-
10	4, 5, 6	-	-	-	229.99	16.77	38.67
5	1, 2, 3	6.17	255.97	0.00	-	-	-
5	4, 5, 6	-	-	-	18.46	0.00	0.00
0.5	1, 2, 3	0.00	0.00	0.00	-	-	-
0.5	4, 5, 6	-	-	-	0.00	0.00	0.00

3.4 Summary

The effort in this Chapter resulted in an experimental test plan and a heat-release-based analysis to calculate the mass of engine lubricating oil that burns in reactivated cylinders that have previously undergone prolonged periods of deactivation.

1. In-cylinder pressure measurements were used to calculate the cumulative gross heat release in all six cylinders, including the effect of heat transfer through cylinder walls.
2. The difference between the heat released by combustion in reactivated cylinders and active cylinders was assumed to be caused solely by the combustion of accumulated engine oil.
3. To eliminate the effects of cylinder-to-cylinder pressure transducer and fuel injector variations, baseline heat release data for each cylinder were collected while each cylinder was actively firing, as opposed to being reactivated. Heat release data in data in reactivated cylinders was compared to the baseline data for the same cylinders.
4. Engine experiments at 800 rpm, 2.54 bar BMEP demonstrated that for CDA times of up to 20 minutes, as much as 462.95 mg of oil had accumulated. This is approximately 20 times greater than the total injected fuel per cycle.
5. In some cases, significant oil masses (on the order of the total injected fuel) had accumulated after CDA times of only 5 minutes.
6. The calculated oil mass varied significantly from cylinder-to-cylinder, with both data sets indicating that cylinders 2 and 4 allowed for the most oil accumulation.

CHAPTER 4: FIRST-FIRE READINESS ANALYSIS

This Chapter presents a study of first-fire readiness for a diesel engine utilizing CDA. As was done for the oil accumulation study presented in Chapter 3, this study utilizes in-cylinder pressure measurements to calculate the heat released in combustion events during the transition from CDA to six cylinder mode. Additionally, the pressure measurements are used to calculate the gross indicated mean effective pressure (GIMEP) that the engine experiences during the mode transition. Any deviation in heat release and GIMEP from normal six cylinder operation during the mode transition is indicative of a lack of first-fire readiness. Experimental results at an engine operating condition of 800 rpm, 2.54 bar BMEP demonstrate that after CDA times of 5, 10, and 20 minutes, the engine is not first-fire ready. The results also show possible first-fire readiness issues for CDA times of as little as 0.5 minutes.

4.1 Analytical Procedure

The study of first-fire readiness in an engine utilizing CDA aims to answer the following question: Will a cylinder behave properly immediately upon reactivation after a prolonged period of deactivation? In this context, a cylinder is said to behave “properly” if it experiences combustion events indistinguishable from those seen in cylinders that have been actively firing for a long period of time. Since the heat release rate is a good indicator of combustion, first-fire readiness can be assessed by comparing the heat release rates of newly reactivated cylinders to those found in cylinders that have been active for an extended period of time. Just as in Chapter 3, it is the gross heat release rate that is of interest, since it represents all of the heat released by the combustion of a cylinder’s contents (injected fuel and accumulated engine oil), including the heat lost through the cylinder walls.

In the study of first-fire readiness, there are a few things to note in a heat release rate profile. Most importantly, it must be noted whether a cylinder exhibits any combustion at all immediately upon reactivation. For long enough periods of deactivation, it is possible for a cylinder to cool down to the extent that it is no longer hot enough to combust a fuel/air mixture properly. This is entirely unacceptable, and therefore is considered the most important first-fire readiness constraint. Another issue that appears in a heat release rate profile is deviation from normal combustion during the pilot injection. Finally, distorted combustion during and after the main injection must also be noted.

Another major first-fire readiness issue is torque oscillations caused by the combustion of accumulated oil, as outlined in Chapter 3. Statistically significant amounts of engine oil accumulate in deactivated cylinders over periods of time greater than five minutes. This oil mixes with injected fuel and combusts upon a cylinder's reactivation, and this is reflected in the heat release analysis in Chapter 3. In terms of first-fire readiness, the additional heat release caused by oil combustion can cause undesirable torque oscillations at the crank shaft, and this is analyzed using GIMEP calculations.

The implementation of any CDA strategy on a full vehicle should be completely transparent to the driver. Accordingly, in this analysis, the engine is determined to be non-first-fire-ready if at least one cylinder exhibits abnormal combustion or the GIMEP exhibits any abnormal fluctuations.

4.2 Experimental Results

The experimental study of first-fire readiness is based on the same test plan presented in Chapter 3. Data sets 1 and 2 from Chapter 3 are again analyzed in this Chapter, this time with a focus on the first-fire readiness issues outlined in Section 4.1. The following subsections discuss first-fire readiness issues in both data sets at each of the four CDA times in the test plan.

20 Minute CDA Time

After 20 minutes of CDA, the engine is not first-fire ready due to both distorted combustion and GIMEP oscillations during the mode transition. Fig. 4.1 shows that after 20 minutes of CDA, combustion in cylinder 5 is extremely distorted during both the pilot and main fuel injections due to the combustion of accumulated oil. In the first, second, and third cycles, very little combustion occurs during the pilot injection, and heat release during and after the main injection is expectedly higher than baseline. In the fourth and fifth cycles, combustion occurs before the pilot (near 340 °), and combustion is markedly greater than baseline during the pilot and after the main. Data from other cylinders also show this kind of distorted combustion.

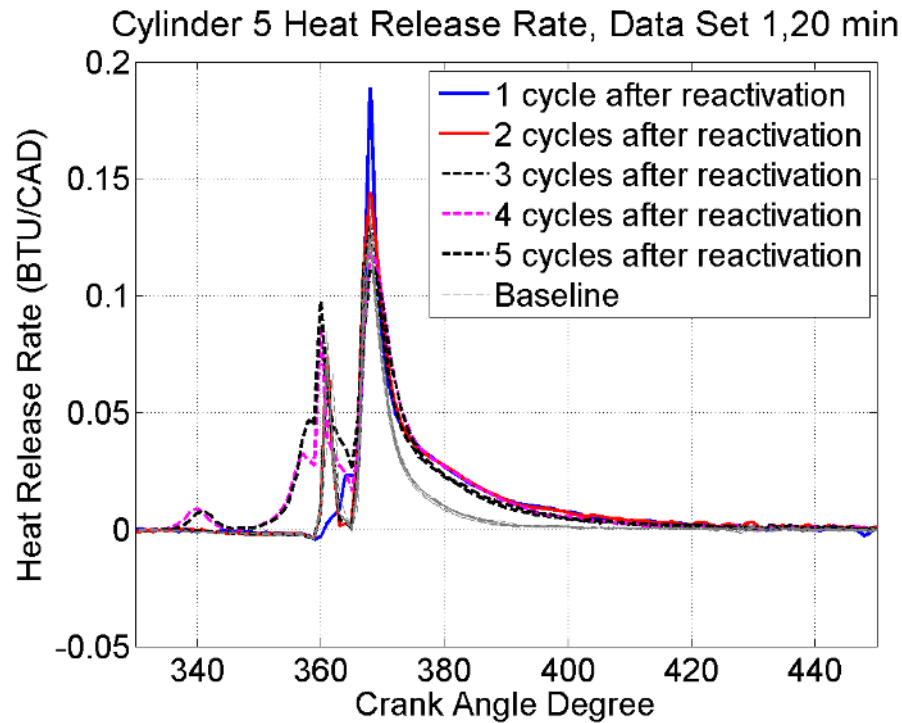


Figure 4.1. Heat release rate as a function of crank angle in cylinder 5 after 20 minutes of CDA.

Since the cumulative heat release during the transition is greater than it is during steady-state six cylinder operation, the large GIMEP fluctuations illustrated in Fig.

4.2 occur. Due to the abnormal combustion and GIMEP oscillations in Figs. 4.1 and

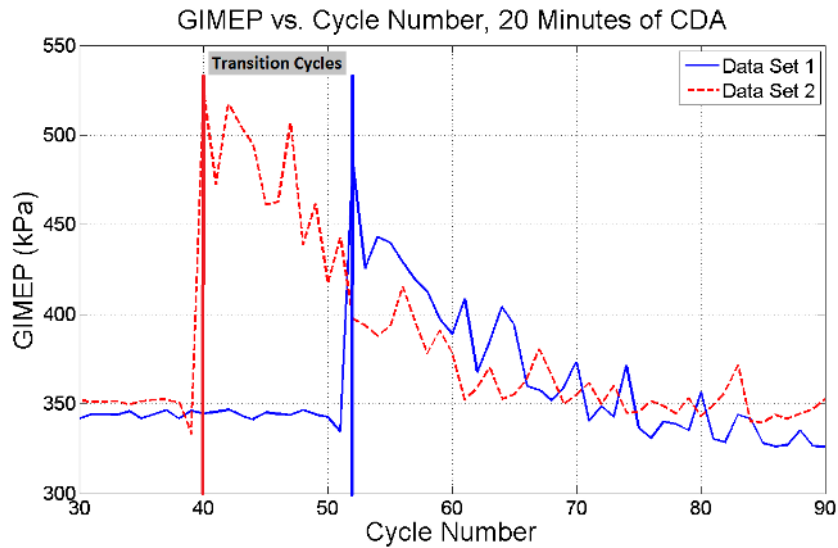


Figure 4.2. GIMEP after 20 minutes of CDA for data sets 1 and 2.

4.2, respectively, the engine is not first-fire ready after 20 minutes of CDA.

10 Minute CDA Time

After 10 minutes of CDA, the engine is not first-fire ready due to both distorted combustion and GIMEP oscillations during the mode transition. Fig. 4.3 shows that after 10 minutes of CDA, combustion in cylinder 1 is quenched during both the pilot and main fuel injections in the first cycle after reactivation. While such quenching is not apparent in the subsequent cycles, there is evidence of oil combustion after the main injection. This oil combustion contributes to the GIMEP oscillations illustrated in Fig. 4.4. While these oscillations are slightly lower in magnitude than those after 20 minutes of CDA, they nonetheless represent a significant deviation from normal six cylinder operation. Due to the abnormal combustion and GIMEP oscillations in Figs. 4.3 and 4.4, respectively, the engine is not first-fire ready after 10 minutes of CDA.

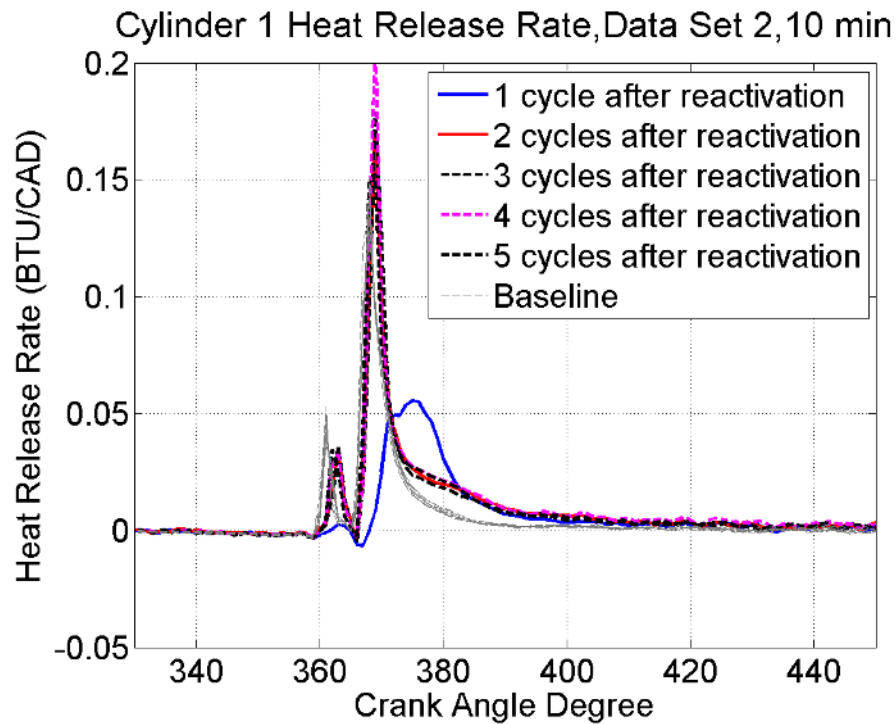


Figure 4.3. Heat release rate as a function of crank angle in cylinder 1 after 10 minutes of CDA.

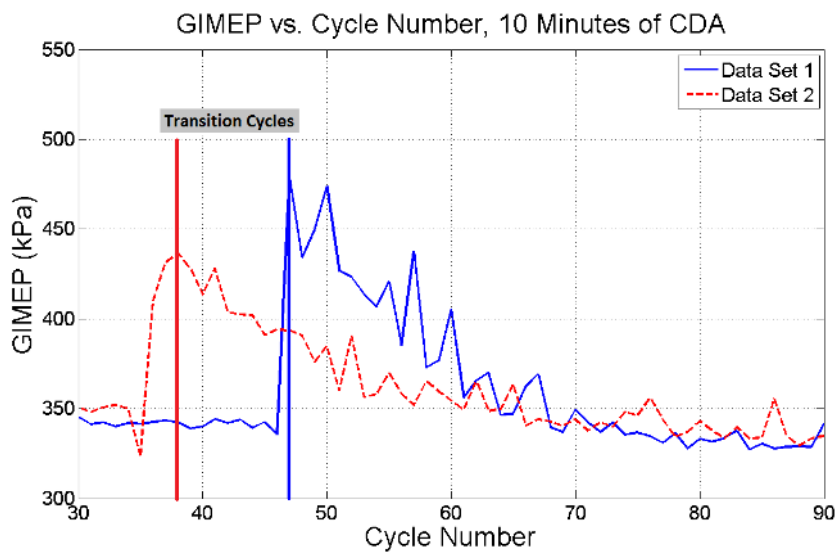


Figure 4.4. GIMEP after 10 minutes of CDA for data sets 1 and 2.

5 Minute CDA Time

After 5 minutes of CDA, the engine is not first-fire ready due to both distorted combustion and GIMEP oscillations during the mode transition. Fig. 4.5 shows that after 5 minutes of CDA, combustion in cylinder 3 is quenched during both the pilot and main fuel injections in the first cycle after reactivation. In the subsequent cycles, quenching is somewhat less drastic but is still present, particularly during the pilot injection. This distorted combustion contributes to the GIMEP oscillations

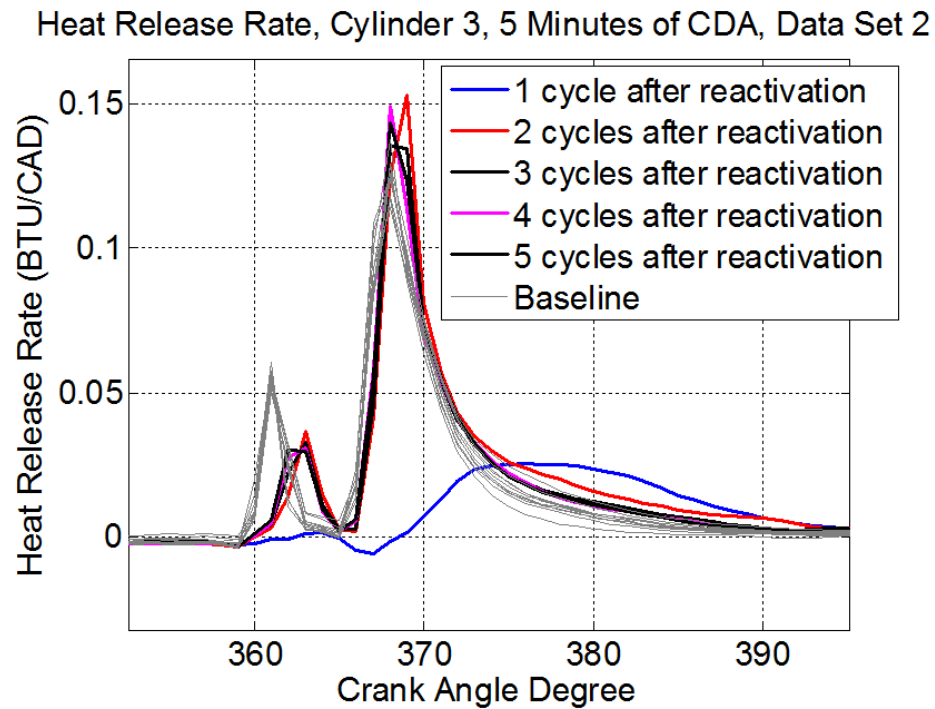


Figure 4.5. Heat release rate as a function of crank angle in cylinder 3 after 5 minutes of CDA.

illustrated in Fig. 4.6. While these oscillations are less pronounced than those after 10 and 20 minutes of CDA, they are significantly different from normal six cylinder operation. Due to the abnormal combustion and GIMEP oscillations in Figs. 4.5 and 4.6, respectively, the engine is not first-fire ready after 5 minutes of CDA.

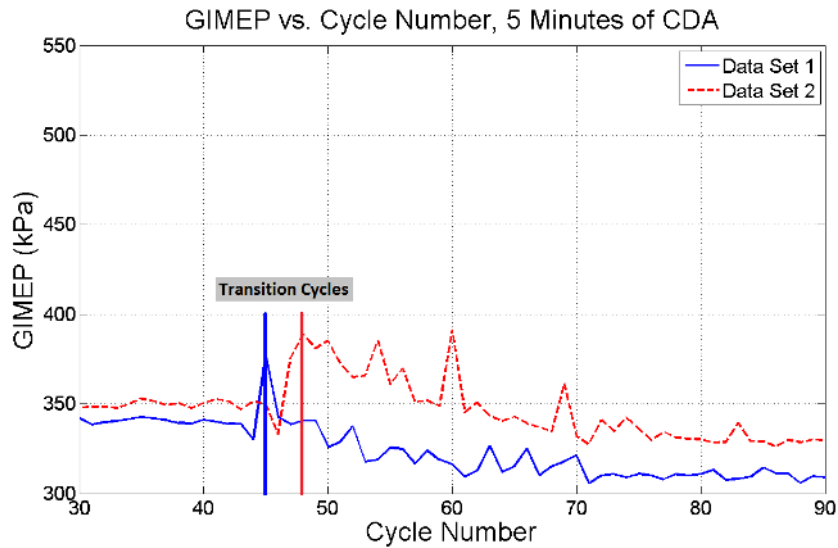


Figure 4.6. GIMEP after 5 minutes of CDA for data sets 1 and 2.

0.5 Minute CDA Time

As the calculations in Chapter 3 demonstrated, little to no oil mass accumulated after only 0.5 minutes of CDA. Thus, significant GIMEP oscillations are not expected during the mode transition, and Fig. 4.7 illustrates this. The slight drop in GIMEP during the transition is due to the increased pumping work required during six cylinder operation. However, the heat release rate is affected during the transition, as is shown in Fig. 4.8. In Fig. 4.8, the heat release rate during the first cycle after reactivation is quenched during the pilot injection and greater than the baseline during the main injection. While the cumulative heat release per cycle, shown in Fig. 4.9, indicates an error bar overlap in the first cycle following the mode transition (i.e. zero calculated oil mass), the abnormal combustion profile in Fig. 4.8 is still noteworthy. While not statistically different from the baseline in terms of cumulative heat release (and thus, GIMEP), this kind of abnormal combustion is present in more than 80% of the 0.5 minute CDA data from data sets 1 and 2. This indicates a probable lack of first-fire readiness, although whether or not this kind of combustion behavior is acceptable is ultimately a decision that must be made by powertrain manufacturers and designers.

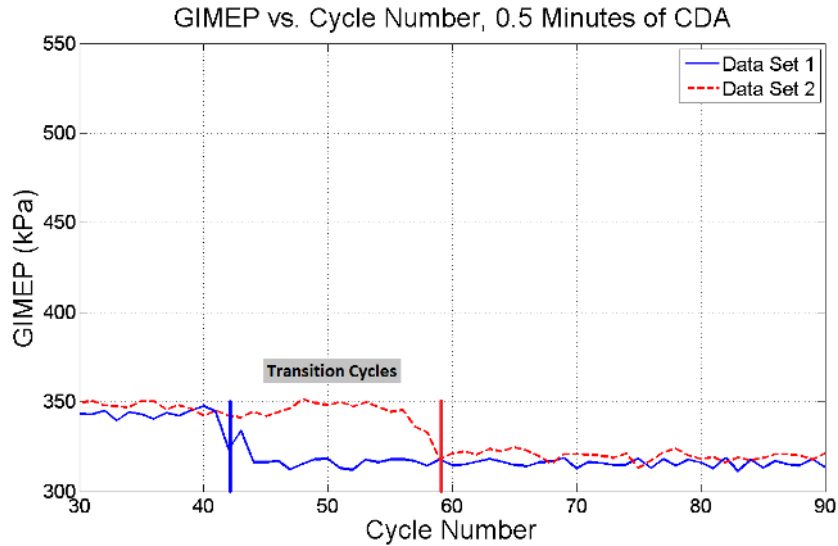


Figure 4.7. GIMEP after 0.5 minutes of CDA for data sets 1 and 2.

4.3 Summary

The effort in this Chapter analyzed the heat release data from Chapter 3 from the perspective of first-fire readiness. It was concluded that after CDA times of 5, 10, and 20 minutes, the engine is not first-fire ready. The engine is also probably not first-fire ready after 0.5 minutes of CDA.

1. The heat release data from Chapter 3 was analyzed from the perspective of first-fire readiness.
2. First-fire readiness was assessed according to deviations in heat release and GIMEP from normal six cylinder operation.
3. CDA times of 5, 10, and 20 minutes were determined not to be first-fire ready.
4. A CDA time of 0.5 minutes was determined to probably not be first-fire ready.

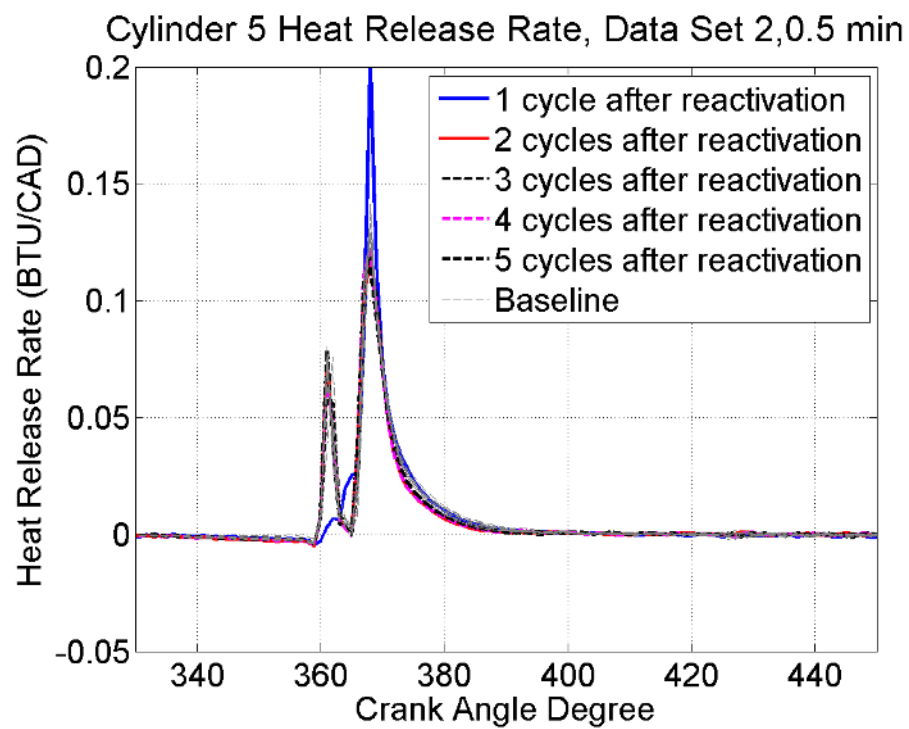


Figure 4.8. Heat release rate as a function of crank angle in cylinder 5 after 0.55 minutes of CDA.

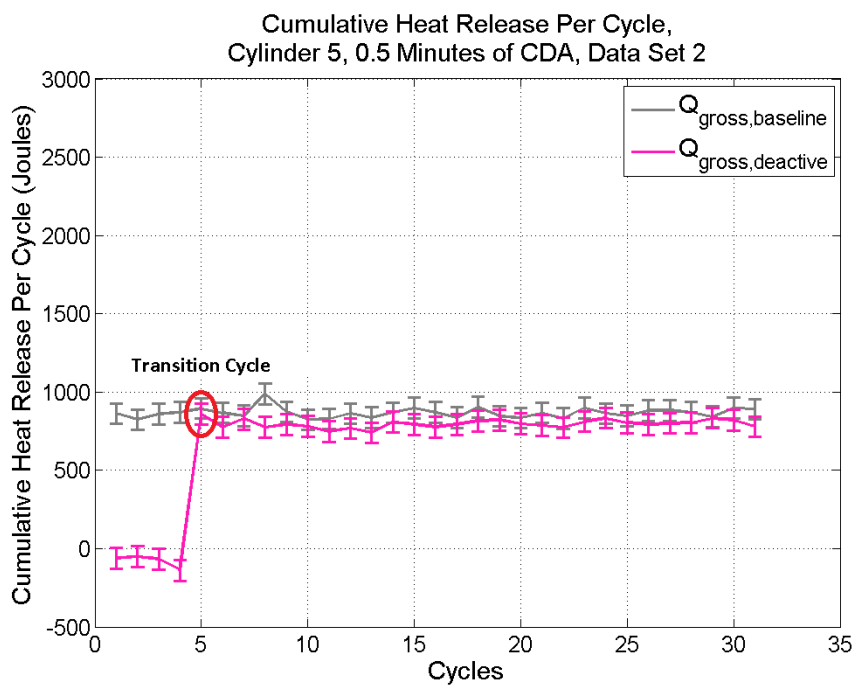


Figure 4.9. Cumulative heat release per cycle in cylinder 5 after 0.5 minutes of CDA in data set 2.

CHAPTER 5: FIRED RECHARGE ALGORITHM DEVELOPMENT AND VALIDATION FOR A DIESEL ENGINE UTILIZING CDA

This Chapter presents the development and implementation of a fired recharge algorithm for a diesel engine utilizing CDA. This algorithm was developed by adding fueling control to the non-fired recharge algorithm developed by the author's colleagues in [15]. The performance of the fired recharge algorithm is validated in this Chapter with plots of injector current, heat release rate, and in-cylinder pressure, which demonstrate that the fired recharge algorithm performed successfully. This Chapter concludes with statements regarding the potential ability of recharge events as a means to mitigate the oil accumulation and first-fire readiness issues discussed in Chapters 3 and 4, respectively. While this Chapter demonstrates that fired recharge capability has been added to the engine test cell, an experimental investigation of the effect of recharge events on oil accumulation and first-fire readiness remains the subject of future work.

5.1 The Fired Recharge Algorithm

The primary goal of this effort is to add functionality to the non-fired recharge algorithm, [15], which is capable of performing fired recharge events for a diesel engine in CDA mode. Ultimately, the entire recharge algorithm (both fired and non-fired recharge events) will enable the experimental analysis of recharge events on oil accumulation and first-fire readiness. The algorithm used in this study behaves in the following way.

First, the user selects between non-fired and fired recharge events. For a non-fired recharge, the series of events illustrated in Fig. 5.1 occur in all six cylinders. In this

case, the recharge event consists of an exhaust valve opening and closing, followed by an intake valve opening and closing. No fuel is injected and no combustion occurs.

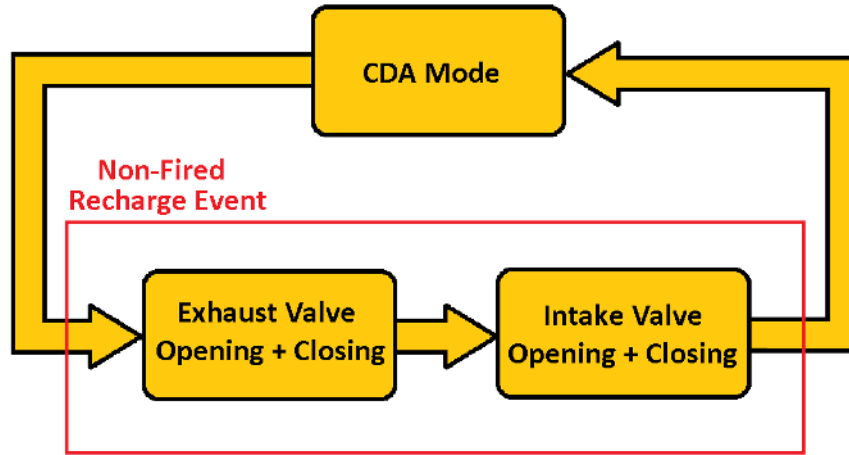


Figure 5.1. Order of events during a non-fired recharge event

During a fired recharge engine cycle, all six cylinders undergo the series of events depicted in Fig. 5.2. First, the cylinder's valve events (opening and closing) happen in the same way as in a non-fired recharge. Next the recharging cylinder experiences a fuel injection, followed by a combustion event. Because the engine used in this study has a firing order of 1-5-3-6-2-4, a successful fired recharge event must also happen in this order.

From an NVH perspective, it is important to maintain a constant torque during the CDA mode transition. Since this particular fired recharge algorithm is essentially an extremely brief transition between three and six cylinder engine operation, an effort must be made to prevent the engine output torque from experiencing dramatic transient fluctuations. In a diesel engine, torque is primarily influenced by the total amount of fuel being injected per cycle. Since entering CDA mode cuts in half the number of cylinders receiving fuel, the total fueling, per cylinder, is commanded to be cut in half during the fired recharge. Thus, the total amount of fuel supplied to all

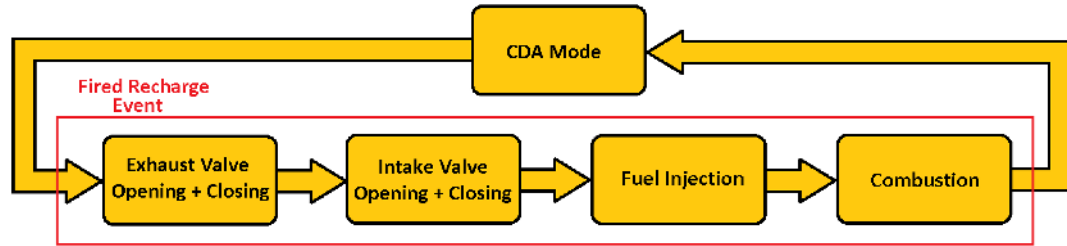


Figure 5.2. Order of Events During a Fired Recharge Event

six cylinders remains constant as the cylinders are reactivated and then immediately deactivated following the fired recharge. While this is not a perfect means of torque control, it yields a reasonably constant torque during the fired recharge event.

5.2 The Implementation and Validation of the Fired Recharge Algorithm

The cycle-to-cycle control of both fueling and valve events results in a non-fired/fired recharge algorithm. In the engine test cell used in this study, all of the valvetrain-related controls are performed using dSPACE. The rest of the engine control systems, including fueling, are handled by the engine control module (ECM). While the test cell is equipped such that dSPACE can communicate with the ECM via a generic serial interface (GSI), such communication can behave unpredictably when fast, transient behavior is desired. While valve event control using dSPACE posed no issues, the implementation of the fired recharge algorithm in dSPACE was difficult due to the lag time between the ECM's fueling command and response.

The valve events during a fired recharge use the exact same dSPACE code developed by the author's colleagues in [14, 15], while the fueling events during a fired recharge were performed using two ECM variables. The two variables and their functions are summarized in Table 5.1.

Table 5.1. ECM variables used in fired recharge algorithm.

ECM Variable	Function
C_CBM_CylCutout_Ov_Value	Specifies which cylinders to stop fueling
C_CBM_CylCutout_Ov_Enable	Stops fueling cylinders specified by C_CBM_CylCutout_Ov_Value when value is 1 and resumes fueling when value is 0

Using these two ECM variables, successful fired recharge events have been performed. In Figs. 5.3 - 5.5, plots of in-cylinder pressure, valve events, injector current, net heat release rate, and the fueling command signal (C_CBM_CylCutout_Ov_Enable) are shown. Additionally, the smaller plot embedded in each of these figures shows injector current and net heat release rate, since those lines are obscured in the larger figures. Since each of these figures contains six lines, most of which represent quantities in different units, the values on the vertical axes are meaningless since some of the lines had to be scaled in order to fit all of them on a single plot. Accordingly, the values on the vertical axes are not shown. Figs. 5.3 - 5.5 primarily serve to demonstrate that events happen in the correct order during a fired recharge, and these figures are discussed with that in mind.

An inspection of Fig. 5.3 shows that the fired recharge event in cylinder 4 began at approximately 5.9 seconds into this particular log of data. Before this time, the solid red line demonstrates that the in-cylinder pressure had decayed to a steady state after several seconds of cylinder 4's deactivation. The dashed red line indicates that the exhaust valve event was the first event, followed by the intake valve event shown by the dashed blue line. After the valve events, the solid blue line shows that cylinder 4's fuel injector received an increase in its actuator's current, and this coincides with a heat release event indicated by the solid black line. Again, these are

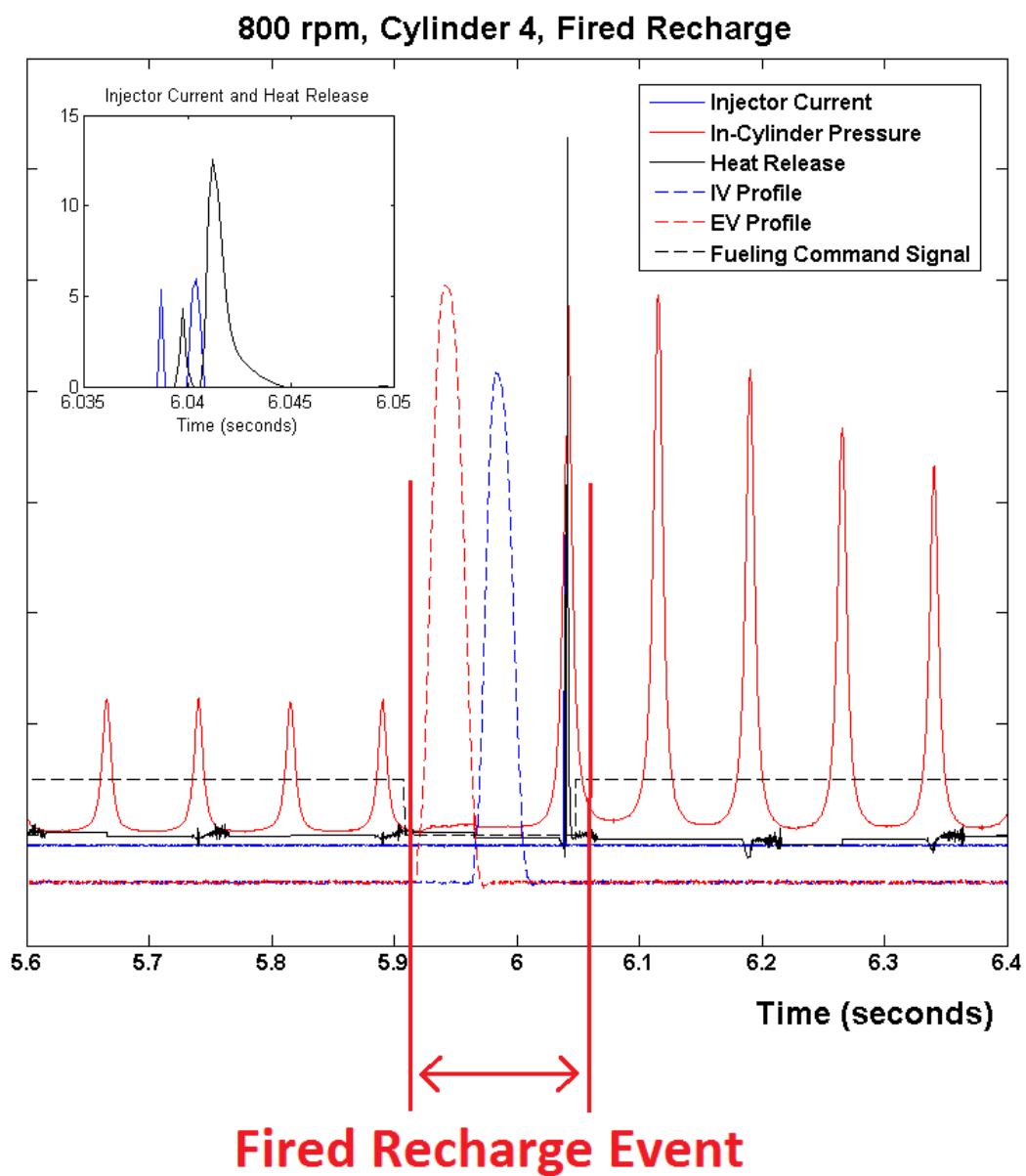


Figure 5.3. Fired recharge in cylinder 4 at 800 rpm

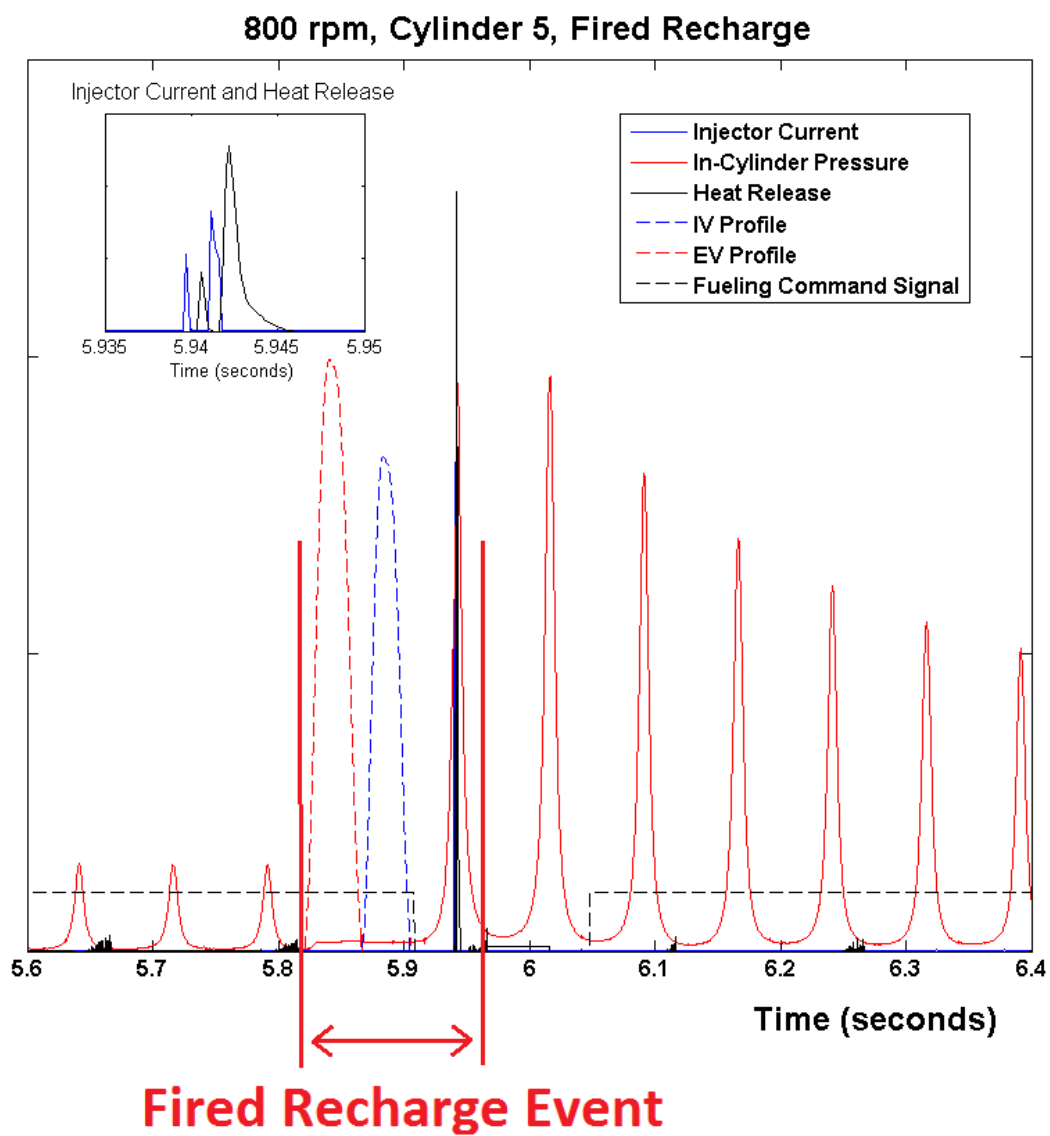


Figure 5.4. Fired recharge in cylinder 5 at 800 rpm

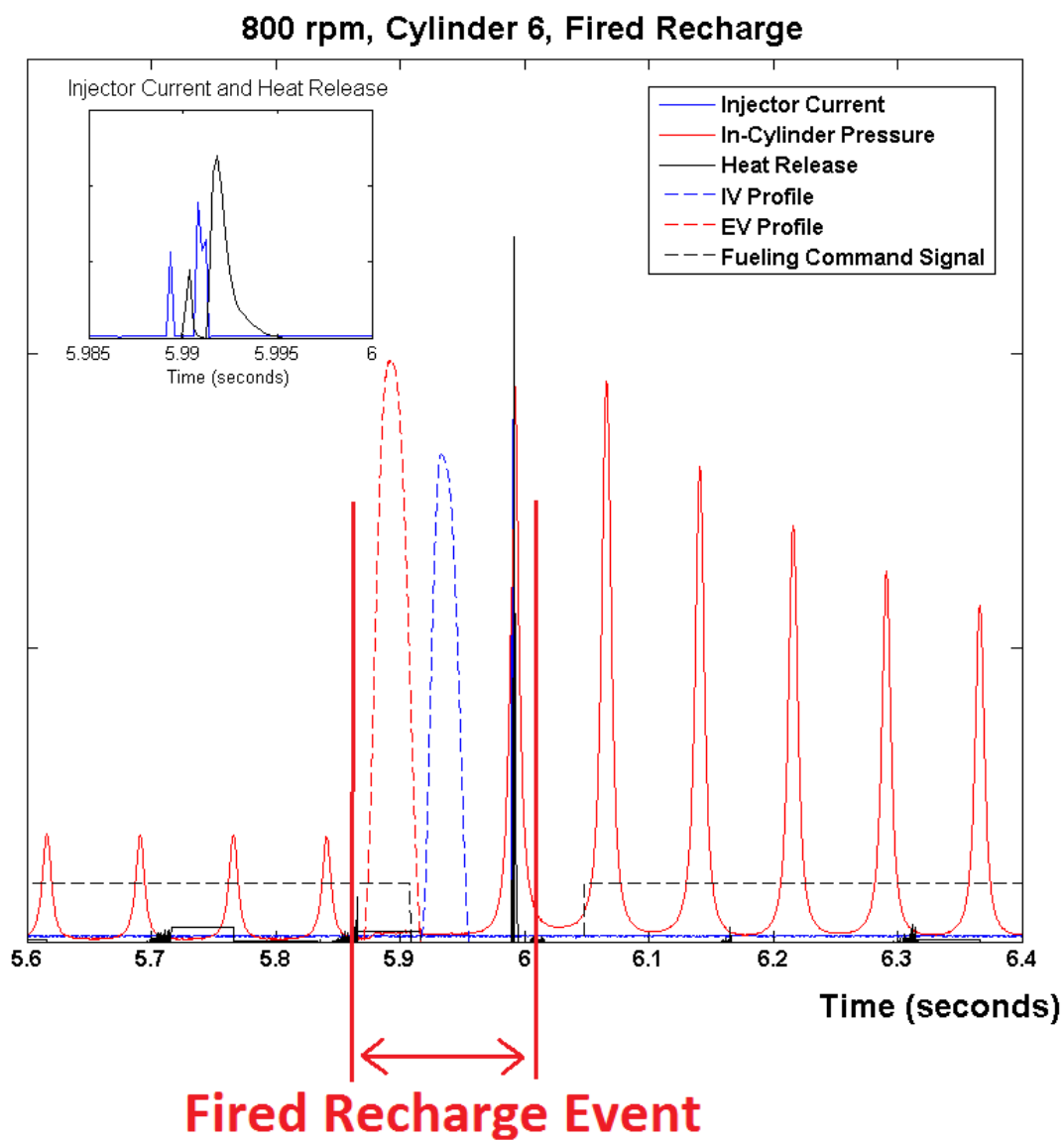


Figure 5.5. Fired recharge in cylinder 6 at 800 rpm

better illustrated by the small plot embedded in Fig. 5.3. The solid red line shows that the in-cylinder pressure experienced the expected increase, one of the goals of a fired recharge strategy. As time passes after the fired recharge, in-cylinder pressure can be seen to again decay.

The black dashed line in Figs. 5.3 - 5.5 represents the fueling command signal. As is described in Table 5.1, when this signal is equal to one, fueling is cut to cylinders 4, 5, and 6. When it is equal to zero, fueling is resumed to all six cylinders, as is desired during the fired recharge cycle. Since the ECM's behavior can be somewhat unpredictable, the best times at which to send and stop sending the fueling command signal during a fired recharge (i.e. setting the signal to zero and then back to one) were determined experimentally. Engine tests were performed at engine speeds of 800 rpm and 1200 rpm, and the times at which the fueling command was sent were varied. These experiments yielded results which led to the successful performance of fired recharge events approximately 90% of the time. Occasionally, cylinder 5 would not exhibit a net heat release rate consistent with combustion, and its injector current would not experience an increase consistent with a fuel injection. This is likely due to some inherent variation in the lag time between ECM command and response when communicating with the ECM using GSI.

The same series of events are shown in Figs. 5.4 and 5.5 for cylinders 5 and 6. Fig. 5.6 better illustrates that cylinders 4, 5, and 6 recharged in the correct order. This figure shows data identical to that of Figs. 5.3 - 5.5, but the order of one cylinder's events relative to another is more clear. Data from cylinders 1, 2, and 3 during the fired recharge engine cycle are not shown since those cylinders are constantly firing. Since the order of events during any one cylinder's fired recharge is that shown in Fig. 5.2 and since the cylinders recharged in the correct order (cylinder 5, then cylinder 6, then cylinder 4), the implementation of this fired recharge algorithm was successful.

The final piece of this fired recharge algorithm that has not yet been illustrated in any of the figures is the maintenance of a constant torque during a fired recharge. In a diesel engine, the brake torque is chiefly influenced by the total injected fuel mass

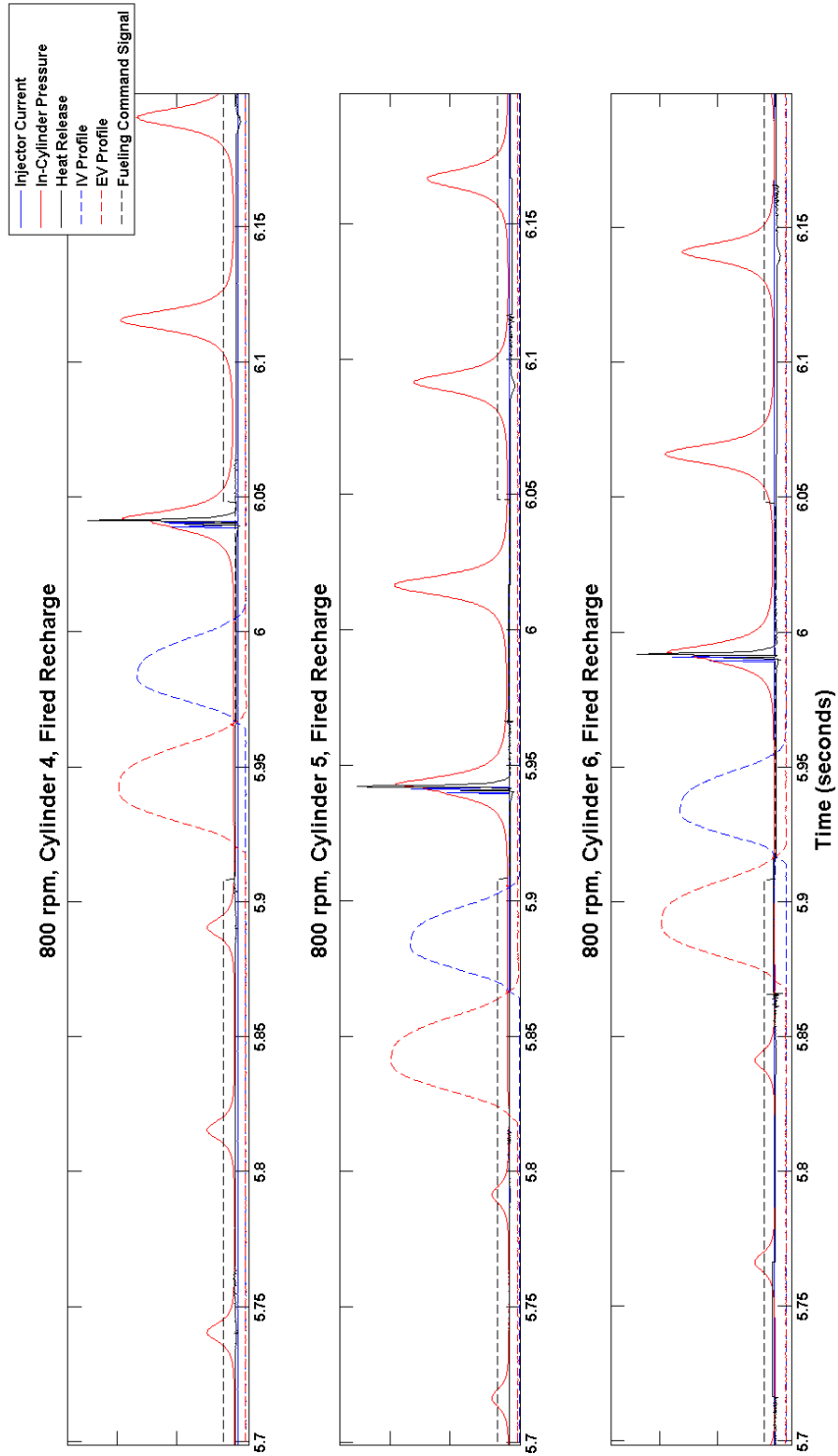


Figure 5.6. Fired recharges in cylinders 4, 5, and 6 at 800 rpm, all on the same time axis

per cycle. Thus, to reduce torque fluctuations, the ECM-commanded total fueling is cut in half during the single-cycle fired recharge event. While the DSpace software in the engine test has been modified to perform this fuel-halving, its efficacy as means of torque control will be investigated in future work.

5.3 The Effect of Recharge Events on Oil Accumulation and First-Fire Readiness

The results presented in this Chapter demonstrate that the ability to perform fired recharge events has been added to the engine test cell. This added capability enables the execution of an important set of experiments that will be conducted in future work, and these experiments will be outlined in this Section.

By leveraging the results presented in Chapters 3 and 4, the effects of fired and non-fired recharge events on oil accumulation and first-fire readiness can be experimentally analyzed. The algorithm presented in this Chapter provides an experimenter with two inputs: the choice between fired and non-fired recharge events and the length of the recharge interval. Since the results in Chapters 3 and 4 indicate that oil accumulation and first-fire readiness are serious issues for CDA times of 5, 10, and 20 minutes, future work should begin by investigating recharge intervals of less than 5 minutes. Since a CDA time of 0.5 minutes also presented probable first-fire readiness issues, it may be necessary to restrict the recharge interval to less than 0.5 minutes. With the proper choice of recharge interval and fired/non-fired recharge event type, it may be possible to mitigate oil accumulation and first-fire readiness sufficiently enough to enable the engine to operate in CDA mode and experience its fuel economy and emissions benefits for extended periods of time.

5.4 Summary

This study resulted in the implementation of a fired cylinder recharging algorithm for a diesel engine utilizing CDA. While the effectiveness of this algorithm in terms

of preventing oil accumulation and improving first-fire readiness is not studied in this thesis, the algorithm could be used to that end in future work. The oil accumulation and first-fire readiness results presented in Chapters 3 and 4 could influence the choice of recharge interval.

1. DSpace software was modified such that a fired cylinder recharge can be performed successfully at user-specified recharge intervals 90% of the time.
2. The ECM-commanded total fueling was cut in half during a fired recharge event to reduce the transient brake torque fluctuations that occur when the total fueling command is not halved.

CHAPTER 6: SUMMARY AND FUTURE WORK

6.1 Parameter Estimation for a Piezoelectric Fuel Injector

Summary

The results in Chapter 2 demonstrate that the parameter estimator in this thesis can correct for an initial error the injector model's needle seat area vs. needle lift relationship. In the presence of an initial parameter error of 25%, the parameter estimator improved the model-based prediction of total injected fuel by approximately 10%. Perhaps most importantly, the prediction of the fuel flow rate during the toe exhibited improvement in most cases after the parameter update, even though the toe is when the injector model is most sensitive.

Future Work

In this paper, a parameter estimation strategy was designed and shown to improve the performance of the state estimator in [26] when there is some initial error in $A_{1,estimator}$. However, only a very basic rule for updating $A_{1,estimator}$ was designed (i.e. update the parameter after 25 boot-shaped injections). A more advanced parameter update law could be a simple extension of the method used in this paper, in which $A_{1,estimator}$ would be updated after a certain number of injection events have occurred. At any rate, the design of a parameter update law is the subject of future work.

In this study, there was no effort to prove that the parameter estimate $\hat{A}_1(x_2)$ converges to its true value. Such a guarantee would certainly be valuable, and is also considered future work.

Finally, Figs. 2.7 - 2.12 along with Table 2.1 show that the parameter update was not quite as effective for $\alpha = 0.75$ as it was for $\alpha = 1.25$. The reason for this lack of symmetry in the parameter estimation strategy in this paper is unknown and could be explored in future work.

6.2 Oil Accumulation, First-Fire Readiness, and Cylinder Recharging Analysis for a Diesel Engine Utilizing CDA

Summary

The results in Chapters 3 and 4 demonstrate that oil accumulation and first-fire readiness are serious issues for a diesel engine operating in CDA mode for 5, 10, and 20 minutes. After 20 minutes of CDA, up to 462.95 mg can accumulate in deactivated cylinders. Furthermore, this oil accumulation can cause distorted combustion and erratic GIMEP fluctuations as the engine transitions from CDA to six cylinder mode. These two problems lead to the conclusion that the engine is not first-fire ready after operating in CDA mode for 5, 10, and 20 minutes, and is likely not first-fire ready after as little as 0.5 minutes of CDA.

The effort in Chapter 5 resulted in a fired cylinder recharging strategy than resumes six cylinder engine operation for a single engine cycle at specified intervals. This strategy aims to prevent oil accumulation and by raising the in-cylinder pressure such that oil cannot seep in through the piston ring seal. This strategy also has the potential to improve first-fire readiness performance.

Future Work

Future work will largely revolve around using the fired recharge strategy presented in Chapter 5 to mitigate oil accumulation and improve first-fire readiness. Experiments can be conducted at different recharge intervals to determine the optimal recharge interval that minimizes oil accumulation while not interfering with the benefits of CDA operation.

Further development of the fired recharge algorithm itself could result in more elaborate cylinder recharging strategies such as not recharging all deactivated cylinders in the same engine cycle. This would require additional software modification, but the ECM is capable of such behavior.

Finally, the effects of torsional vibrations during fired and non-fired recharge events could be studied. Since these torsional vibrations are undesirable, the cylinder recharging strategy will be designed to minimize their magnitudes.

LIST OF REFERENCES

LIST OF REFERENCES

- [1] *Meeting EPA 2010*. <http://www.factsaboutscr.com/scr/engine-control-standards.aspx>, June 2008.
- [2] D. Hareendranath, N. Gajarlawar, M. Manickam, and G. Pundlik. Low end performance improvement by effective use of multiple injection strategy in common rail diesel engine. In *Proceedings of the ASME Internal Combustion Engine Division 2009 Spring Technical Conference*, Milwaukee, Wisconsin, USA.
- [3] S. Mendez and B. Thirouard. Using multiple injection strategies in diesel combustion: Potential to improve emissions, noise and fuel economy trade-off in low cr engines. *SAE 2008-01-1329*, 2008.
- [4] G. Dober, S. Tullis, G. Greeves, N. Milovanovic, M. Hardy, and S. Zuelch. The impact of injection strategies on emissions reduction and power output of future diesel engines. *SAE Technical Paper 2008-01-0941*, 2008.
- [5] J. Kashdan, P. Anselmi, and B. Walter. Advanced injection strategies for controlling low-temperature diesel combustion and emissions. *SAE 2009-01-1962*, 2009.
- [6] R. Payri, F.J. Salvador, J. Gimeno, and J. De la Morena. Influence of injector technology on injection and combustion development part 1: Hydraulic characterization. *Applied Energy 10681074*, 2011.
- [7] B.J. MacLachlan, N. Elvin, C. Blaurock, and N.J. Keegan. Piezoelectric valve actuator for flexible diesel operation. In *Smart Structures and Materials 2004: Industrial and Commercial Applications of Smart Structures Technologies*, San Diego, California, USA.
- [8] J.M. Desantes, J. Benajes, S. Molina, and C.A. Gonzales. The modification of the fuel injection rate in heavy-duty diesel engines. part 1: Effects on engine performance and emissions. *Applied Thermal Engineering 2701-2714*, 2004.
- [9] J.W. Hwang, H.J. Kal, M.H. Kim, J.K. Park, L. Shenghua, A.A. Martychenko, and J.O. Chae. Effect of fuel injection rate on pollutant emissions in di diesel engine. *SAE Technical Paper 1999-01-0195*, 1999.
- [10] M. Ghaffarpour, M. Azarfam, and A. Noorpoor. Emission reduction in diesel engines using new fuel injection system. *JSME International Journal Series B Fluids and Thermal Engineering*, 49(4), 2006.
- [11] T.G. Leone and M. Pozar. Fuel economy benefit of cylinder deactivation - sensitivity to vehicle applications and operating constraints. *SAE 2001-01-3591*, 2001.

- [12] Haijun Mo, Yongquan Huang, Xiaojian Mao, and Bin Zhuo. The effect of cylinder deactivation on the performance of a diesel engine. *Journal of Automobile Engineering*, 2014.
- [13] Jean-Paul Zammit, Michael J. McGhee, , Paul J. Shayler, and Ian Pegg. The influence of cylinder deactivation on the emissions and fuel economy of a four-cylinder direct injection diesel engine. *Journal of Automobile Engineering*, 2014.
- [14] Leighton Roberts, Mark Magee, David Fain, Gregory M. Shaver, Eric Holloway, Raymond Shute, Jim McCarthy, Edward Koeberlein, Douglas Nielsen, and David Koeberlein. Analysis of the impact of diesel engine cylinder deactivation at loaded and unloaded idle on thermal management and efficiency. In *ASME IC Engine Division Fall Technical Conference*, 2014.
- [15] Mark Magee. *Exhaust Thermal Management Using Cylinder Deactivation*. PhD thesis, Purdue University, 2013.
- [16] Leighton Roberts. *Analysis of the Impact of Early Exhaust Valve Opening and Cylinder Deactivation on Aftertreatment Thermal Management and Efficiency for Compression Ignition Engines*. PhD thesis, Purdue University, 2014.
- [17] K. Tanabe, S. Kohketsu, K. Mori, and K. Kawai. Innovative injection rate control with next generation common rail fuel injection system. In *Proceedings of Seoul FISITA World Automotic Congress*, Seoul, Korea, 2000.
- [18] Chienshin Wu and Zongxuan Sun. Design and control of a direct fuel injector with rate shaping capability. In *American Control Conference*, Washington, D.C., USA, 2013.
- [19] F Gu, A D Ball, and K K Rao. Diesel injector dynamic modelling and estimation of injection-parameters from impact response part 2 : prediction of injection parameters from monitored vibration. *Proceedings of the Institution of Mechanical Engineers, Part D: Journal of Automobile Engineering*, 1996.
- [20] J J Moskwa. Estimation of dynamic fuel parameters in automotive engines. *Journal of Dynamic Systems, Measurement, and Control*, 1994.
- [21] Ru Changhai, Sun Lining, Rong Weibin, and Chen Ligu. Adaptive inverse control for piezoelectric actuator with dominant hysteresis. In *International Conference on Control Applications*, 2004.
- [22] U-Xuan Tan, Win Tun Latt, Ferdinan Widjaja, Cheng Yap Shee, Cameron N. Riviere, and Wei Tech Ang. Tracking control of hysteretic piezoelectric actuator using adaptive rate-dependent controller. *Sensors and Actuators A: Physical*, 2009.
- [23] C. Satkosky and et. al. Dynamic modeling of a piezoelectric actuated fuel injector. *ASME Journal of Dynamic Systems, Measurement, and Control*, 133, 2011.
- [24] D. Le, N.S. Ruikar, J. Shen, and G.M. Shaver. Dynamic modeling of a piezoelectric fuel injector during rate shaping. *International Journal of Engine Research*, 2013.

- [25] Chris A. Satkoski, Neha S. Ruikar, Scott D. Biggs, and Gregory M. Shaver. Piezoelectric fuel injection cycle-to-cycle control of tightly space injections. *Control Engineering Practice*, 2012.
- [26] Jin Shen, Bradley W. Pietrzak, Neha Ruikar, Dat Le, and Gregory M. Shaver. Model-based within-a-cycle estimation of rate shaping for a piezoelectric fuel injector. *In review at Control Engineering Practice*, 2013.
- [27] Dat Le, Bradley W. Pietrzak, and Gregory M. Shaver. Dynamic surface control of a piezoelectric fuel injector during rate shaping. *IFAC Control Engineering Practice*, 2014.
- [28] Alan Falkowski, Mark McElwee, and Mike Bonne. Design and development of the daimlerchrysler 5.7l hemi engine multi-displacement cylinder deactivation system. *SAE 2004-01-2106*, 2004.
- [29] Alberto Boretti and Joseph Scalco. Piston and valve deactivation for improved part load performances of internal combustion engines. *SAE 2011-01-0368*, 2011.
- [30] Zheng Ma. Oil transport analysis of a cylinder deactivation engine. *SAE 2010-01-1098*, 2010.
- [31] Ertan Yilmaz, Tian Tian, Victor W. Wong, and John B. Heywood. The contribution of different oil consumption sources to total oil consumption in a spark ignition engine. *SAE 2004-01-2909*, 2004.
- [32] Kent Froelund and Ertan Yilmaz. Impact of engine oil consumption on particulate emissions. *SAE 960581*, 1996.
- [33] W. Bosch. Fuel rate indicator: A new measuring instrument for display of the characteristics of individual injection. *SAE 660749*, 1966.
- [34] Dat Le. *Physically-Based Modeling, Estimation, and Control of Piezoelectric Fuel Injection During Rate Shaping Operation*. PhD thesis, Purdue University, 2014.
- [35] Bradley W. Pietrzak, Dat Le, and Gregory M. Shaver. Model-based estimation of piezoelectric fuel injector parameters. In *American Controls Conference*, Portland, OR, USA, 2014.
- [36] Amit Garg, Kainou Kazunari, and Tinus Pulles. *2006 IPCC Guidelines for National Greenhouse Gas Inventories*. 2006.
- [37] J. Heywood. *Internal Combustion Engine Fundamentals*. McGraw-Hill, New York, NY USA, 1998.
- [38] Lyle Kocher, Ed Koeberlein, Dan Van Alstine, Karla Stricker, and Gregory M. Shaver. Physically-based volumetric efficiency model for diesel engines utilizing variable intake valve actuation. *International Journal of Engine Research*, 2012.
- [39] G. Woschni. A universally applicable equation for the instantaneous heat transfer coefficient in the internal combustion engine. *SAE 670931*, 1967.
- [40] Donald W. Stanton. Systematic development of highly efficient and clean engines to meet future commercial vehicle greenhouse gas regulations. *SAE 2013-01-2421*, 2013.